Channel Section Cantilevered Beam Subjected to Restrained Torsional Loading

Submitted by

Osman Karim Abdullah

For the Degree of MSc in Structural Engineering

London South Bank University,

Department of Urban Engineering,

Faculty of Engineering, Science and the Built Environment,

October / 2012

ABSTRACT

This project describes the state and behaviour of shear stress distribution and warping shear flow due to an applied torque on thin-walled channel cross section under restrained torsion. When the warping is restrained, warping normal stresses will be induced. These warping normal stresses will induce warping shears, which will provide a torsional restraining moment. This moment is defined as a warping torsional moment. In addition the pure torsional moment provides equilibrium in the system, which is discussed in chapter 4. Also it describes the state of the bending stress, shear stress and displacement of a rectangular section when subjected to a point load at the free end of the cantilever beam, which is discussed in chapter 3. Moreover, it will be seen that the maximum bending stress occur at the top and bottom surfaces of the cross section of the beam and it varies linearly. The longitudinal stress is zero at the free end of the cantilever beam and the maximum deflection occurs at the free end.

The theories and assumptions for thin-walled open section beam under restrained torsion and pure torsion are explained in the literature review (see chapter 2).

Theoretical analyses has been approved for thin-walled channel section subjected to restrained torsion-bending and investigate how the direct stress system is induced by axial constraint and a variety of warping stress, warping displacement and angle of twist in the longitudinal axis. Also, warping stress, shear flow and warping displacement round section profile (see chapter 5).

Finite element analysis solutions and results are obtained and organized by Strand 7 software. Finite element and theoretical results are compared by tables and graphs to provide percentages of error for thin-walled channel section cantilever beam under restrained torque loading (see chapter 6&7).

ACKNOWLEDGEMENTS

I thank God for giving me good health and opportunities to finish my dissertation.

I would like to thank my supervisor Dr Mahmood Datoo for all his friendly help in preparing this dissertation.

I would like to take this opportunity to thank all the staff from the Perry library help desk that has been helpful towards me during my studies at London South Bank University.

Finally, I wish to thank my immediate family, especially my mother, sisters, brothers and my friends for their prayer and support throughout my studies.

Contents

List of figures

List of tables

List of symbols

L = length of beam

z = longitudinal axis

b = flange width or width of cross section

h = web depth or depth of cross section

t = thickness of the beam wall

e = distance from shear centre to the web of section beam

T = torque

p = force

J = torsion constant

E = young's modulus

v = Poisson's ration

G = shear modulus of material

I_w = torsion-bending constant (warping constant)

s = distance round profile of section beam

w = sectorial coordinate

W = primary warping

W^* = secondary warping

μ = factor

θ = rotation

$\frac{\partial \theta}{\partial z}$ = rate of twist

f_w = warping stress

τ = shear stress

q_Γ = warping shear flow

A_E = first sectorial moment

$A_{E,0}$ = swept area

T_J = torsion torque (unrestrained torsion)

T_w = warping torque (restrained torsion)

CHAPTER (1)

INTRODUCTION

Chapter 1: Introduction

1.1 Background

The thin-walled structure is the most modern and optimal, designed for minimum weight and maximum stiffness. Thin-walled structures are fabricated from thin steel plates into thick beam section and thin-walled beam section. Thin-walled beams are commonly used in civil engineering structures generally in torsion due to high strength and low weight. In addition, any shapes of open cross sections are torsionally very flexible and twists readily when a torque is applied.

Torque is a common form of load in aircraft structures. A torque is a moment or couple that has the unit N.m. The difference between a torque and bending moment is that the torque acts about the longitudinal axis of a beam, whereas a bending moment acts about an axis that is perpendicular to the longitudinal axis of the beam.

According to the St. Venant theory; in the case of uniform torsion, in which it is assumed that when a torque is applied to unrestrained members then the cross sectional shape is maintained but that the plane of the cross section can warp freely along the member and no longitudinal stresses develop. This is applied for all cross section without any axial constraint of longitudinal members and the angle of twist will be constant along the longitudinal axis of the members.

According to the Wagner theory; in the case of nonuniform torsion (restrained torsion) cross sections are not free to warp and longitudinal stresses will occur which is varying along the member. In addition warping shear flow induces due to restrained torsion and the angle of twist will no longer be constant but will vary along the axis of the member.

When transverse load is applied to a thin walled section, the torque will occur if the load does not pass through the shear centre of the cross section.

While the member is restrained from warping, such as the fixed end of the cantilever beam in Fig (5.1), the resulting torsion at the point of warping restraint is called warping torsion. The warping stresses are shear (different from the St. Venant shear stresses) and longitudinal stresses. These longitudinal stresses will directly add to bending

stresses if the member is also subjected to major or minor axis bending moments. Along the length of the cantilever beam, both St. Venant and warping torsional stresses are present.

According to the theories of the St. Venant and Bredt-Batho, it was assumed that there is no warping stress along the beam longitudinal axis and there are no any effects of axial constraint. In the development of the Wagner theory for open section under torque, it was investigated that the direct stress along the span longitudinal axis is induced by axial constraint. In Fig (5.1), warping stress is not zero due to axial constraint at one end and associated shear stress systems induced.

According to Timoshenko theory of thin-walled I cross-section beam, if a torsion is applied to unrestrained beam then warp occurs along the beam and angle of rotation is constant along the beam, then this case is called pure torsion. The shear stresses distribution is induced around profile due to pure torsion and it is the same for all section. In addition, Timoshenko explained that “For a beam of thin-walled open section it can be assumed with reasonable accuracy that the shearing stress at any point is parallel to the corresponding tangent to the middle line of the cross section and is proportional to the distance from that line” see Fig (4.5). Furthermore, it has been explained by Saint-Venant and Bredt-Batho torsion theories and Wagner, Vlasov’s torsion bending theories. Also, some research has been done by Loughlan, J., Ata, M., Gotluru, B. P., Schafer, B. W. and Pekoz, T., (see chapter 2).

In chapter (5); the theoretical analysis has been executed for a thin-walled channel cantilever beam subjected to restrained torsional loading by calculating warping displacement (primary warping), warping stress, angle of twist, warping shear flow and location of the shear centre, which depends on type of the cross section as indicated in appendix (A). In addition in chapter (6); finite element analysis has been carried out for analysis thin-walled channel cantilever beam subjected to restrain torsional loading. Also, the theoretical and finite element results are compared and discussed in chapter (7).

1.2 Aim and objectives of the project

The aims of this dissertation are to study the analysis of the thin-walled structural form of single cell open section beam by determining stresses, shear flow constraint and displacements produced by restrained torsion, and investigate the effects of axial constraint on channel section cantilever beam. Direct and shear stress systems in open section beams are also modified by axial constraint.

The main objectives of the project are

- To study and research on thin-walled open section cantilever beam subject to restrained torsional loading and describe torsion under axial constraint.
- To design suitable cross section due to torsion bending and gain a better understanding of thin walled open beam under restrained torsion.
- To analysis and validate theoretical and finite element data.

1.3 Research Methodology

This project involves the theoretical analysis of the thin-walled channel cantilever beam under restrained torsional loading; the finite element program Strand 7 was used. The structure was simplified and material properties assumed, in order to obtain results of the warping stresses, shear flow, an angle of twist and displacements occurring in the structure. Also, to compare theoretical and Strand 7 results, including list of tables and graphs.

CHAPTER (2)

LITERATURE REVIEW

2.1 Saint-Venant and Bredt-Batho torsion theories

The theory of St. Venant is a generalisation of the problem of twisting of a circular shaft. A twisting of a shaft without restrain, does not produce any longitudinal stresses (compressions or tensions), but only pure shear stresses will be induced and the maximum value of shear stress occurs at the surface of the wall around section of the beam. The longitudinal warping stress is not induced, which is called free warping. Free warping at the cross section is referring to Saint-Venant's assumption; it is that when a torque applies on any cross section then it does remain undistorted in their own planes. The work of Saint-Venant (1853) revealed the classical torsion theory to the French Academy of Science. Bach, C. in (1909), is revealed that the classical torsion assumption will not determine warping stresses. Hence, the shear centre will not be coincided with the centroid of the section.

Also Saint-Venant investigated that the rate of twist for uniform torsion along the length of the section beam is constant and there is no longitudinal axial constraint affects on the cross section of the beam and warping is free along whole the beam.

The significant principle of St. Venant is that while statically equivalent systems of forces acting on a body produce largely different local effects the stresses at sections distant from the surface of loading are essentially the same.

2.2 Wagner theory

Wagner assumption for thin walled arbitrary section under restrained torsion exposed that the cross section remains undistorted and the shear stress and strain at the central line of the wall cross section is negligible except shear load.

Wagner developed a general theory of flexural torsional buckling and produced that if a thin-walled open section beam was subjected to restrained torsion then warping deformation is induced and warping is not longer constant at any point in the cross section. Thus, direct stress will be induced in longitudinal direction of the beam.

Furthermore, bending and torsional deformation occur around rotation centre due to generate torsional moment by apply shear load at any point (except centre of twist point) of thin-walled open cross section of the beam. However, if the force applies to the centre of twist point then bending deformation will be occurred at the section and torsional deformation will not be induced, (1929).

2.3 Timoshenko's theory and assumption

Timoshenko presented a paper on the effects of warping torsion in I-beam. In some cases Timoshenko explained and established that where the conditions are such as to cause one or more cross sections to remain plane and the question arises as to how such prevention of warping affects, the angle of twist and distribution of stresses. When a thin-walled open cross section subjected to torsion then warping will prevent by bending of the flange and depending on the rigidity of the flange. A simple case of this is I-beam which is twisted by a couple applied at the middle and beam is supported at the ends. From symmetry, the cross-section of the web at the middle I-beam must remain plane during twist and the consequent rotation of this cross-section with respect to the end cross-section is accompanied by bending of the flange. Timoshenko assumption for a thin-walled open section beam, it is assumed that the thicknesses of the flanges and of the web are small so that the stresses due to bending of these parts in the directions perpendicular to their surfaces can be neglected. In such a case, the action between the upper flange and the web is represented only by shearing stresses. These stresses produce bending and compression on the flange, (1905). Also, Timoshenko's and Goodier did research on elastic theory of a member subjected to torsion (1970).

2.4 Previous studies for open section beam under warping torsion

N S TRAHAIR (2011) studied on the torsion and buckling behaviour of beams which derive from a theory developed by Wagner, who extended Timoshenko's treatment of the elastic buckling of I section beams and columns to members of a general thin-walled open cross-section. The first-order Wagner effect leads to the torsional buckling

of cruciform columns, and modifies the flexural torsional buckling of monosymmetric beams, cantilevers, and arches. Theoretical predictions have been confirmed by test results. The second-order Wagner effect becomes important at large twist rotations. While large twist rotations do not occur in well-designed structures, the existence of the second-order Wagner effect shows that the post buckling of beams is imperfection insensitive, suggests that the design strengths of very slender beams are equal to their minor axis strengths, and provides assurance that approximate plastic collapse analyses of torsion will be conservative.

Argyris, J. H. and Dunne, P. C showed that the calculation of the shear stress distribution at a built-in end is a relatively simple problem in that the solution is obtained for arbitrary beam sections and loading condition by statics. The determination of stress distributions along the length of the beam is a more complex problem. This stress, for the section case are shown to be the sum of the generalized Bredt-Batho stresses plus stresses due to systems of self-equilibrating end loads. For a beam supporting shear loads the resulting complex stress system may be similarly expressed as the sum of the Engineer's theory stresses plus stresses caused by systems of self-equilibrating end loads. In both cases the basic systems of Bredt-Batho and Engineer's theory stresses are statically equivalent to applied loading (1949).

St. Venant development on a member subjected to torsion had been improved and extended by Seaburg & Heins (1963), Timoshenko & Goodier (1970), Bradford & Trahair (1991), and Johnson & Salmon (1996) investigated that total torsional resistance of thin-walled open section beam under restrained torsion is equal to the sum of uniform torsion due to St. Venant theory and nonuniform torsion due Wagner & Vlasov theories and assumptions.

Galambos did research on St. Venant classical approach development, that maximum shear stress occur at the surface of the wall cross section and its proportional to the maximum thickness of the cross section and first derivative of angle of twist (1968).

The effect of axial constraint on beams of an open section is similar to the constraint of closed section beams in that the free warping is restricted and self-equilibrating stress

systems are induced; the analysis is however, based on a different approach. In fact two methods are in use; the first and oldest is the torsion bending theory of Wagner (1929) and Kappus (1937), whilst a more modern treatment is due to Vlasov (1961), which is applicable to a variety of loading conditions. Vlasov's work has been conveniently summarized by Zbirohowski-Koscia (1967). Either method is capable of analysing beams of arbitrary section, although Vlasov's method has the added advantage of allowing applied loading systems other than pure torsion to be considered. The theory and results for open section beams presented in B.C.S.A publication No.31 relies on Vlasov's approach.

2.5 Vlasov's theory

Vlasov development and theory about stress distribution of thin walled open cross section beam, if a beam subjected to bending and twisting then a different type of stress will be induced as; (a) Shear stress occur around profile due to St. Venant theory. (b) Shear stress will induce due to restrained on end of the beam (warping restraint). (c) Axial stress around profile along the beam due to warping restraint. The major value will occur at different point of the cross section and depends on the shape of the cross section and thickness of the wall. The stress due to warping restraint can be neglected; this is only applied for closed section and solid section. This is because the torsion constant in closed section is of extremely large value due to massive value of enclosed area in closed section. Also, Vlasov developed stiffness matrix formula (see appendix E).

Vlasov's theory is based on the assumption that the outline of a section of a thin-walled beam remains unchanged under an action of external loading. It means that the dimension and angles between the flanges and the web remains unchanged, (1941).

According to Zbirohowski-Koscia, K. (1967), that "a shear stress in a fibre of a thin-walled beam caused by a flexural twist is equal to the product of this flexural twist multiplied by the sectorial statical moment of this point and divided by the wall thickness (at this point) and the principal sectorial moment of inertia".

2.6 Loughlan, J. and Ata, M. research

The analysis procedure was carried out for the restrained torsional response of an open section carbon fibre composite beam (1995). The method is used to modify torsion theory between isotropic and non isotropic material for the composite beam and to determine the behaviour stiffness of the beam under St. Venant and Warping torsion using the suitable comparable engineering elastic constants of the composite material. The theoretical results compared with finite element results for warping displacement and warping stress along the beam and around cross-section, and the rotation along the beam. The model built-up for Z-section beam which is restrained at one end and free in other end then applied torque at the free end of the beam. The warping shear flow results at mid-span have been drawn on the graph which is illustrated in Fig. (2.1)

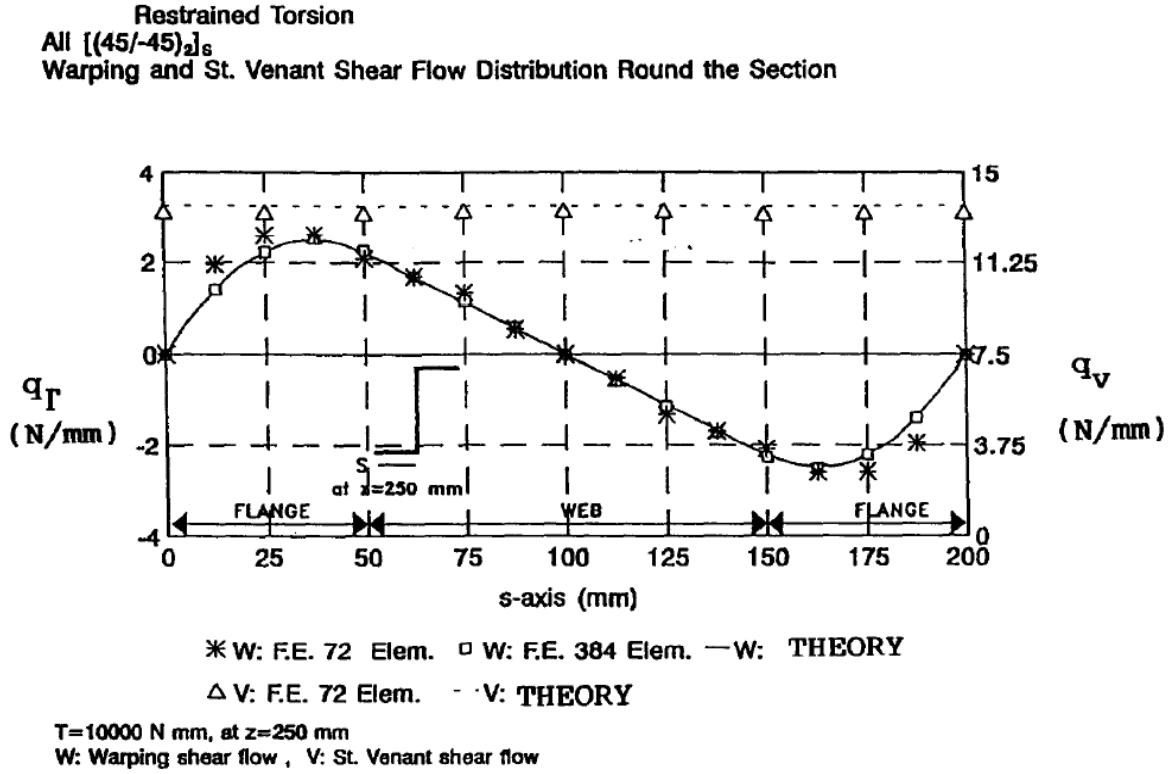

Figure 2.1 Warping and St. Venant shear flow distribution round the Z-section subjected to restrained torsion.

Source: From reference (36) by Loughlan, J. and Ata, M. (1995).

In Fig (2.1); it is clear that shear flow around web is varies linearly and zero at centre of the web but shear flow is parabolic at the flange and shows that the maximum value occurs at the middle of the flange section.

2.7 Gotluru, B. P., Schafer, B. W. and Pekoz, T. research

The analysis procedure was carried out for the behaviour of thin-walled cold-formed steel beams which has lipped channel sections where the centroid and shear center do not coincide, under torsion and bending (2000). Torque is induced due to transverse load, which is applied away from the shear centre. Hence, warping induce in the beam.

The studies of lateral torsional buckling and warping stress distributions have been analysed for a simply unbraced supported beam with two points loading applied at the flange-web junction.

LB denotes the local buckling and LTB for lateral torsional buckling. In Fig (2.2) it's clear when the rotation increases the local buckling load decreased and lateral torsional buckling increases. When the load increase the beam starts to rotate gradually and the horizontal displacement occurs so lateral torsional buckling start to develop and the failure is started by yielding of the material. The beam passes through huge rotation before failure.

.

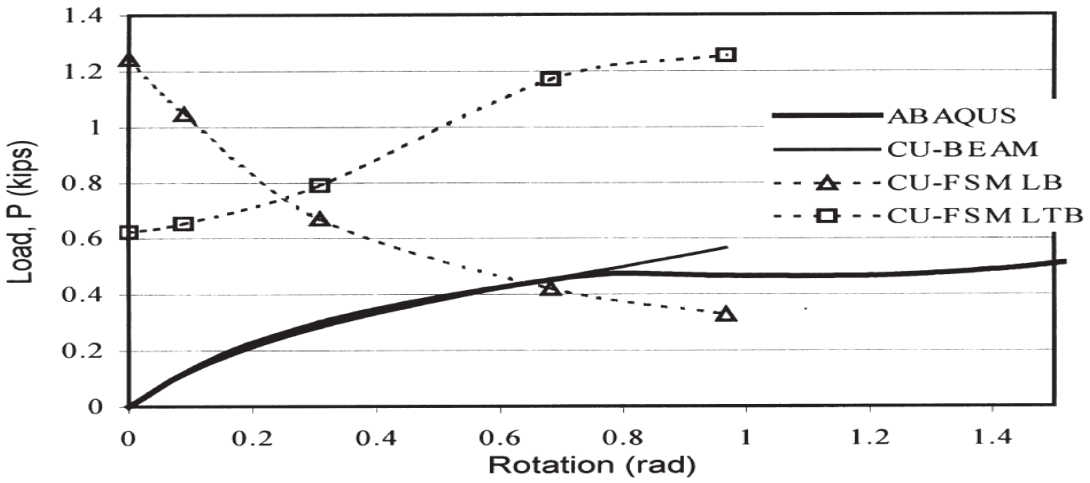

Fig. 10. C14U — local and lateral-torsional buckling analysis by finite strip method.

Figure 2.2 Local and lateral-torsional buckling analysis by finite strip method.

Source: From reference (8) by Gotluru, B. P., Schafer, B. W. and Pekoz, T. (2000).

CHAPTER (3)

FAMILIRISATION OF THE SOFTWARE

Finite element modelling (FEM) software, Strand7 has been used to model a 1.2m rectangular beam which is fixed at one end and free at the other end. The breadth of the beam is 50mm and depth is 150mm. There is a load of 1 KN acting downwards at the free end and the Young's Modulus, E is 200 $^{KN}/_{mm^2}$ and Poisson's ratio, v = 0.3.

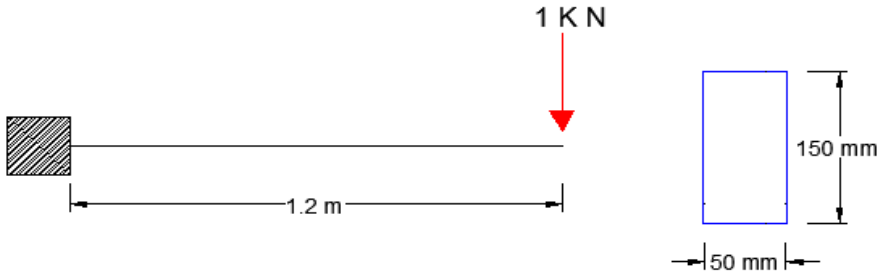

Figure 3.1 Cantilever beam with point load at the free end with its section.

3.1 Problem Formulation

The beam is modelled by apply five different mesh densities as shown in section (3.3) where mesh 1 and mesh 2 consist of one element, mesh 3 consists of four elements, mesh 4 consists of eight elements and mesh 5 consists of 16 elements. The five meshes are modelled in Strand7 software and are run in order to obtain the analysis results. When zero error is obtained from the solver, it means that the beam is successfully modelled.

The values of deflection, bending stress and shear stress along the beam surface and at mid-span are able to obtain from the listing menu for each mesh. The results are shown in chapter (6). In order to check that these results are good, theoretical calculations are done. Theoretical calculation for the deflection on the top surface of the beam is done using Macaulay's method, the bending stress is calculated using the bending stress formula and shear stress is calculated using shear stress formula. All the theoretical results are shown in the following section (3.2).

Further modelling has been performed to get more results for comparison. Mesh 5 consists of 16 elements. Therefore, for the new model, a mesh with 32 elements was

considered and the model was run and the results were compared to the results obtained for the previous meshes and with the theoretical results.

Tables and graphs in chapter (6) and summarize all the results obtained from the Strand7 modelling and from theoretical results are discussed in chapter (7).

3.2 Theoretical Results

In this section, hand calculations have been carried out to calculate the vertical deflection, the bending stress and the shear stress of a cantilever beam. These theoretical results will then be used to compare with the modelling results in chapter (7).

3.2.1 Vertical deflection on top surface of beam

The vertical deflection is going to be calculated using Macaulay's method.

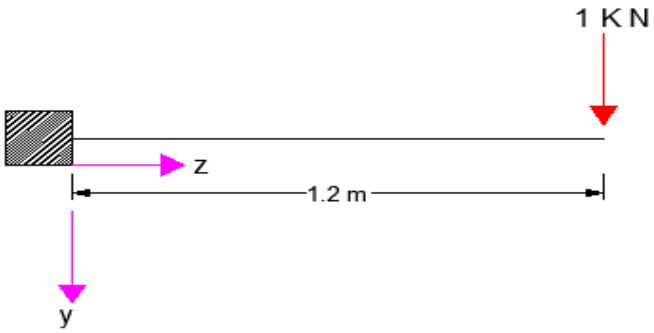

Bending moment is considered from the free end, as then the reactions at the fixed end need not to be determined.

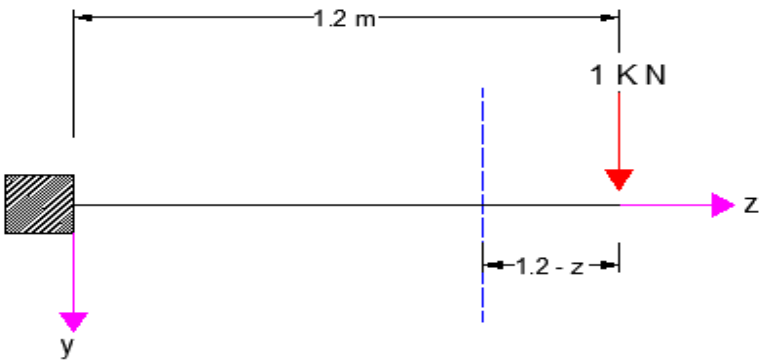

Moment, M = -1 (1.2 –z) valid throughout the beam span $0 \leq z \leq 1.2$

Moment curvature equation:

$$\frac{d^2y}{dz^2} = -\frac{M}{EI}$$

$$EI\frac{d^2y}{dz^2} = -M$$

Substituting the moment expression into the moment curvature equation:

$$EI\frac{d^2y}{dz^2} = -M = 1(1.2 - z)$$

Integrating with respect to$Z$, gives the slope equation:

$$EI\frac{dy}{dz} = -0.5(1.2 - z)^2 + A$$

Integrating with respect to$Z$, gives the deflection equation:

$$EIy = 0.167(1.2 - z)^3 + Az + B$$

When z = 0 (at the fixed end), the slope, $\frac{dy}{dz} = 0$. From the slope equation:

$$EI\frac{dy}{dz} = -0.5(1.2 - z)^2 + A$$

$$0 = -0.5(1.2 - 0)^2 + A$$

Therefore, A = 0.72

Substituting the constant A in the deflection equation, gives

$$EIy = 0.167(1.2 - z)^3 + 0.72z + B$$

When z = 0 (at the fixed end), the deflection, y = 0

$$0 = 0.167(1.2)^3 + 0.72(0) + B$$

B = -0.2886

Thus, the slope and deflection equations are given as:

$$EI\frac{dy}{dz} = -0.5(1.2 - z)^2 + 0.72$$

$$EIy = 0.167(1.2 - z)^3 + 0.72z - 0.2886$$

By inspection, the maximum deflection will occur at the free end, where z = 1.2m:

$$EIy_{1.2} = 0.167(1.2 - 1.2)^3 + 0.72(1.2) - 0.2886$$

$EIy_{1.2} = 0.5754$

Calculation of EI value, given E = 200$^{KN}/_{mm^2}$, b = 50 mm and d = 150mm

$$I = \frac{bd^3}{12} = \frac{50 \times 150^3}{12} = 14.1 \times 10^6 mm^4$$

$$EI = \frac{200 \times 14.1 \times 10^6}{10^6} = 2.82 \times 10^3 kNm^2$$

Therefore, $y_{1.2m} = \frac{0.5754}{EI} = \frac{0.5754}{2.82 \times 10^3} = 2.04 \times 10^{-4} m = 0.204mm$

$$EIy = 0.167(1.2 - z)^3 + 0.72z - 0.2886$$

Where z = 0m:

$$EIy = 0.167(1.2)^3 + 0 - 0.2886$$

Deflection, y = 0

Where z = 0.15m:

$$EIy = 0.167(1.2 - 0.15)^3 + (0.72 \times 0.15) - 0.2886$$

$$EIy = 0.0127$$

Deflection, y = 0.0045mm

Where z = 0.3m:

$$EIy = 0.167(1.2 - 0.3)^3 + (0.72 \times 0.3) - 0.2886$$

$$EIy = 0.0491$$

Deflection, y = 0.0174mm

Where z = 0.45m:

$$EIy = 0.167(1.2 - 0.45)^3 + (0.72 \times 0.45) - 0.2886$$

$$EIy = 0.1059$$

Deflection, y = 0.0376mm

Where z = 0.6m:

$$EIy = 0.167(1.2 - 0.6)^3 + (0.72 \times 0.6) - 0.2886$$

$$EIy = 0.179$$

Deflection, y = 0.0635mm

Where z = 0.75m:

$$EIy = 0.167(1.2 - 0.75)^3 + (0.72 \times 0.75) - 0.2886$$

$$EIy = 0.2666$$

Deflection, y = 0.0945mm

Where z = 0.9m:

$$EIy = 0.167(1.2 - 0.9)^3 + (0.72 \times 0.9) - 0.2886$$

$$EIy = 0.3665$$

Deflection, y = 0.13mm

Where z = 1.05m:

$$EIy = 0.167(1.2 - 1.05)^3 + (0.72 \times 1.05) - 0.2886$$

$$EIy = 0.4706$$

Deflection, y = 0.1668mm

Following the same procedure, the deflection at different distance along the top surface of the beam is calculated and shown in the Table (3.1).

Table 3.1 Theoretical deflections along the span of the cantilever beam.

Distance, Z (mm)	Deflection, y (mm)
0	0.0000
75	0.0010
150	0.0045
225	0.0100
300	0.0174
375	0.0270
450	0.0376
525	0.0500
600	0.0635
675	0.0790
750	0.0945
825	0.1120
900	0.1300
975	0.1480
1050	0.1668
1125	0.1850
1200	0.2040

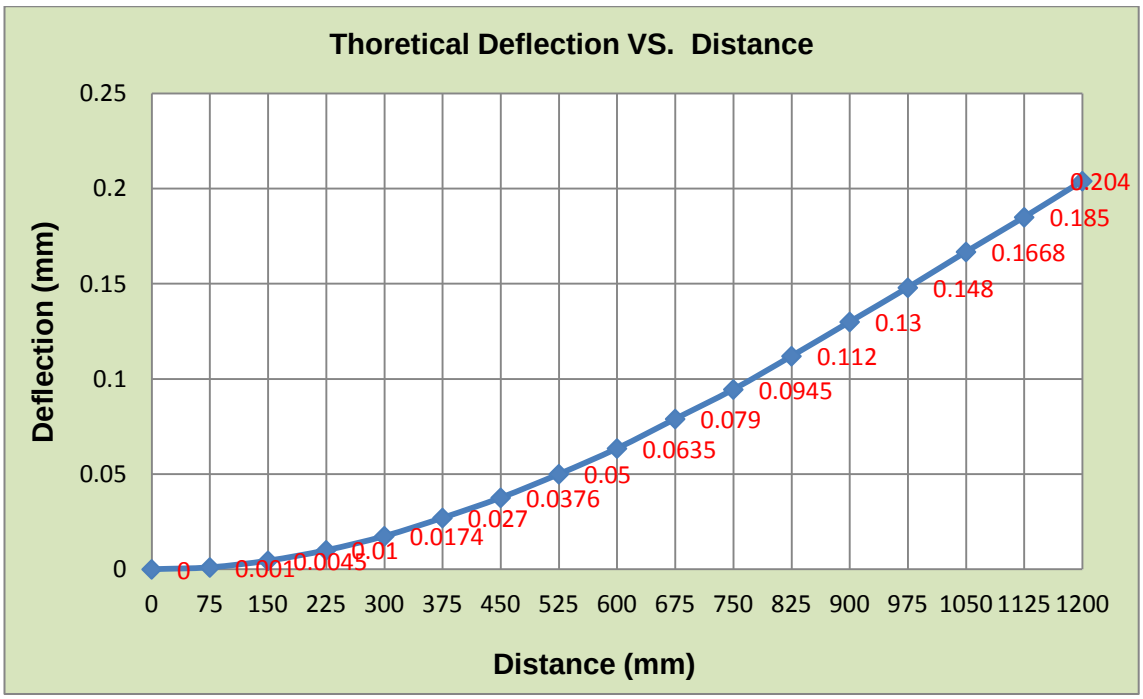

Figure 3.2 Deflection results along the span of the cantilever beam.

3.2.2 Bending Stress on top surface of the beam

The bending stress will occur along the centre of the beam i.e. at depth, y = 75mm. The bending stress, σ will be calculated for different distance, z starting from the free end where z = 0. The longitudinal stress σ_{zz} is zero at the end of the cantilever z = 0. The bending stress directly is proportional to the vertical distance from the neutral axis, and thus the stress will vary linearly from the top to the bottom surface, with a zero stress at the neutral axis.

Bending stress, $\sigma = \frac{My}{I} = \frac{Fzy}{I}$

Where z = 0 mm, $\sigma = \frac{1000 \times 0 \times 75}{14.1 \times 10^6}$ = 0 MPa

Where z = 150 mm, $\sigma = \frac{1000 \times 150 \times 75}{14.1 \times 10^6}$ = 0.8 MPa

Where z = 300 mm, $\sigma = \frac{1000 \times 300 \times 75}{14.1 \times 10^6}$ = 1.6 MPa

Where z = 450 mm, $\sigma = \frac{1000 \times 450 \times 75}{14.1 \times 10^6}$ = 2.4 MPa

Where z = 600 mm, $\sigma = \frac{1000 \times 600 \times 75}{14.1 \times 10^6}$ = 3.2 MPa

Where z = 750 mm, $\sigma = \frac{1000 \times 750 \times 75}{14.1 \times 10^6}$ = 4.0 MPa

Where z = 900 mm, $\sigma = \frac{1000 \times 900 \times 75}{14.1 \times 10^6}$ = 4.8 MPa

Where z = 1050 mm, $\sigma = \frac{1000 \times 1050 \times 75}{14.1 \times 10^6}$ = 5.6 MPa

Where z = 1200 mm, $\sigma = \frac{1000 \times 1200 \times 75}{14.1 \times 10^6}$ = 6.4 MPa

Following the same procedure, the bending stress at different distance along the top surface of the beam is calculated and shown in the Table (3.2).

Table 3.2 Theoretical bending stresses along the cantilever beam.

Distance, z (mm)	Bending stress, σ (MPa)
0	0.00
75	0.40
150	0.80
225	1.20
300	1.60
375	2.00
450	2.40
525	2.80
600	3.20
675	3.60
750	4.00
825	4.40
900	4.80
975	5.20
1050	5.60
1125	6.00
1200	6.40

3.2.3 Bending Stress of the cross-section area at mid-span of the beam

Using the same method for bending stress as section 3.2.2, the bending stress at mid-span is calculated. Here, value of distance, Z remains 600 mm (mid-span) and value of the beam depth, y changes. It will be seen that the top and bottom surfaces of the beam at $y = \pm \frac{1}{2} d$ are free both of normal stress ($\sigma_{yy=0}$) and of shear stress.

Bending stress, $\sigma = \frac{My}{I} = \frac{Fzy}{I}$

Where y = -75 mm, $\sigma = \frac{1000 \times 600 \times -75}{14.1 \times 10^6}$ = -3.2 MPa

Where y = -37.5 mm, $\sigma = \frac{1000 \times 600 \times -37.5}{14.1 \times 10^6}$ = -1.6 MPa

Where y = 0 mm, $\sigma = \frac{1000 \times 600 \times 0}{14.1 \times 10^6}$ = 0 MPa

Where y = 37.5 mm, $\sigma = \frac{1000 \times 600 \times 37.5}{14.1 \times 10^6}$ = 1.6 MPa

Where y = 75 mm, $\sigma = \frac{1000 \times 600 \times 75}{14.1 \times 10^6}$ = 3.2 MPa

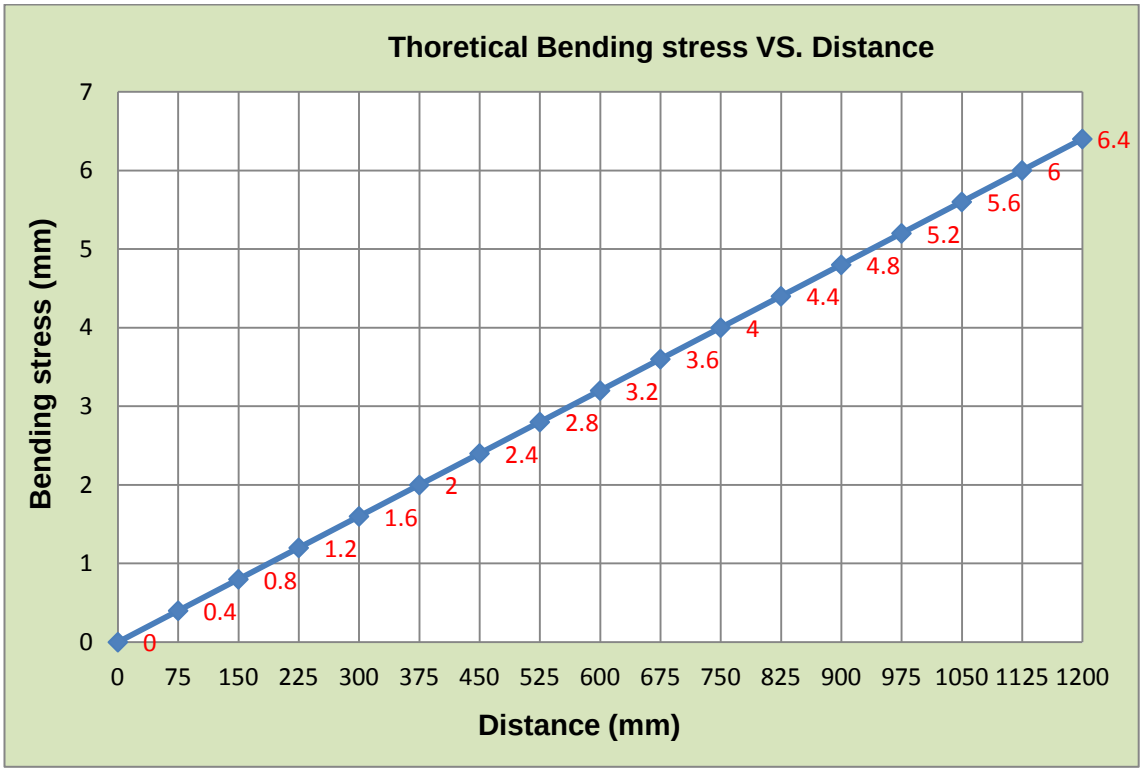

Figure 3.3 Bending stress results along the span of the cantilever beam.

Table 3.3 Theoretical bending stresses cross-section area at mid-span of the cantilever beam.

Depth, y (mm)	Bending stress, σ (MPa)
-75	-3.2
-37.5	-1.6
0	0
37.5	1.6
75	3.2

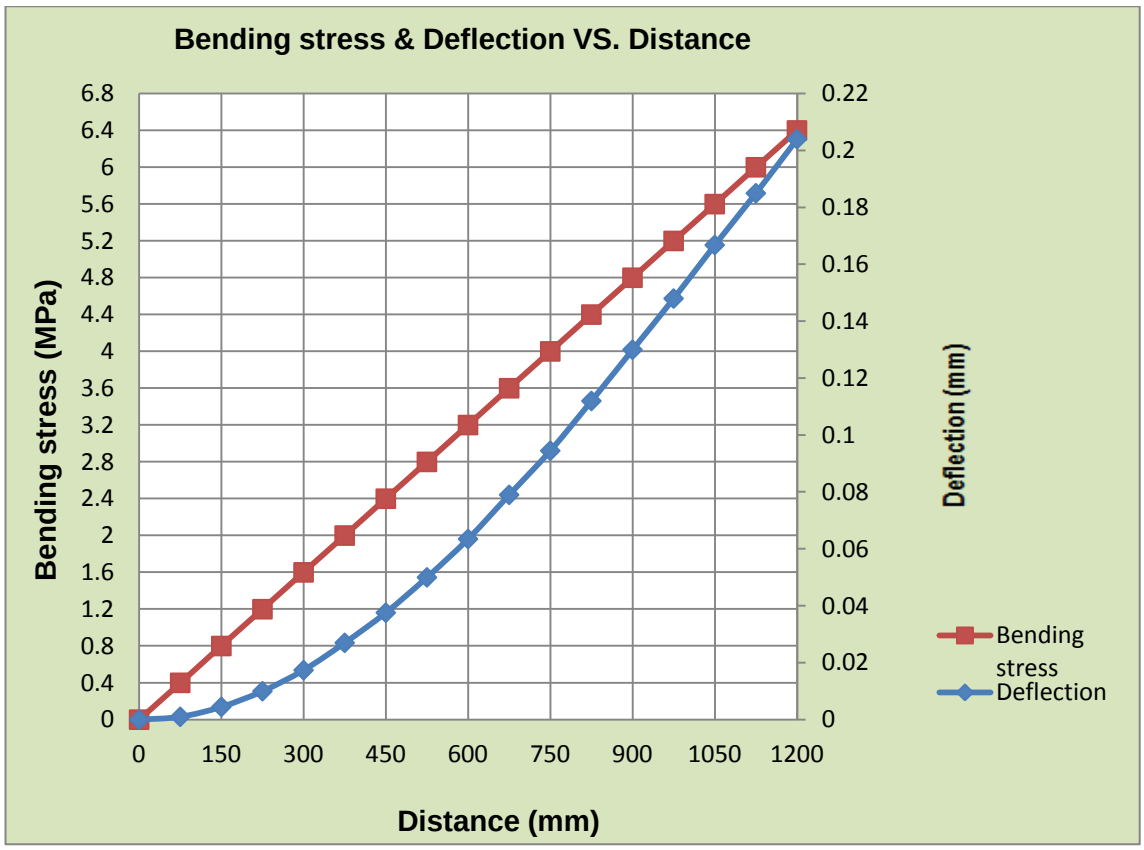

Figure 3.4 Bending stress and deflection along the span of the cantilever beam.

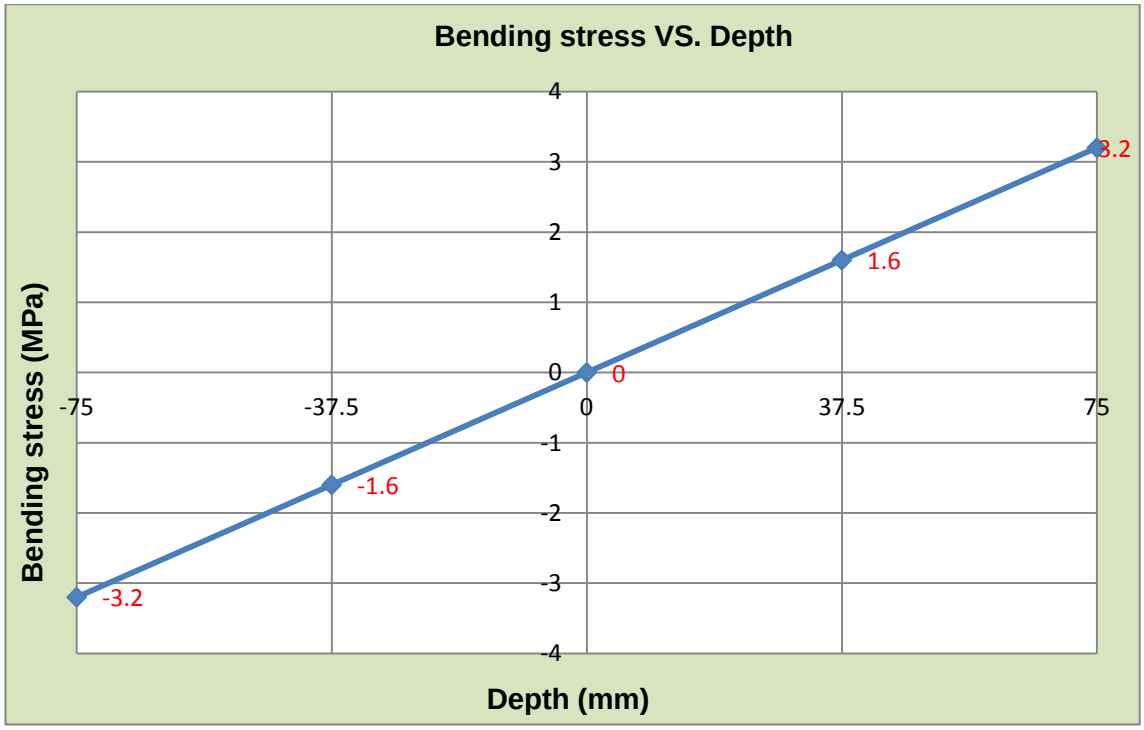

Figure 3.5 Bending stress of the cross-section area at mid-span of the cantilever beam.

3.2.4 Shear Stress of the cross-section area at mid-span of the beam

Shear stress, $\tau = \dfrac{FAy}{Ib}$

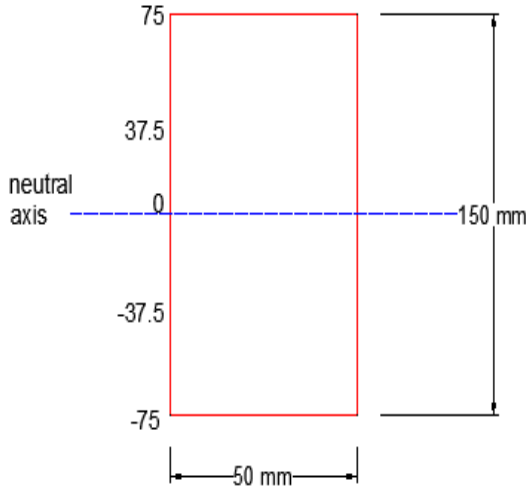

Where,

F : Shear force

A : Cross-sectional area

y : Distance of centroid from neutral axis

I : Second moment of area

b : Width of beam

Considering this first case:

Shear stress (τ);

$$\tau = \frac{1000 \times (50 \times 37.5) \times 56.25}{14.1 \times 10^6 \times 50} = 0.15\ MPa$$

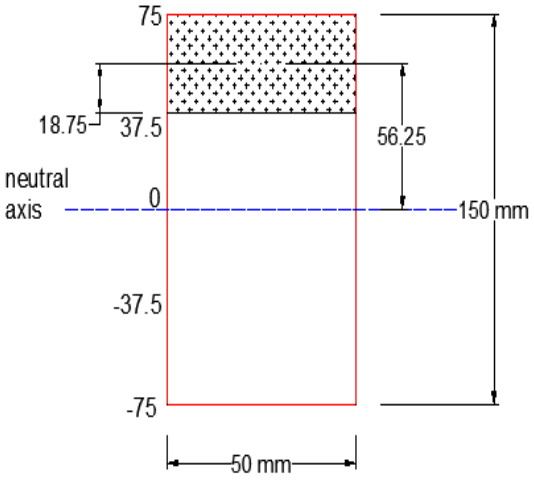

Second case:

Shear stress (τ);

$$\tau = \frac{1000 \times (50 \times 75) \times 37.5}{14.1 \times 10^6 \times 50} = 0.197\ MPa$$

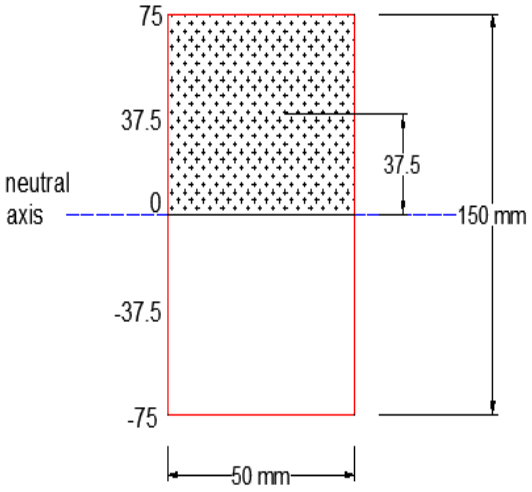

Third case:

Shear stress (τ);

$$\tau = \frac{1000 \times (50 \times 37.5) \times -56.25}{14.1 \times 10^6 \times 50} = -0.15$$

MPa

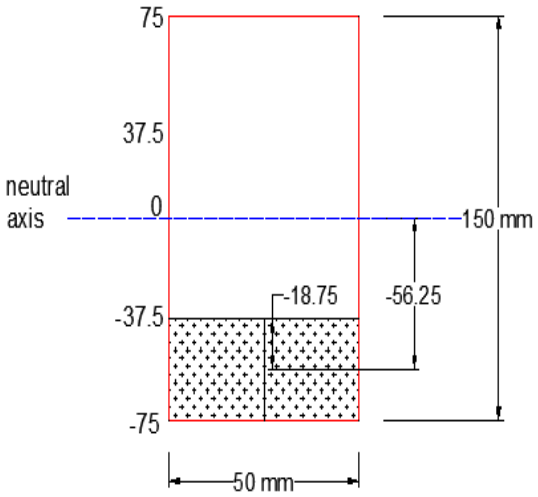

Fourth case:

Shear stress (τ);

$$\tau = \frac{1000 \times (50 \times 75) \times -37.5}{14.1 \times 10^6 \times 50} = -0.197 \ \ MPa$$

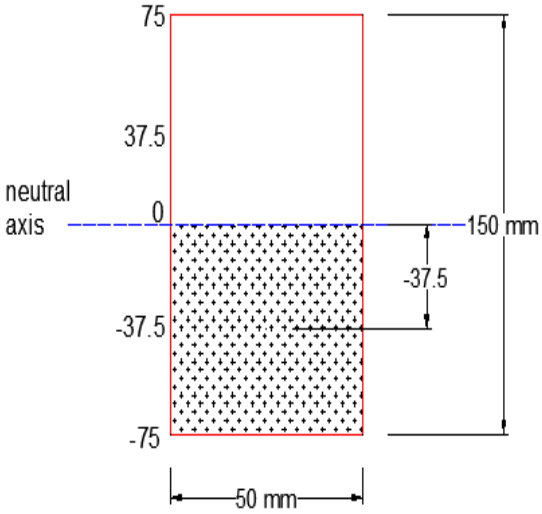

At depth = 0 mm, shear stress, τ = 0

Table 3.4 Theoretical shear stresses cross-section area at mid-span of the cantilever beam.

Depth, y (mm)	Shear stress, τ (MPa)
-75	0
-37.5	-0.150
0	-0.197
37.5	-0.150
75	0

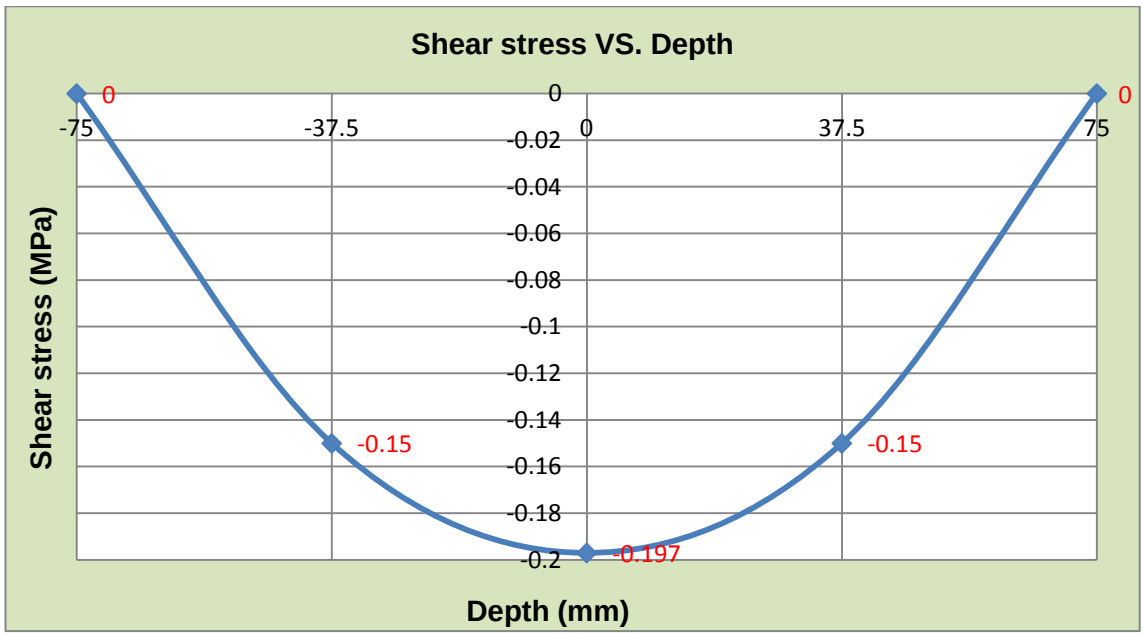

Figure 3.6 Shear stresses of the cross-section area at mid-span of the cantilever beam.

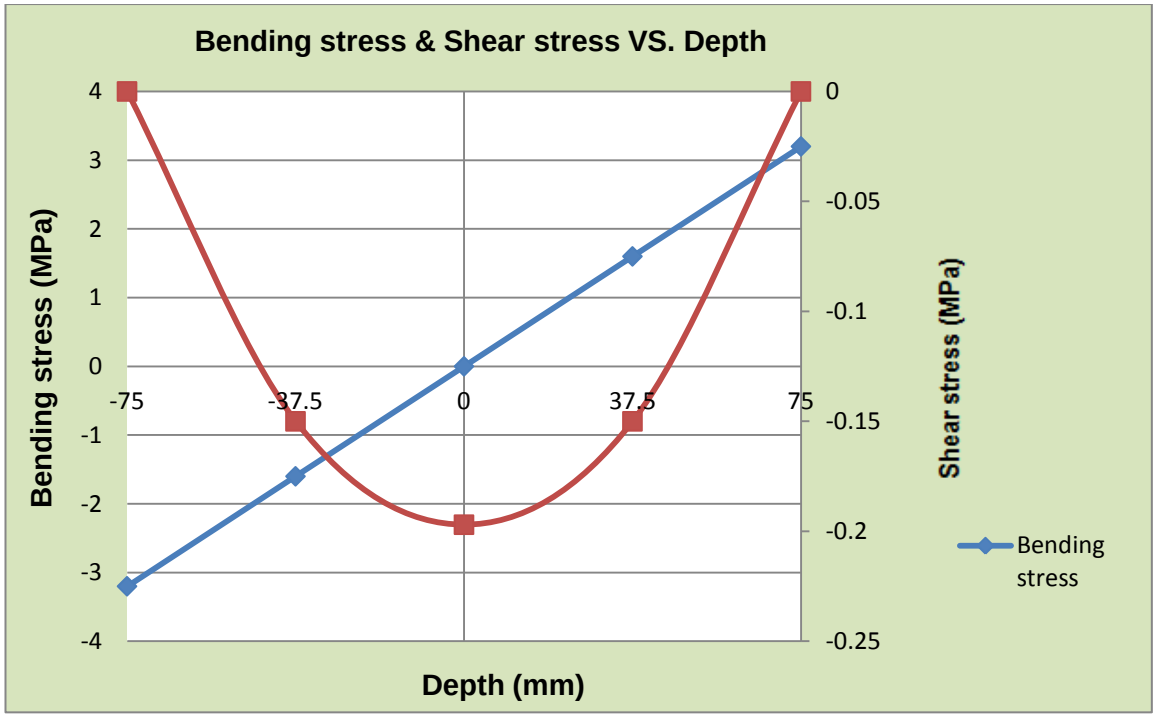

Figure 3.7 Bending stress and shear stress of the cross-section area at mid-span of the cantilever beam.

3.3 Scaled diagrams of the mesh densities

Mesh 1: One 4-node element

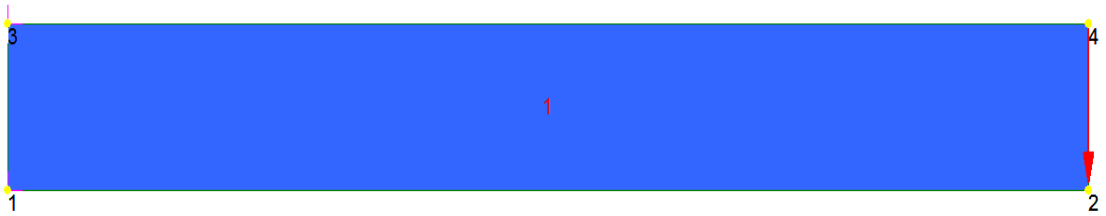

Figure 3.8 Model (1) one 4-node element (2D).

Mesh 2: One 8-node element

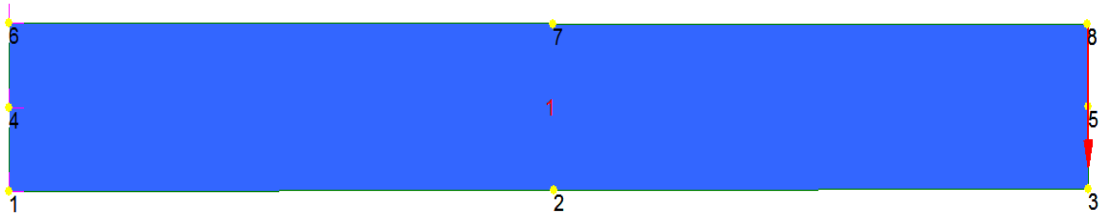

Figure 3.9 Model (2) one 8-node element (2D).

Mesh 3: Four 8-node element

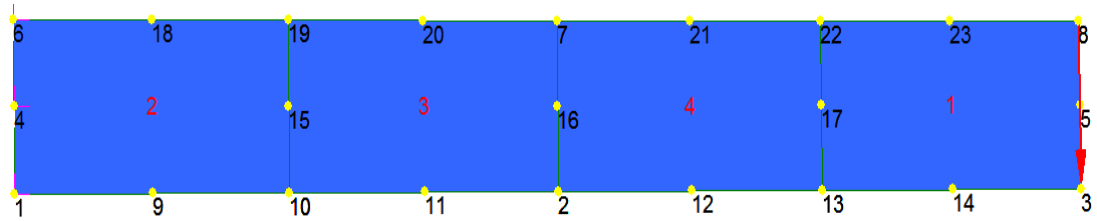

Figure 3.10 Model (3) four 8-node element (2D).

Mesh 4: Eight 8-node element

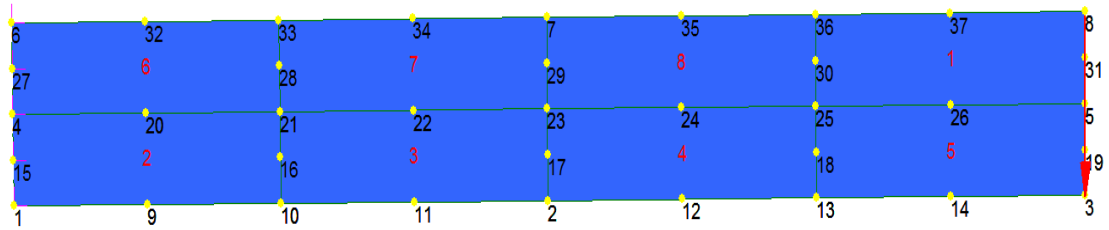

Figure 3.11 Model (4) eight 8-node element (2D).

Mesh 5: Sixteen 8-node element

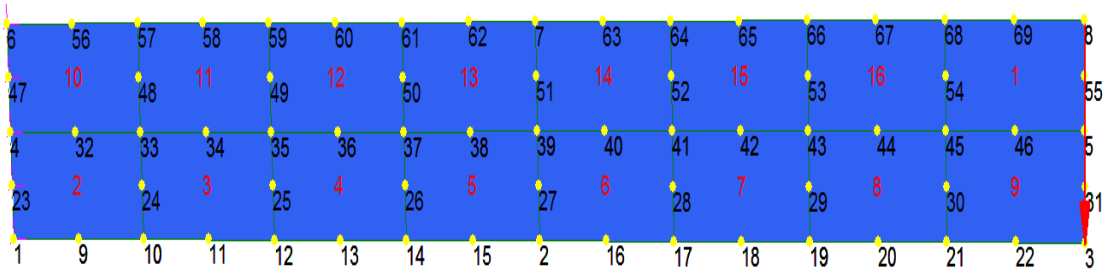

Figure 3.12 Model (5) sixteen 8-node element (2D).

Mesh own: Thirty-two 8-node element

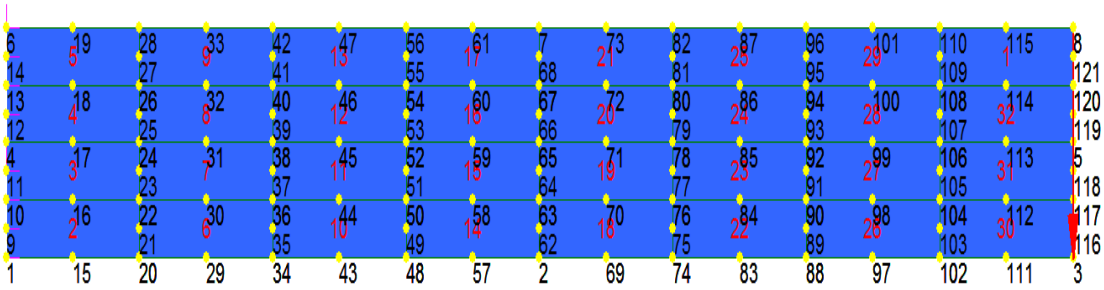

Figure 3.13 (Own model) thirty-two 8-node element (2D).

CHAPTER (4)

THIN-WALLED AN OPEN SECTION BEAM

UNDER RESTRAINED TORSION

Chapter 4: Thin-walled an open section beam under restrained torsion

4.1 Thin-walled open section beam properties and behaviour under restrained torsion

Thin-walled sections are such that the structural thickness is everywhere small as compared with the overall dimensions of the section. There is no clearly defined kind of demarcation between thin-walled and thick-walled sections, it is suggested that thin-walled theory may be applied with reasonable accuracy to sections if:

$$t_{max}/_{b} \leq 0.1 \text{ ---------- (4.1)}$$

Where t_{max} is the maximum thickness of the section and b is a typical cross-sectional dimension.

Most structures in civil engineering may be regarded as having either a thick-walled or thin-walled section as shown in Fig (4.1), for an I-section and Channel section beam.

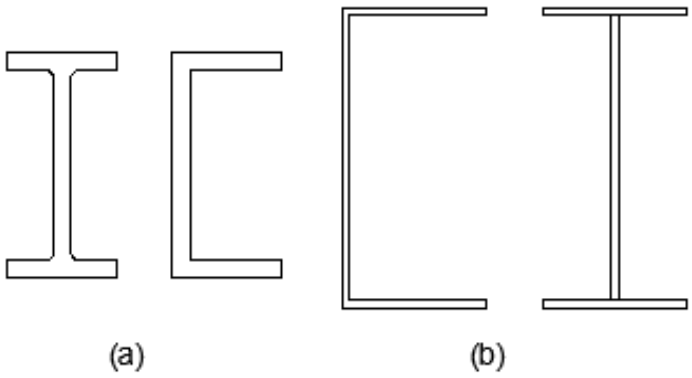

Figure 4.1 (a) Thick beam section, (b) Thin-walled beam section.

The analysis of the thin-walled open cross section depends on the boundary condition of the member and it is obtained by determining primary warping, warping stress, shear flow and angle of rotation. There are two types of torsion; (a) unrestrained torsion or free torsion due to St. Venant & Bredt-Batho theories, (b) restrained torsion or warping torsion due to Wagner & Vlasov theories.

In the unrestrained torsion, there is no axial constraint in longitudinal axis. The cross section is free to warp completely and longitudinal warping stress is not induced around profile along the member. Also, the angle of twist remains constant along the member.

In the restrained torsion, if the end of a torsion member is restrained then the cross section is prevented from warping, and warping stress is induced around profile along the member. Also, the angle of twist is not longer constant along the member.

The percentage of the torque carried in each way depends on the dimensions of the cross section and the length of the member.

Restrained warping will be significant during the twisting of a thin-walled beam when the applied twisting moment or the boundary conditions create an internal twisting moment that varies along the beam axis.

4.2 Shear center of thin-walled an open section beam

Loading on a beam will usually produce combined bending and twisting. It is possible to locate a point in the cross-sectional plane through which the resultant forces must pass if there is to be no twisting. This point is called shear center.

When a beam bends without twisting, due to some external load system, shearing stresses are set up on the cross sections of the beam. The centroid of this external shear force system is often referred to as the shear center for the particular section. The resultant external shear load at this section must pass through the shear centre of the section if twist of the section is to be prevented. Thus, if the shear centre is known, it is possible to represent the external load influences by two systems, one that causes flexure and other which causes only twist. It is necessary to know or to be able to determine the position of the shear centre of all types of section. For some cross section which is illustrated in Fig (4.2) the position of the shear centre is at the intersection of the walls. Also, where a section has axis of symmetry, then the shear centre must lie on this axis shown in Fig (4.3). The position of the shear centre of channel cross section is determined by calculating e value, as illustrated in Fig (4.4).

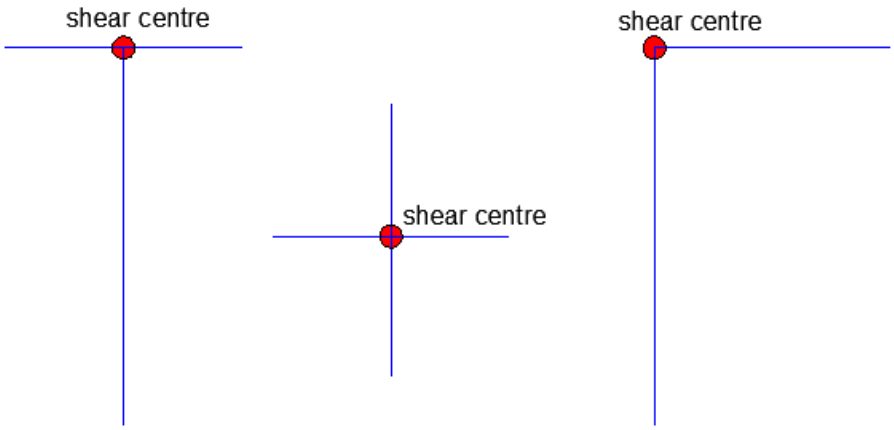

Figure 4.2 Shear centre position for angle, cruciform, and T- sections.

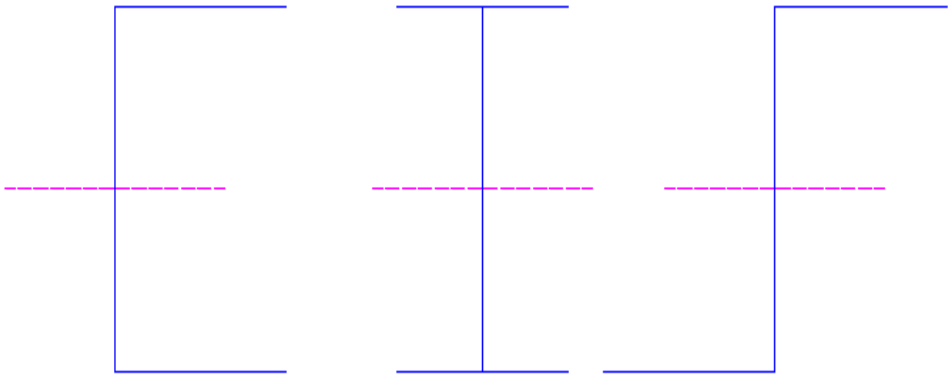

Figure 4.3 Shear centre will lie on the axis symmetry for channel, T- and Z- sections.

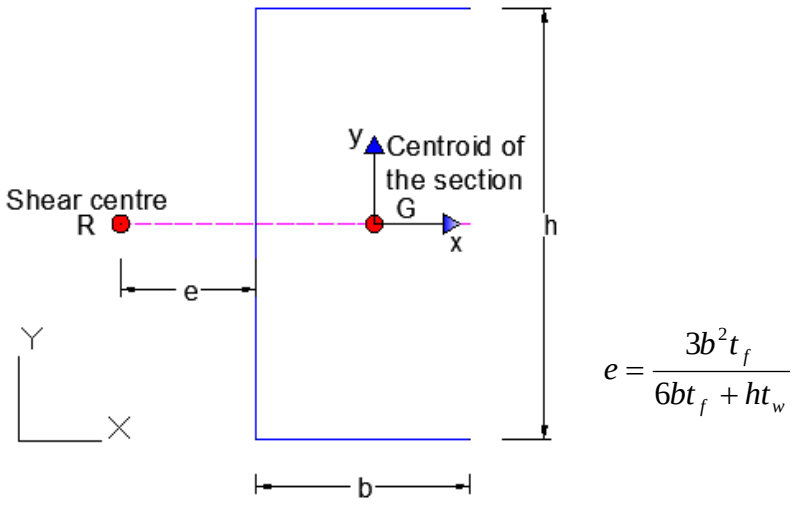

Figure 4.4 Location of channel shear centre.

4.3 Torsion of thin-walled an open section beam

Approximate expressions for the shear distribution and rate of twist in a thin-walled open section beam are based on the derivation of a thin rectangular strip, the membrane analogy and St. Venant warping functions.

The assumptions on which the theory is based are similar to those for the torsion of a closed section in that the cross section is assumed not to distort in its own plane and that stresses, other than St. Venant shear stresses, are assumed constant across the wall thickness. Theses stresses would in fact be axial constraint stresses which are explained in section (4.4 & 4.6).

The shear stress distribution in a thin-walled open section beam subjected to a torque as shown in Fig (4.5) has two possible components, f_{zs} in the direction of the tangent to the section wall and f_{zn} normal to the tangent. It may be shown that

$$f_{zs} = 2Gn\frac{d\theta}{dz}, \qquad f_{zn} = 0 \quad \text{---------- (4.2)}$$

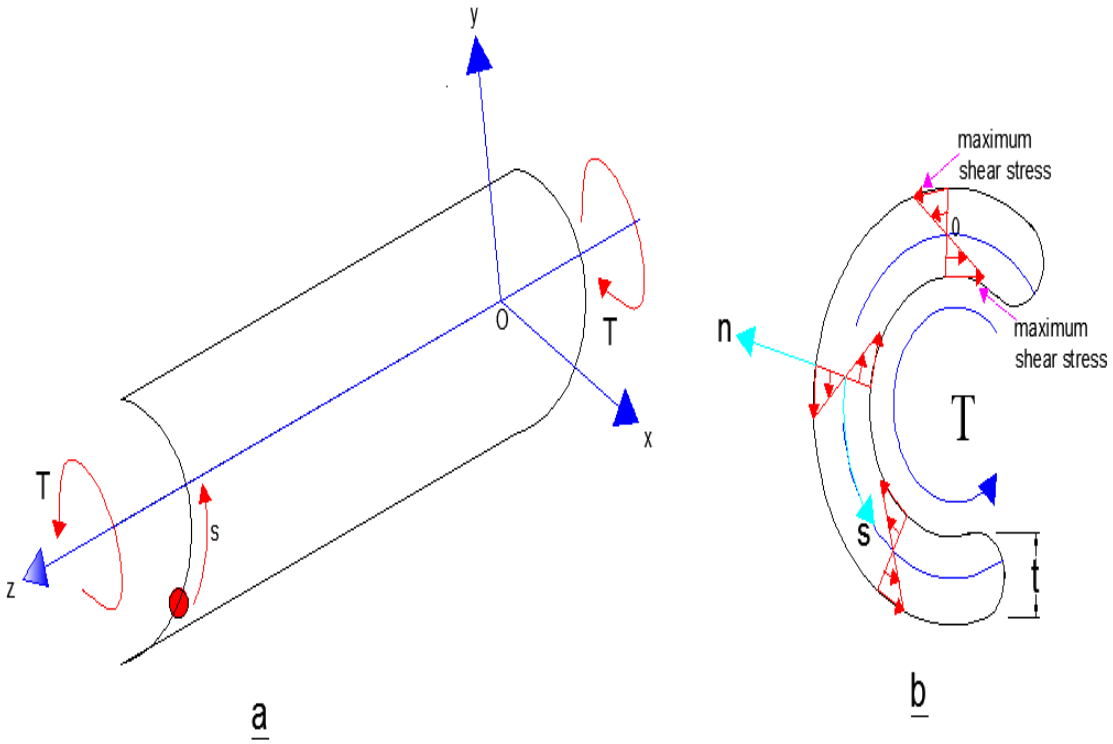

Figure 4.5 (a) Torsion of an open section beam, (b) Shear stress distribution across the wall of an open section beam subjected to torsion.

Giving the linear distribution of f_{zs} across the thickness of the section wall shown in Fig 4.5(b). The maximum value of f_{zs} occurs at the inner and outer surfaces of the wall where $n = \pm {}^{t}/_{2}$ and is

$$f_{zs} = \pm Gt\frac{d\theta}{dz} \text{ ---------- (4.3)}$$

The shear stress varies linearly across the wall thickness, and zero at mid-plane.

The rate of twist ${}^{d\theta}/_{dz}$ is expressed in terms of the applied torque, the shear modulus G and the torsion constant J by the relationship;

$$T = GJ\frac{d\theta}{dz} \text{ ---------- (4.4)}$$

$$J = \sum \frac{st^3}{3} \text{ ---------- (4.5)}$$

The shear modulus (G) depends on Poisson's ration, Young's modulus and Section properties, which expressed in Eq. (4.6)

$$G = \frac{E}{2(1+v)} \text{ ---------- (4.6)}$$

4.4 Warping of thin-walled an open section beam under restrained torsion

Warping is the displacement along the beam longitudinal axis and it is a difficult phenomenon to visualize. In the general case of open cross-section warping takes place, i.e., the cross-section does not remain plane. There are two types of warping associated with open sections; primary warping, in which the complete cross-section suffers displacements normal to its plane, and secondary warping, which involves longitudinal displacements across the thickness of the walls of the section. For thin-walled sections secondary warping is negligibly small. However primary warping displacements are relatively large and any form of axial constraint in which this primary warping is restrained produces significant values of direct stress and changes in shear stress.

It has been showed in Section (4.3) that the torsion of a thin-walled, open section axially unrestrained beam induces a constant rate of twist along the length of the beam and a shear stress distribution which varies linearly across the thickness of the walls of the beam and is zero at the middle plane see Fig 4.5(b).

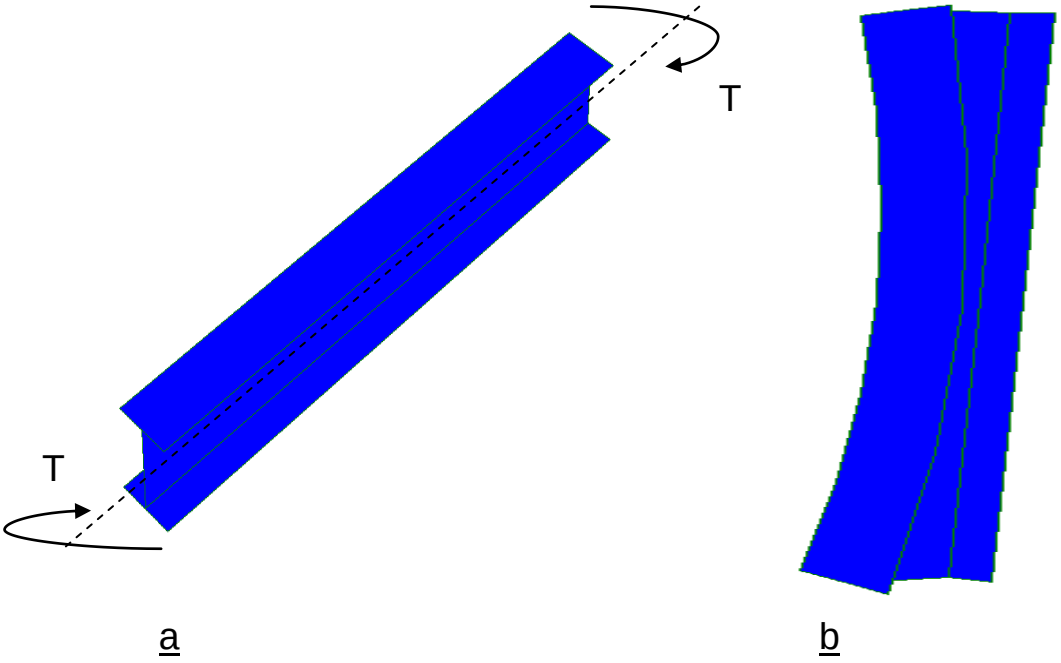

Figure 4.6 (a) Torsion of a thin-walled I-section beam, (b) Warping of I-section under uniform twisting moment showing undistorted shape of flanges.

It follows that, although the beam cross-section and middle plane warp, there is no shear distortion of the middle plane. This is clearly demonstrated in Fig 4.6(b), where the middle plane of each flange of the I-section remains rectangular, although twisted, after torsion. In Fig 4.7(a) it has been shown that the warping of the one end of the beam is restrained. This restraint causes some longitudinal strains and stresses. The warping is not induced at the fix end of the beam due to the effect of applying restraint to one end of the beam. Also, the flange will move from its plane and will bend into the shape shown in Fig 4.7(b). In addition, the angle of rotation will vary and is zero at fix end. A total twisting moment is a sum of a pure St. Venant twist and restrained warping torsion, which is expressed below;

$$T_{Total} = T_J + T_w$$

Where $T_J = GJ\frac{d_\theta}{d_z}$ from the unrestrained torsion of open section beams, but in which $\frac{d_\theta}{d_z}$ is not constant and T_w is obtained from a consideration of the bending of the flanges. In both the Wagner and Vlasov methods Eq. (4.7) is expressed as a second order differential equation in $\frac{d_\theta}{d_z}$ from which $\frac{d_\theta}{d_z}$ is obtained for a particular beam having given loading and support conditions.

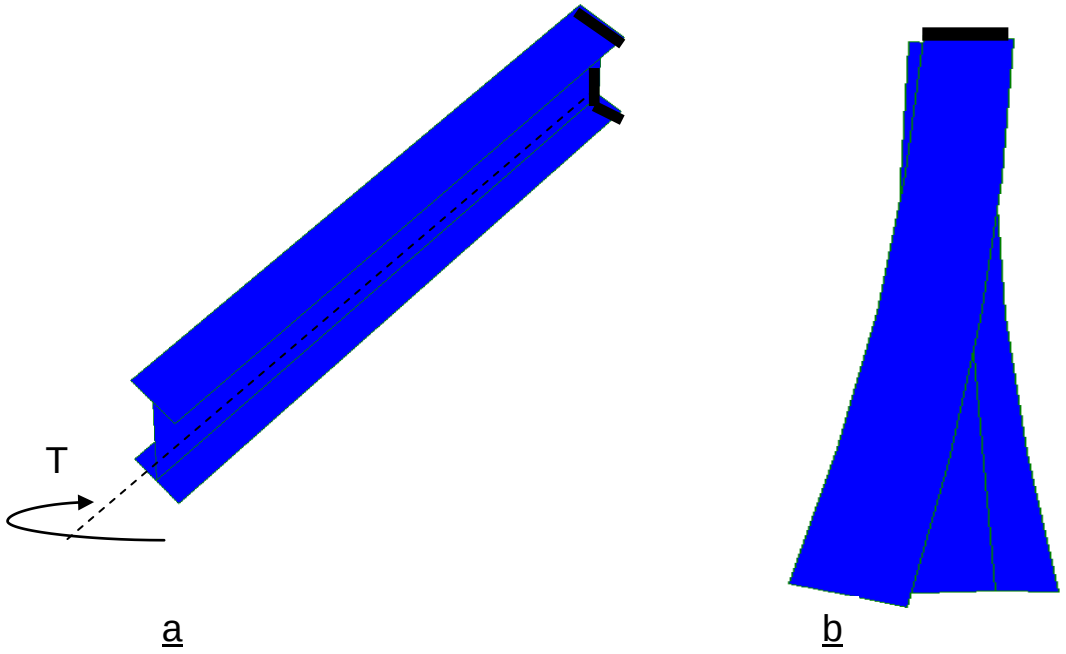

Figure 4.7 (a) Thin-walled I-section cantilever beam subjected to a torque, (b) Bending effect of axial constraint on flanges of I-section beam subjected to restrained torsion.

If the warping is restrained, warping normal stresses will be induced. These warping normal stresses will induce warping shears, which will provide a tensional restraining moment. This moment, defined as a warping tensional moment, in addition to the pure tensional moment provide equilibrium in the system.

The combination of St. Vanent and warping torsion gives a model for torsion which can give reasonable predictions of behaviour.

The primary warping (W) round a section profile is determined by Eq. (4.7);

$$W = w(s)\frac{d\theta}{dz} \text{ ---------- (4.7)}$$

The primary warping in opens sections depends on the rate of twist of the section and the section property known as the sectorial coordinate, $w(s)$.

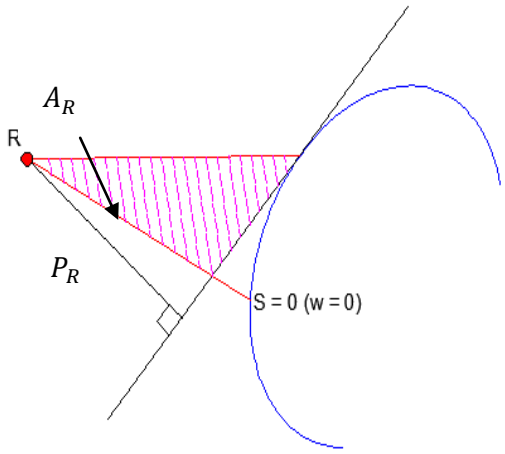

Figure 4.8 Warping of an open section beam.

The sectorial coordinate $w(s)$ round section beam is determined by Eq. (4.8)

$$w(s) = \int_0^s P_R ds \text{ ---------- (4.8)}$$

Megson, T. H. G, (1974) explained that "The integral in the expression for primary warping represents twice the area A_R swept out by a generator rotating about the centre of twist (R) from the point of zero warping" as shown in Fig (4.8). Thus the primary warping may be written as

$$W = -2A_R\frac{d\theta}{dz} \text{ ---------- (4.9)}$$

Or in term of the applied torque

$$W = -2A_R\frac{T}{GJ} \text{ ---------- (4.10)}$$

The sign convention adopted for A_R is that perpendicular P_R from the centre of twist R to the tangent at any point is positive in sign if movement in the positive direction of s of the foot of P_R along the tangent causes anti-clockwise rotation about (R).

Secondary warping becomes significant in sections (e.g. T-section & angle section) where their primary warping is zero.

The secondary displacement warping (W^*) longitudinal across the thickness of the walls of the section is determined by Eq. (4.11) and the sectorial computed by Eq. (4.12)

$$W^* = w^*(s)\frac{d\theta}{dz} \text{ ---------- (4.11)}$$

$$w^*(s) = \int_0^n n_R dn \text{ ---------- (4.12)}$$

The shear centre location for channel section is determined by Eq. (4.13)

$$e = \frac{3b^2 t_f}{6bt_f + ht_w} \text{ ---------- (4.13)}$$

Torsion bending constant is determined by Eq. (4.14) or (4.15)

$$I_w = \int_s [w(s)]^2 dA \text{ ---------- (4.14)}$$

$$I_w = \int_s [w(s)]^2 t\, ds \text{ ---------- (4.15)}$$

4.5 Rate of twist in thin-walled open section beam under torsion

The rate of twist in open section is determined by Eq. (4.16)

$$\frac{d\theta}{dz} = \frac{T}{GJ}\left[1 - \frac{\cosh \mu(L-z)}{\cosh \mu L}\right] \text{ ---------- (4.16)}$$

The first term in Eq. (4.16) is seen to be the rate of twist derived from the St. Venant torsion theory. The hyperbolic second term is therefore modification introduced by the axial constraint.

According to the Vlasov torsion-bending theory, (μ) value is determined from stiffness matrix equations as follow;

$$\mu = \sqrt{\frac{GJ}{EI_w}} \text{ ---------- (4.17)}$$

Integrating Equation (4.16) with respect to z, gives:

$$\theta = \frac{T}{GJ}\left[z + \frac{\sinh \mu(L-z)}{\mu \cosh \mu L} \right] + K$$

At the built-in end, where $z = 0,\ \theta = 0$:

$$\theta = \frac{T}{GJ}\left[0 + \frac{\sinh \mu L}{\mu \cosh \mu L} \right] + K$$

$$\therefore K = -\left[\frac{\sinh \mu L}{\mu \cosh \mu L} \right]$$

And so

$$\theta = \frac{T}{GJ}\left[Z + \frac{\sinh \mu(L-z)}{\mu \cosh \mu L} - \frac{\sinh \mu L}{\mu \cosh \mu L} \right] \text{---------- (4.18)}$$

The maximum twist occurs at the free end where, $z = L$. So from equation (4.19)

$$\theta_{\max} = \frac{TL}{GJ}\left[1 - \frac{\tanh \mu L}{\mu L} \right] \text{---------- (4.19)}$$

4.6 Warping stress; calculations

According to Wagner torsion-bending theory, when axial constraints are present $\frac{d_\theta}{d_z}$ is no longer constant so that the longitudinal strain $\frac{\mathrm{dw}}{\mathrm{dz}}$ is not zero and direct stresses are induced, given by Eq. (4.20)

$$\frac{dW}{dz} = w(s)\frac{d^2\theta}{dz^2} \text{---------- (4.20)}$$

The rate of twist is no longer constant along the beam due to induced warping strain. From Hook's law, the warping stress is defined as:

$$f_w = E\frac{dW}{dz} \text{---------- (4.21)}$$

And substituting for the strain

$$f_w = Ew(s)\frac{d^2\theta}{dz^2} \text{---------- (4.22)}$$

The rate of twist is given by Eq. (4.16)

$$\frac{d\theta}{dz} = \frac{T}{GJ}\left[1 - \frac{\cosh \mu(L-z)}{\cosh \mu L}\right]$$

And the second order of $\frac{d_\theta}{d_z}$

$$\frac{d^2\theta}{dz^2} = \frac{T}{GJ}\mu\frac{\sinh(L-z)}{\cosh \mu L}$$

So

$$f_w = Ew(s)\frac{T}{GJ}\mu\frac{\sinh \mu(L-z)}{\cosh \mu L}$$

The warping stress round the profile at any section, gives by Eq. (4.23)

$$f_w = \frac{E}{G}x\frac{T\mu}{J}x\frac{\sinh \mu(L-z)}{\cosh \mu L}x\,w(s) \text{ ---------- (4.23)}$$

4.7 Axial constraint; calculations

When a restriction is happened in any thin walled cross section of the beam due to discontinuities of the loads then, an axial constraint effect occurs in that section. Thus axial direct stress arises in longitudinal direction. This direct stresses is proportional to the longitudinal strain and to the second derivative of angle of twist.

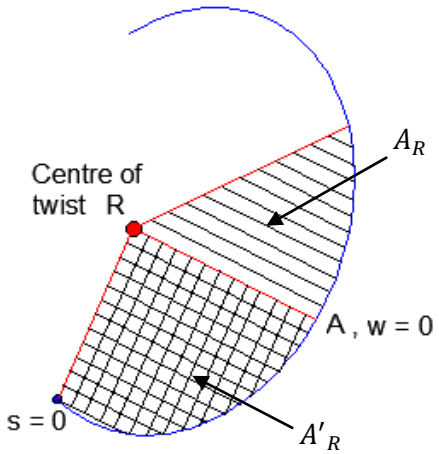

Figure 4.9 Determination of swept area A_R.

In Fig (4.9); a positive sectorial coordinate starts from the reference line (RA), in clockwise direction and negative starts from the reference line (RA), in anti-clockwise direction.

The sectorial coordinate is always from the reference line from zero warping point in section to shear centre and it depends on the section shape (section properties) and the location of the shear centre.

It is necessary to have a reference line in order to sweep the sectorial coordinate.

In section 4.4 it has been showed that the primary warping w of a thin-walled beam of open section was given by Eq. (4.9)

$$W = -2A_R \frac{d\theta}{dz}$$

When axial constraints are present $\frac{d_\theta}{d_z}$ is no longer constant so that the longitudinal strain $\frac{\mathrm{dw}}{\mathrm{dz}}$ is not zero and direct stresses are induced, so

$$f_w = E\frac{dw}{dz} = -2A_R \frac{d^2\theta}{dz^2} \text{ ---------- (4.24)}$$

The warping stress system must be self-equilibrating since the applied load is a pure torque. Therefore at any section the resultant end load is zero and

$$\int_{section} f_w t ds = 0 \text{ ---------- (4.25)}$$

From Eq. (4.24) and observing that $\frac{d^2\theta}{dz^2}$ is a function of z only,

$$\int_{section} 2A_R t ds = 0 \text{ ---------- (4.26)}$$

The limits of integration of Eq. (4.26) are as yet unknown since A_R is zero when w is zero at an unknown value of s. Let

$$2A_R = 2A_{R_0} - 2A'_R$$

Where A_{R_0} is the area swept out from $(s = 0)$ and A'_R is the value of A_{R_0} at $(w = 0)$, as shown in Fig (4.9). Then in Eq. (4.26)

$$\int_{section} 2A_{R_0} tds - 2A'_R \qquad \int_{section} tds = 0$$

And

$$2A'_R = \frac{\int_{section} 2A_{R_0} tds}{\int_{section} tds}$$

Given

$$2A_R = 2A_{R_0} - \frac{\int_{section} 2A_{R_0} tds}{\int_{section} tds} \text{ ---------- (4.27)}$$

For equilibrium of the element in the z-direction and neglecting body forces, it is obtained Eq. (4.28)

$$\frac{\partial q}{\partial s} + t\frac{\partial f_Z}{\partial z} = 0 \text{ ---------- (4.28)}$$

The axial constraint shear flow system q_Γ is in equilibrium with the self-equilibrating direct stress system. Thus from Eq. (4.28)

$$\frac{\partial q_\Gamma}{\partial s} + t\frac{\partial f_w}{\partial z} = 0$$

Hence

$$\frac{\partial q_\Gamma}{\partial s} = -t\frac{\partial f_w}{\partial z}$$

Substituting for f_w from Eq. (4.24) and noting that $q_\Gamma = 0$ when $s = 0$, then

$$q_\Gamma = E\frac{d^3\theta}{dz^3}\int_0^s 2A_E t\, ds$$

Now

$$T_w = \int_{section} p_R q_\Gamma ds$$

Through the integrations by part

$$T_w = -EI_w\frac{d^3\theta}{dz^3} \text{ ---------- (4.29)}$$

T_w is termed the torsion bending constant and purely a function of the geometry of the cross-section.

The total torque, T which is the sum of the St. Venant and the Wagner torsion bending torque, is then written

$$T = GJ\frac{d\theta}{dz} - EI_w\frac{d^3\theta}{dz^3} \text{ ---------- (4.30)}$$

Or

$$\frac{d^3\theta}{dz^3} - \frac{GJ}{EI_w}\frac{d\theta}{dz} + \frac{T}{EI_w} = 0 \text{ ---------- (4.31)}$$

So

$$\frac{d^3\theta}{dz^3} = -\frac{T}{EI_w}\left[\frac{\cosh(L-z)}{\cosh(\mu L)}\right] \text{ ---------- (4.32)}$$

T_J, St. Venant torsion is given by

$$T_J = GJ\frac{d\theta}{dz} = T\left[1 - \frac{\cosh\mu(L-z)}{\cosh\mu L}\right] \text{ ---------- (4.33)}$$

T_w, Wagner torsion-bending (warping torque) is given by

$$T_w = -EI_w\frac{d^3\theta}{dz^3} = T\ \frac{\cosh\mu(L-z)}{\cosh\mu L} \text{ ---------- (4.34)}$$

CHAPTER (5)

THEORETICAL ANALYSIS FOR

THIN-WALLED CHANNEL SECTION

CANTILEVER BEAM

SUBJECTED TO RESTRAINED TORSION

Chapter 5: Theoretical analysis for thin-walled channel Section cantilever beam subjected to torsion

A thin walled singly symmetric channel section cantilevered beam is subjected to restrained torsional loads as shown in the Fig (5.1). The section has a uniform thickness of 2 mm.

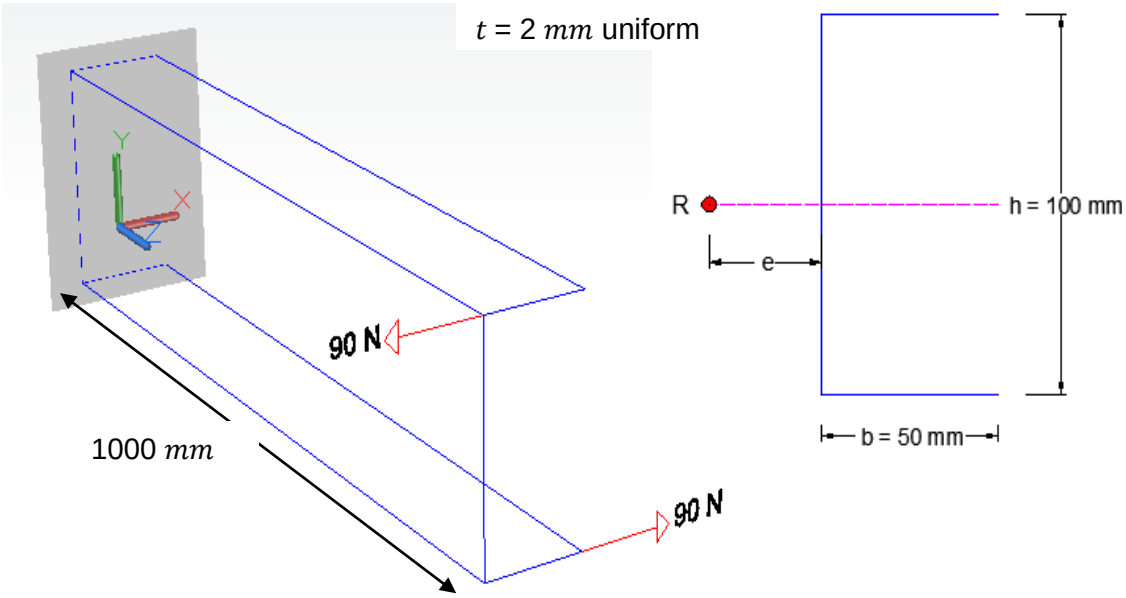

Figure 5.1 The dimensions of a channel cantilevered beam under a torque loading.

(Aluminium Alloy : 1050 - O); has been chosen for a plate material

Young's modulus (E) = 69000 MPa

Poisson's ratio (ν) = 0.334

Shear modulus (G) = $\frac{E}{2\,(1+\nu)}$ = $\frac{69000}{2\,(1+0.334)}$ = 25862 MPa

Torsion (T) = $p \times h$

Where; p = 90 N

Where; h = 100 mm

$\therefore T$ = 90 × 100 = 9000 $N.mm$

$$e = \frac{3b^2 t_f}{6bt_f + ht_w}$$

Where; b = 50 mm, h = 100 mm, t = 2 mm (uniform thickness)

$$\therefore e = \frac{3 \times 50^2 \times 2}{(6 \times 50 \times 2) + (100 \times 2)} = 18.75mm$$

5.1 Sectorial coordinates; calculations

Sectorial coordinate is always calculated from the reference line, from zero warping point to shear centre. It is necessary to have a reference line in order to sweep the sectorial coordinate. Sectorial coordinate depends on the section shape and the location of shear centre. The sectorial zero point is at the intersection of the axis of symmetry and the profile of the beam.

In element 1-2: $0 \le s_1 \le 50$

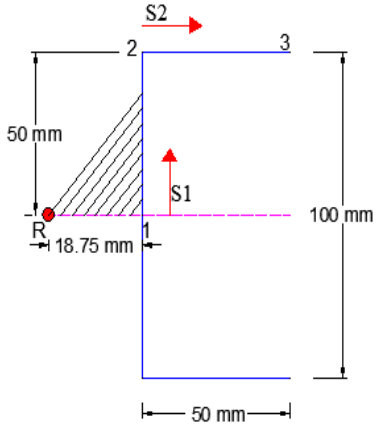

$$w(s_1) = -2 \times \frac{1}{2} \times 18.75 \times s_1$$

$$\therefore w(s_1) = -18.75 s_1$$

Where; s_1 = 0

$$w_1 = -18.75 \times 0 = 0$$

Where; s_1 = 50

$$w_2 = -18.75 \times 50 = -937.5mm^2 \qquad \text{(Linear in - between)}$$

In element 2-3: $0 \le s_2 \le 50$

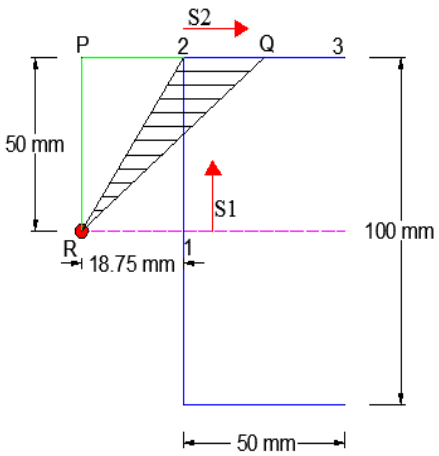

Area R2Q = area RPQ – area RP2

$$= \frac{1}{2} \times (18.75 + S_2) \times 50 - \frac{1}{2} \times 18.75 \times 50$$

Area R2Q $= \frac{1}{2} \times 50 \times S_2$

$$w(s_2) = -937.5 + (2 \times \frac{1}{2} \times 50 \times s_2)$$

$$\therefore w(s_2) = -937.5 + 50s_2$$

Where; s_2 = 0

$$w_2 = -937.5 + 50 \times 0 = -937.5 mm^2$$

Where; s_2 = 50

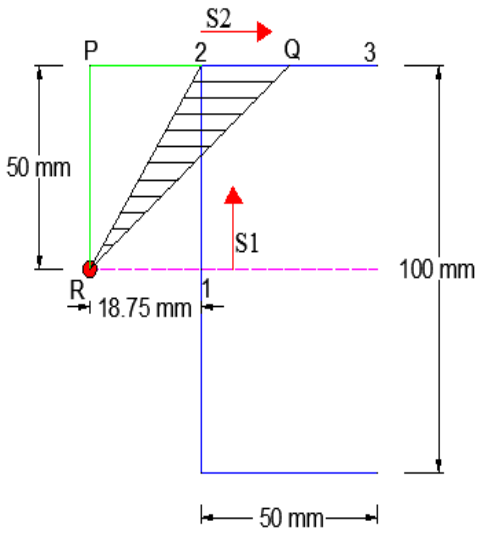

$$w_3 = -937.5 + (50 \times 50) = 1562.5 mm^2 \qquad \text{(Linear in - between)}$$

5.2 Warping (Torsion-Bending) constant; calculations

$$I_w = \int_s [w(s)]^2 t \, ds$$

$$I_w = 2\left[\int_0^{50} (-18.75 s_1)^2 \times 2 \times ds_1 + \int_0^{50} (-937.5 + 50 s_2)^2 \times 2 \times ds_2\right]$$

$$= 2\left[703.13\left(\frac{S_1^3}{3}\right)_0^{50} + \frac{2\left[(-937.5 + 50 s_2)^3\right]_0^{50}}{3 \times 50}\right] = 2\left[29.3 \times 10^6 + 50.9 \times 10^6 + 10.9 \times 10^6\right]$$

$$\therefore I_w = 1.8 \times 10^8 \, mm^6$$

5.3 Torsion-Bending related; calculations

$$J = \sum \frac{st^3}{3} = \frac{50 \times 2^3}{3} + \frac{100 \times 2^3}{3} + \frac{50 \times 2^3}{3} = 533 mm^4$$

$$\mu = \sqrt{\frac{GJ}{EI_w}} = \sqrt{\frac{25862 \times 533}{69000 \times 1.8 \times 10^8}} = 1.1 \times 10^{-3} \quad 1/mm$$

$$\mu L = 1.1 \times 10^{-3} \times 1000 = 1.1$$

5.4 Rate of twist at mid-span; calculations

Where; Z = 500mm

$$\frac{d\theta}{dz} = \frac{T}{GJ}\left[1 - \frac{\cosh \mu(L-z)}{\cosh \mu L}\right] = \frac{9000}{25862 \times 533}\left[1 - \frac{\cosh 1.1 \times 10^{-3}(1000-500)}{\cosh 1.1}\right]$$

$$\frac{d\theta}{dz} = 2 \times 10^{-4}$$

5.5 Warping distribution (Primary warping) round the profile; calculations

$$W = w(s)\frac{\partial \theta}{\partial z}$$

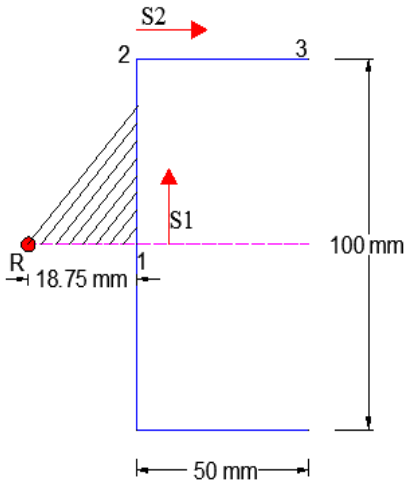

$$W = w(s) \times 2 \times 10^{-4}$$

Where; Z = 500mm

In element 1-2: $0 \le s_1 \le 50$

Where; s_1 = 0

$$w_1 = -18.75 \times 0 = 0$$

$$W_1 = 0 \times 2 \times 10^{-4} = 0$$

Where; s_1 = 50

$$w_2 = -18.75 \times 50 = -937.5mm^2 \quad \text{(Linear in - between)}$$

$$W_2 = -937.5 \times 2 \times 10^{-4} = -0.19mm \quad \text{(Linear in - between)}$$

In element 2-3: $0 \le s_2 \le 50$

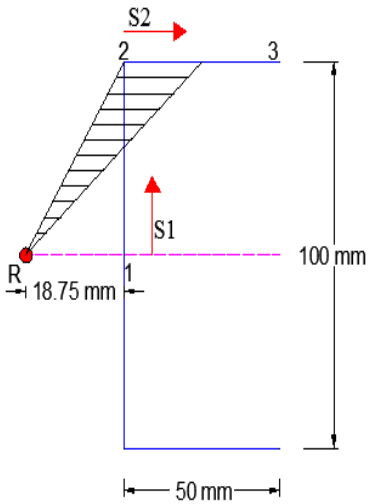

Where; s_2 = 0

$$w_2 = -937.5 + 50x0 = -937.5mm^2$$

$$W_2 = -937.5x2x10^{-4} = -0.19mm$$

Where; s_2 = 50

$$w_3 = -937.5 + (50 \times 50) = 1562.5mm^2 \quad \text{(Linear in - between)}$$

$$W_3 = 1562.5 \times 2 \times 10^{-4} = 0.31mm \quad \text{(Linear in - between)}$$

The warping displacement round the other half the section will be established by inspection of the section symmetry as shown in Fig (5.2).

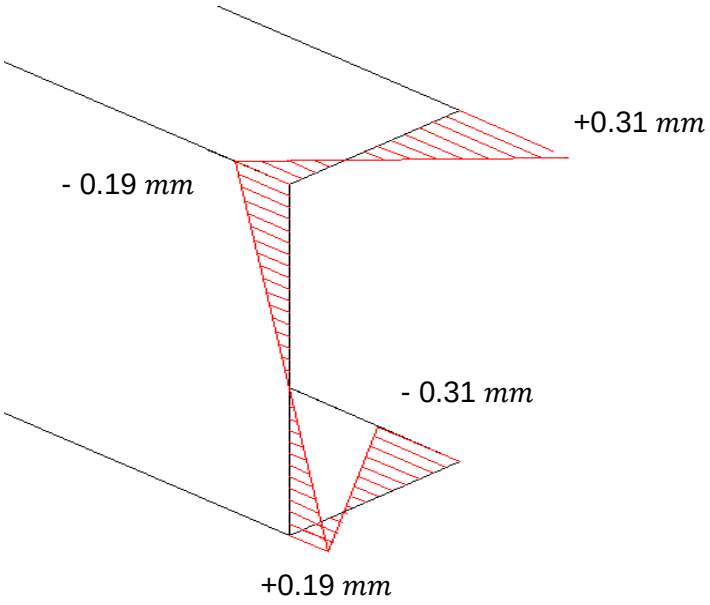

Figure 5.2 Warping distribution of the channel section cantilevered beam under a torque loading.

Table 5.1 Warping displacement results at mid-span of the channel section beam

Distance, s (mm)	0	50	100	150	200
Warping, W (mm)	0.31	- 0.19	0.00	0.19	- 0.31

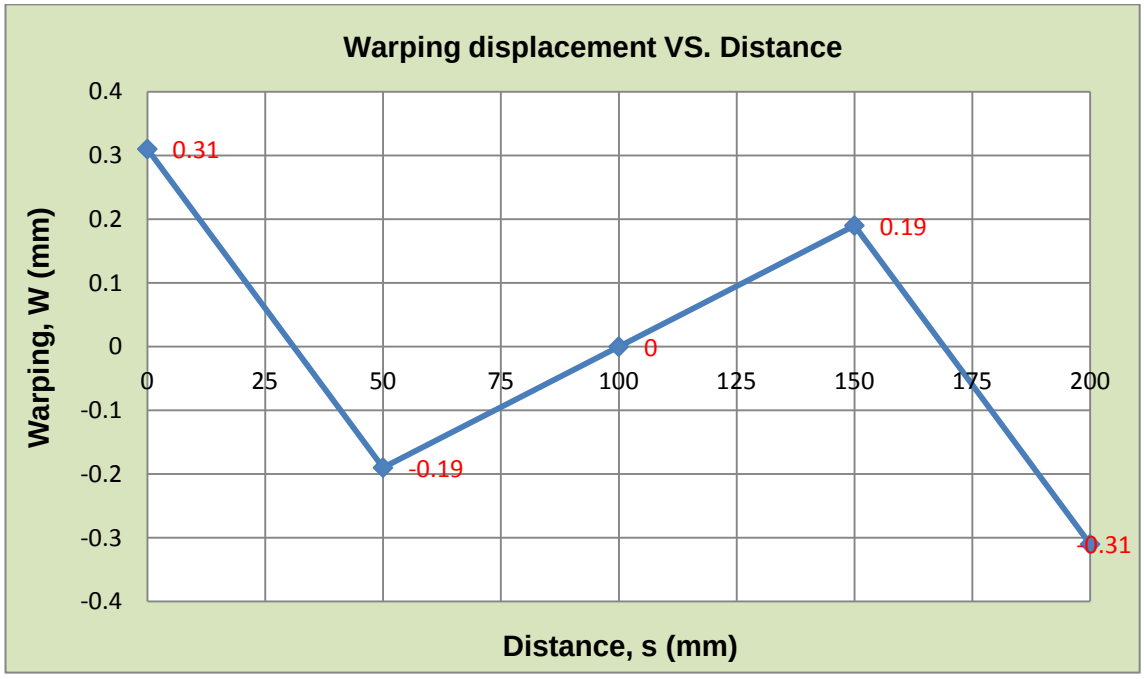

Figure 5.3 Warping distribution for the channel section at mid-span.

5.6 Warping at flange tip–along span; calculations

At fixed end, where; $Z = 0$

$$W = w(s)\frac{\partial\theta}{\partial z}$$

$$\frac{d\theta}{dz} = \frac{T}{GJ}\left[1 - \frac{\cosh\mu(L-z)}{\cosh\mu L}\right]$$

$$\therefore W = \frac{T}{GJ}\left[1 - \frac{\cosh\mu(L-z)}{\cosh\mu L}\right] x\, w(s)$$

$$W = \frac{9000}{25862\times 533}\left[1 - \frac{\cosh 1.1\times10^{-3}(1000-z)}{\cosh 1.1}\right]\times 1562.5$$

$$\therefore W = 1.02\left[1 - \frac{\cosh\left[1.1\times10^{-3}(1000-z)\right]}{1.67}\right]$$

Where; $Z = 0$

$W = 0$

Where; $Z = 100$

$$W = 1.02\left[1 - \frac{\cosh\left[1.1\times10^{-3}(1000-100)\right]}{1.67}\right] = 0.08mm$$

Use the same process to calculate the warping displacement values at regular sections of 100mm. The results are tabulated in table (5.2).

Table 5.2 Warping distribution results for the channel section at flange tip–along span.

Length, Z (mm)	Warping, W (mm)
0	0.00
100	0.08
200	0.16
300	0.22
400	0.27
500	0.31
600	0.35
700	0.38
800	0.40
900	0.41
1000	0.41

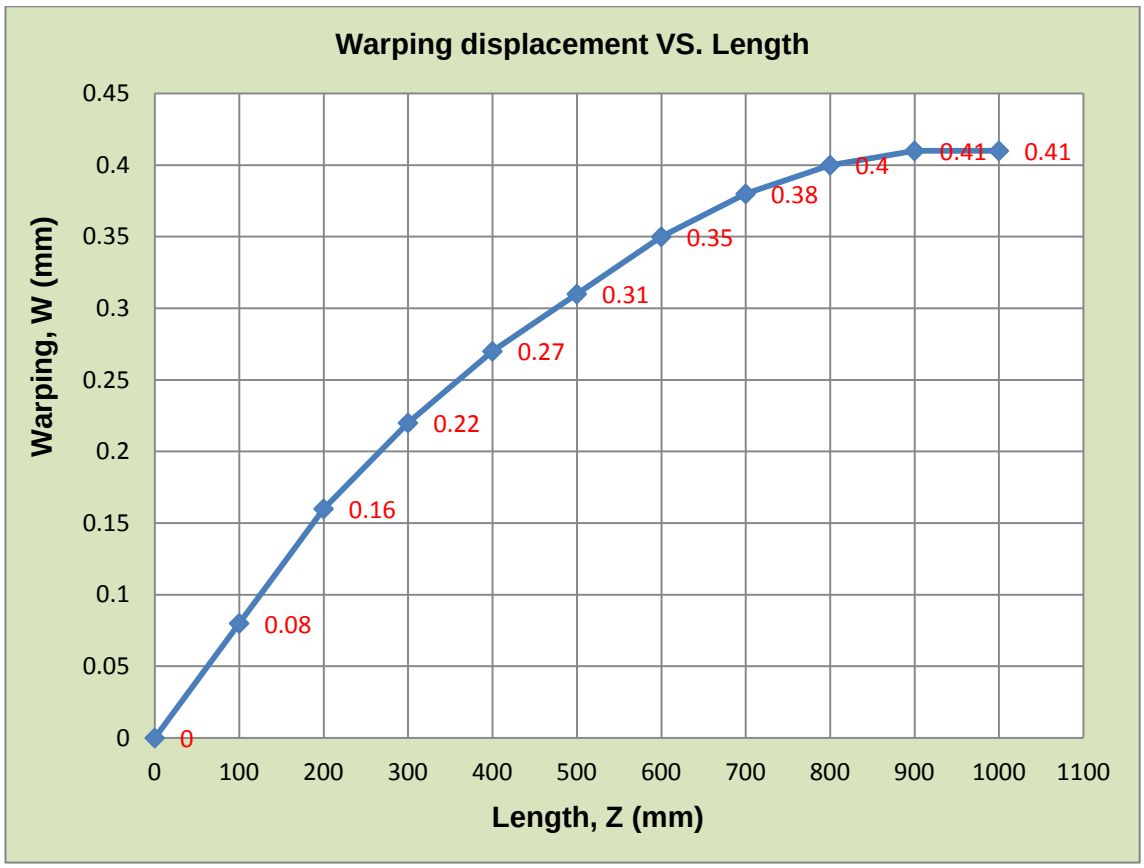

Figure 5.4 Warping distribution of the channel section along the span.

.

5.7 Warping stress distribution at top flange tip-along span; calculations

$$f_w = \frac{E}{G} \times \frac{T\mu}{J} \times \frac{\sinh \mu(L-z)}{\cosh \mu L} \times w(s)$$

$$w(s) = w_3$$

$$w_3 = 1562.5 mm^2$$

$$f_w = \frac{69000}{25862} \times \frac{9000 \times 1.1 \times 10^{-3}}{533} \times \frac{\sinh \mu(L-z)}{\cosh 1.1} \times 1562.5$$

$$f_w = 2.67 \times \frac{9000 \times 1.1 \times 10^{-3}}{533} \times \frac{\sinh \mu(L-z)}{1.67} \times 1562.5$$

$$f_w = 46.4 \times [\sinh \mu(L-z)]$$

$$\therefore f_w = 46.4 \times \sinh[1.1 \times 10^{-3}(1000-z)]$$

Where; $Z = 0$

$$f_w = 62 N/mm^2$$

Where; $Z = 100$

$f_w = 53.8N/mm^2$

Use the same process to calculate the warping stress values at regular sections of $100mm$. The results are tabulated in table (5.3).

Table 5.3 Warping stress results at top flange tip–along span.

Length, Z (mm)	Warping stress, f_w $(^N/_{mm^2})$
0	62
100	53.8
200	46.3
300	39.4
400	32.9
500	26.8
600	21.1
700	15.6
800	10.3
900	5.1
1000	0

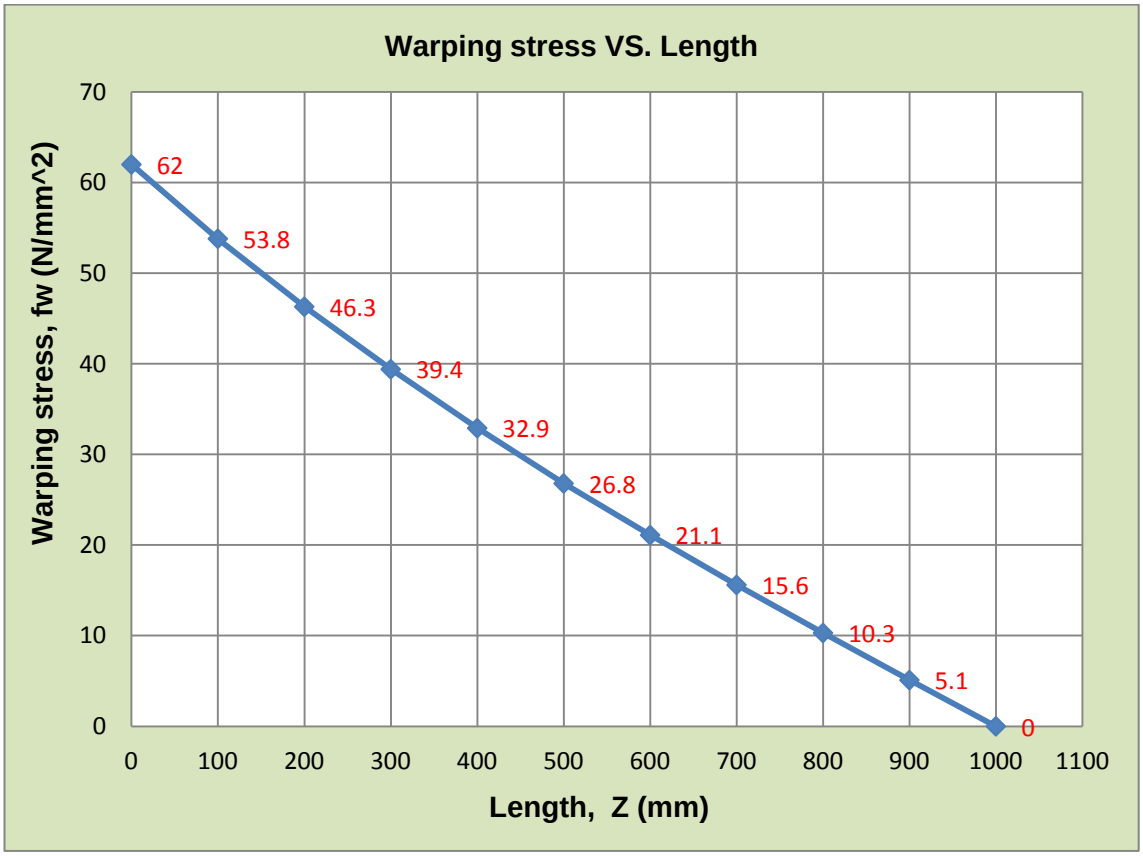

Figure 5.5 Warping stress at top flange tip-along the span of the beam.

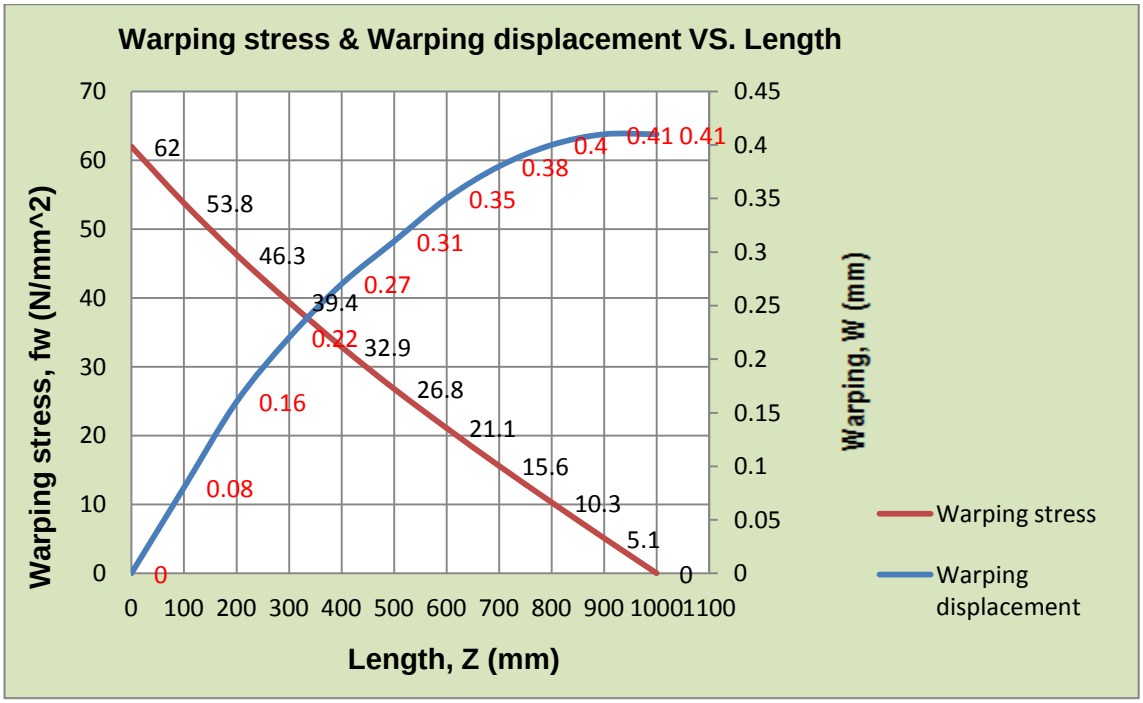

Figure 5.6 Warping stress and warping displacement along-span of the beam.

5.8 Warping stress at the built-in end; calculations

$$f_w = \frac{E}{G} \times \frac{T\mu}{J} \times \frac{\sinh \mu(L-z)}{\cosh \mu L} \times w(s)$$

Where; $Z = 0$

$$f_w = \frac{E}{G} \times \frac{T\mu}{J} \times \frac{\sinh \mu L}{\cosh \mu L} \times w(s)$$

$$f_w = \frac{E}{G} \times \frac{T\mu}{J} \times \tanh \mu L \times w(s)$$

$$f_w = \frac{69000}{25862} \times \frac{9000 \times 1.1 \times 10^{-3}}{533} \times \tanh(1.1) \times w(s)$$

$$f_w = 2.67 \times \frac{9000 \times 1.1 \times 10^{-3}}{533} \times \tanh(1.1) \times w(s)$$

$$\therefore f_w = 0.04 w(s)$$

Where; $w_1 = 0$

$$f_{w_1} = 0.04 \times 0 = 0$$

Where; $w_2 = -937.5\ mm^2$

$$f_{w_2} = 0.04 \times (-937.5) = -37.5 N/mm^2$$

Where; $w_3 = 1562.5\ mm^2$

$f_{w_3} = 0.04 \times (1562.5) = 62.5 N/mm^2$

The warping stress round the other half the section will be established by inspection of the section symmetry as shown in Fig (5.7), and unit for f_w is $^N/_{mm^2}$.

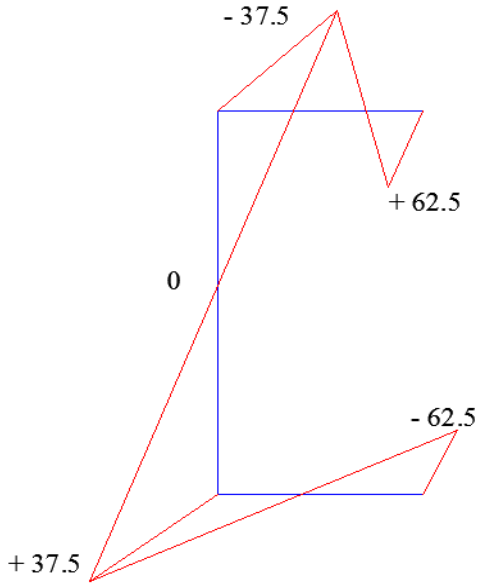

Figure 5.7 Warping stress due to restrained torsion round profile at built-in end.

Table 5.4 Warping stress results round profile at built-in end.

Distance, s (mm)	0	50	100	150	200
Warping stress, $f_w(^N/_{mm^2})$	62.5	- 37.5	0.00	37.5	- 62.5

5.9 Warping stress round profile at mid-span; calculations

At mid-span, where; L = 500 mm

$$f_w = \frac{E}{G} \times \frac{T\mu}{J} \times \tanh \mu L \times w(s)$$

$$\mu L = 1.1x10^{-3}\, x500 = 0.55$$

$$f_w = \frac{69000}{25862} \times \frac{9000 \times 1.1 \times 10^{-3}}{533} \times \tanh(0.55) \times w(s)$$

$$f_w = 2.67 \times \frac{9000 \times 1.1 \times 10^{-3}}{533} \times \tanh(0.55) \times w(s)$$

$f_w = 0.025w(s)$

Where; $w_1 = 0$

$f_{w_1} = 0.025 \times 0 = 0$

Where; $w_2 = -937.5\ mm^2$

$f_{w_2} = 0.025 \times (-937.5) = -23.4 N/mm^2$

Where; $w_3 = 1562.5\ mm^2$

$f_{w_3} = 0.025 \times (1562.5) = 39.1 N/mm^2$

The warping stress round the other half of the section will be established by inspection of the section symmetry as shown in Fig (5.8), and unit for f_w is $^N/_{mm^2}$.

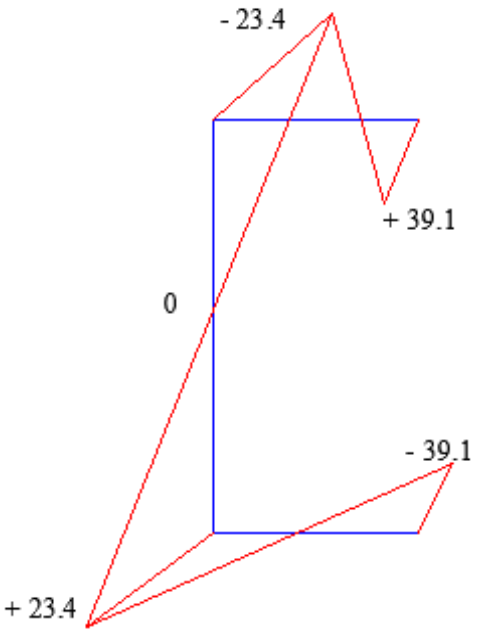

Figure 5.8 Warping stress due to restrained torsion round profile at mid-span.

.

Table 5.5 Warping stress results round profile at mid-span.

Distance, s (mm)	0	50	100	150	200
Warping stress, f_w $(^N/_{mm^2})$	39.1	- 23.4	0.00	23.4	- 39.1

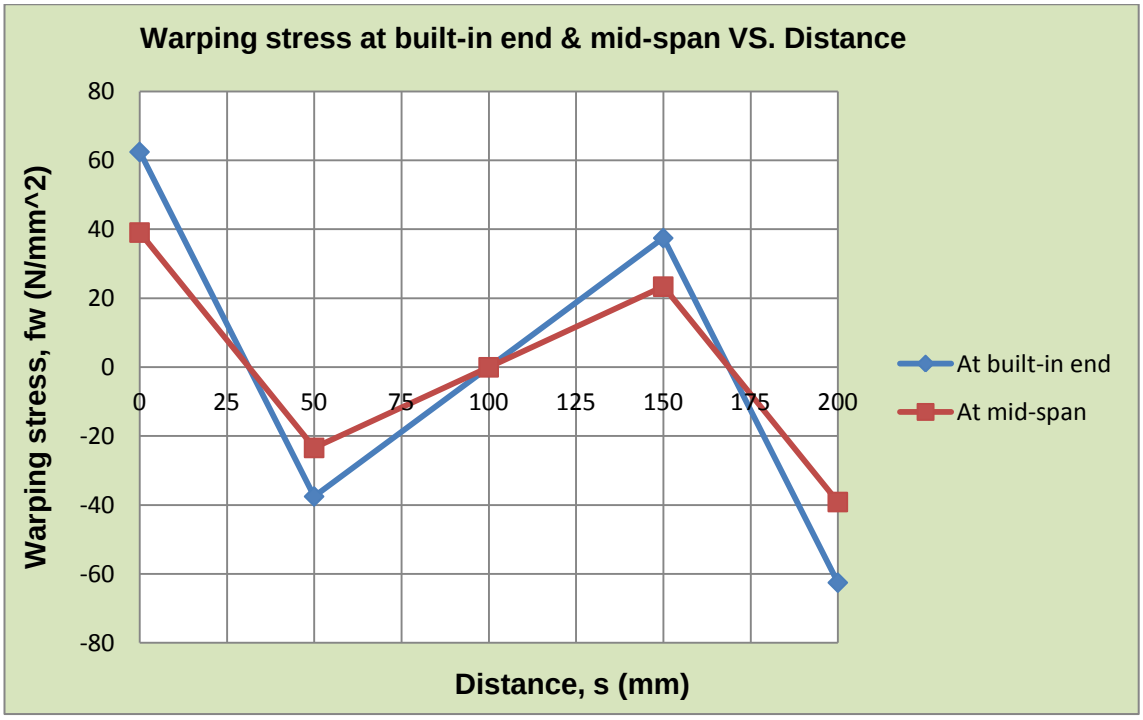

Figure 5.9 Distribution of axial constraint direct stress round section at built-in end and mid-span of the beam.

5.10 The rotation at flange tip-along span; calculations

Where; $Z = 0$ (At built-in end)

$$\frac{d\theta}{dz} = \frac{T}{GJ}\left[1 - \frac{\cosh \mu(L-z)}{\cosh \mu L}\right] = \frac{9000}{25862 \times 533}\left[1 - \frac{\cosh 1.1\times10^{-3}(1000-0)}{\cosh 1.1}\right]$$

$$\frac{d\theta}{dz} = 6.53\times10^{-4}\left[1 - \frac{\cosh\left[1.1\times10^{-3}(1000)\right]}{\cosh 1.1}\right] = 0$$

$$\therefore \theta = 0$$

$$\theta = \frac{T}{GJ}\left[z + \frac{\sinh \mu(L-z)}{\mu \cosh \mu L} - \frac{\sinh \mu L}{\mu \cosh \mu L}\right]$$

$$\theta = \frac{9000}{25862 \times 533}\left[z + \frac{\sinh \mu(L-z)}{1.1\times10^{-3} \times \cosh 1.1} - \frac{\sinh 1.1}{1.1\times10^{-3} \times \cosh 1.1}\right]$$

$$\therefore \theta = 6.53\times10^{-4}\left[z + \frac{\sinh\left[1.1\times10^{-3}(1000-z)\right]}{1.84\times10^{-3}} - 727.7\right]$$

Where; $Z = 0$

$$\theta = 0$$

Where; $Z = 100\ mm$

$$\theta = 6.53\times10^{-4}\left[100 + \frac{\sinh\left[1.1\times10^{-3}(1000-100)\right]}{1.84\times10^{-3}} - 727.7\right] = 1.73\times10^{-3}\ rad$$

$$\therefore \theta_{\deg} = \theta_{rad}\times\frac{180}{\pi} = 1.73\times10^{-3}\times\frac{180}{\pi} = 0.099^{\circ}$$

Use the same process to calculate the angle of twist values at regular sections of 100 mm. The results are tabulated in table (5.6).

Table 5.6 The angle of twist results at top flange tip–along span.

Length, $Z\ (mm)$	Angle of twist, $\theta_z\ (rad)$	Angle of twist, $\theta_z\ (degree)$
0	0.00000	0.000
100	0.00173	0.099
200	0.00961	0.551
300	0.02179	1.248
400	0.03762	2.155
500	0.05649	3.237
600	0.07785	4.460
700	0.10116	5.796
800	0.12592	7.215
900	0.15163	8.688
1000	0.17781	10.188

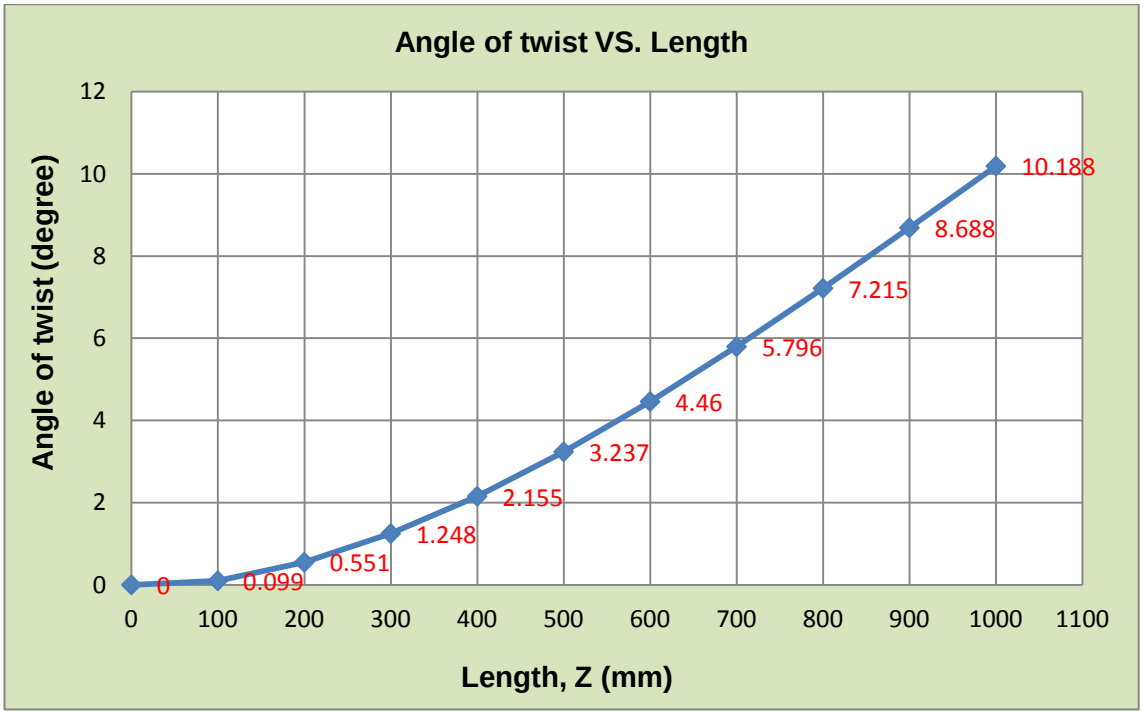

Figure 5.10 Angle of twist at top flange tip-along the span of the beam.

5.11 Wagner torsion-bending and St. Venant torsion computations along-span; calculations

$$T_J = GJ\frac{d\theta}{dz} \qquad \text{(St. Venant Torsion)}$$

$$\frac{d\theta}{dz} = \frac{T}{GJ}\left[1 - \frac{\cosh \mu(L-z)}{\cosh \mu L}\right]$$

$$T_J = T\left[1 - \frac{\cosh \mu(L-z)}{\cosh \mu L}\right]$$

$$T_J = 9000\left[1 - \frac{\cosh\left[1.1\times10^{-3}(L-z)\right]}{\cosh 1.1}\right]$$

Where; $Z = 0$ (At built-in)

$$T_J = 9000\left[1 - \frac{\cosh 1.1\times10^{-3}(1000-0)}{\cosh 1.1}\right] = 0$$

Where; $Z = 100$

$$T_J = 9000\left[1 - \frac{\cosh 1.1\times10^{-3}(1000-100)}{\cosh 1.1}\right] = 739.6Nmm$$

$$T_w = -EI_w\frac{d^3\theta}{dz^3} = T\ \frac{\cosh \mu(L-z)}{\cosh \mu L} \qquad \text{(Warping restraint)}$$

$$T_w == 9000\times\frac{\cosh\left[1.1\times10^{-3}(1000-z)\right]}{\cosh 1.1}$$

Where; $Z = 0$ (At built-in)

$$T_w = 9000\times\frac{\cosh 1.1\times10^{-3}(1000-0)}{\cosh 1.1} = 9000Nmm$$

Where; $Z = 100$

$$T_w = 9000\times\frac{\cosh 1.1\times10^{-3}(1000-100)}{\cosh 1.1} = 8260.4Nmm$$

Use the same process to calculate St. Venant torsion and Warping restraint values at regular sections of 100mm. The results are tabulated in table (5.7).

Table 5.7 St. Venant torsion and Wagner torsion-bending values along span.

Length, Z (mm)	St. Venant torsion, T_J $(N.mm)$	Warping restraint, T_W $(N.mm)$
0	0	9000
100	739.6	8260.4
200	1379	7620.9
300	1926.4	7073.6
400	2388	6612.1
500	2769.4	6230.6
600	3075.4	5924.6
700	3309.6	5690.4
800	3475	5525.1
900	3573.3	5426.7
1000	3606	5394

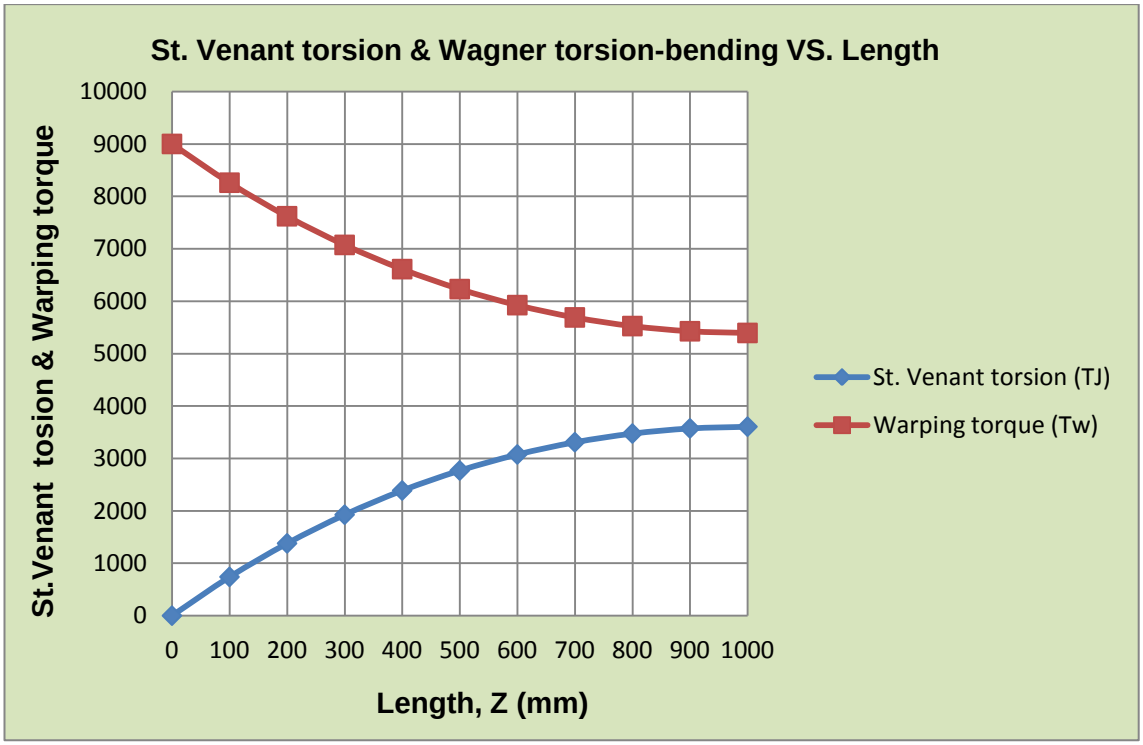

Figure 5.11 St. Venant torsion and Wagner torsion-bending along span of the beam.

$T_{total} = T_J + T_W$

Where;

T_{total} = total resistance to torsion

T_J = unrestrained torsion

T_W = restrained torsion

Where; $Z = 0$

$T_{total} = 0 + 9000$ = 9000 $N.mm$

$\frac{T_J}{T} = \frac{0}{9000} = 0$

$\frac{T_W}{T} = \frac{9000}{9000} = 1$

Use the same process to calculate (T_{total}, $\frac{T_J}{T}$ & $\frac{T_W}{T}$) values at regular sections of $100mm$. The results are tabulated in table (5.8).

Table 5.8 ${}^{T_J}/_{T}$, ${}^{T_W}/_{T}$ and T_{total} results for channel section of cantilevered beam.

Length, Z (mm)	T_{total} $(N.mm)$	$\frac{T_J}{T}$	$\frac{T_W}{T}$
0	9000	0.000	1.000
100	9000	0.082	0.918
200	9000	0.153	0.847
300	9000	0.214	0.786
400	9000	0.265	0.735
500	9000	0.308	0.692
600	9000	0.342	0.658
700	9000	0.368	0.632
800	9000	0.386	0.613
900	9000	0.397	0.603
1000	9000	0.401	0.599

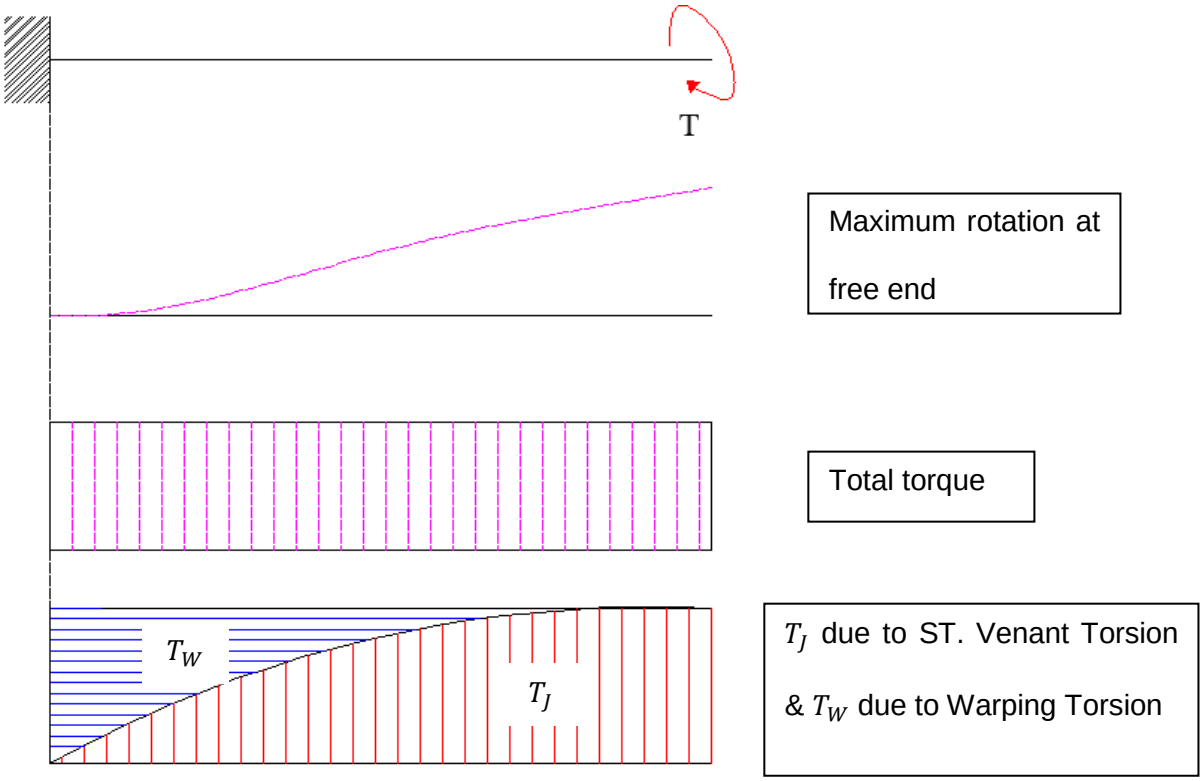

Figure 5.12 Distribution of the twist (θ), Torsional moment (T_J) & Warping moment (T_W) in the channel cantilever beam under restrained torsion.

In Fig (5.11 & 5.12); it can be seen that at built-in end of the beam the St. Venant torsion is zero, and it is maximum at free end of the beam but Warping torsion is the maximum value at fix-end and it is zero at free end of the channel cantilever beam. Moreover, the St. Venant part of the torsional moment is proportional to the first derivative of the angle of twist; the warping torsion on the other hands is proportional to the third derivative of the angle of twist. The angle of twist is the maximum value at free end of the channel cantilever beam.

5.12 Axial constraint shear flow round profile; calculations

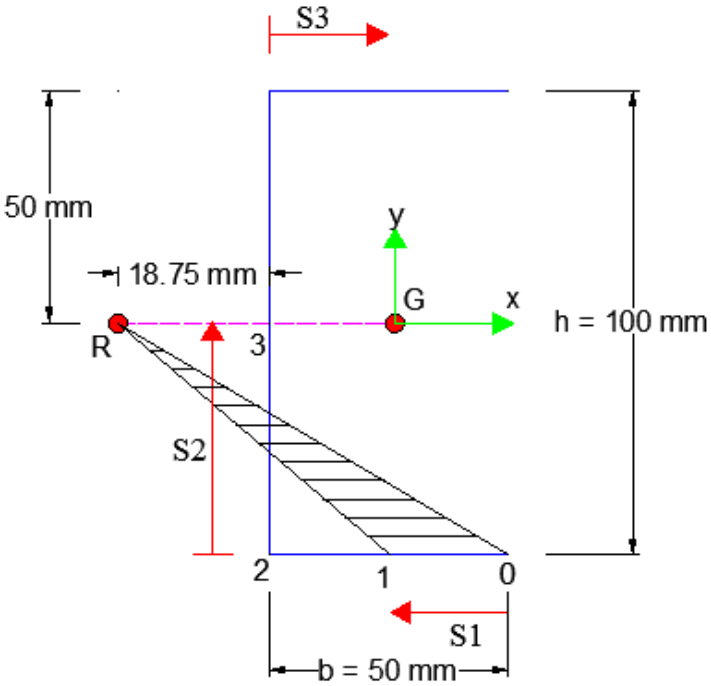

Figure 5.13 Axial constraint shears flow distribution round cross-section of the beam.

5.12.1 At mid-span (where Z = 500mm)

$$q_{\Gamma} = E\frac{d^3\theta}{dz^3}\int_0^s 2A_E t\,ds \quad \text{(Axial constraint shear flow)}$$

$$\frac{d^3\theta}{dz^3} = -\frac{T}{EI_w}\left[\frac{\cosh\mu(L-z)}{\cosh(\mu L)}\right]$$

$$\frac{d^3\theta}{dz^3} = -\frac{9000}{69000\times 1.8\times 10^8}\left[\frac{\cosh[1.1\times 10^{-3}(1000-500)]}{\cosh(1.1)}\right]$$

$$\therefore \frac{d^3\theta}{dz^3} = -5\times 10^{-10}$$

Sectorial coordinates calculations; from Fig (5.13):

$$w_S = 2A_{E,0} = \int_0^s \frac{h}{2}\,ds = \frac{h}{2}s \qquad \text{For } 0 \le s \le b$$

$$w_S = 2A_{E,0} = \frac{h}{2}b + (-)\int_b^s e\,ds = \frac{bh}{2} - e(s-b) \qquad \text{For } b \le s \le b+h$$

$$w_S = 2A_{E,0} = \frac{bh}{2} - e(b+h-b) + \int_{b+h}^s \frac{h}{2}ds = \frac{h}{2}(s-2e-h) \qquad \text{For } b+h \le s \le 2b+h$$

Integrating by part;

$$2A'_E = \frac{1}{A}\int_0^{2b+h} 2A_{E,0}\,dA$$

$$2A'_E = \frac{1}{2bt+ht}\left\{\int_0^b \frac{h}{2}s\,t\,d_s + \int_b^{b+h}\left[\frac{bh}{2} - e(s-b)\right]t\,ds + \int_{b+h}^{2b+h}\frac{h}{2}(s-2e-h)\,t\,ds\right\}$$

$$\therefore 2A'_E = \frac{h}{2}(b-e)$$

In element 0-2: $0 \le s \le b$

$$2A_E = 2A_{E,0} - 2A'_E$$

$$2A_E = \frac{h}{2}s_1 - \frac{h}{2}(b-e)$$

$$\int_0^{s_1} 2A_E\,t\,ds_1 = \frac{1}{2}hts_1\left(\frac{1}{2}s_1 - b + e\right)$$

$$\Rightarrow q_\Gamma = E\frac{d^3\theta}{dz^3}\int_0^s 2A_E\,t\,ds$$

$$\therefore q_\Gamma = E\frac{d^3\theta}{dz^3}\times\frac{1}{2}hts_1\left(\frac{1}{2}s_1 - b + e\right)$$

At point (0); s_1 = 0 mm

$\therefore q_{\Gamma 0} = 0$

At point (1); $s_1 = \frac{1}{2}\ b \Rightarrow\ \therefore s_1 = \frac{1}{2}50 \Rightarrow s_1 = 25mm$

$$q_\Gamma = -69000 \times 5x10^{-10}\left[\frac{1}{2}\times 100 \times 2 \times s_1(\frac{1}{2}s_1 - b + e)\right]$$

$$q_\Gamma = -3.45\times 10^{-5}\left[100\, s_1(\frac{1}{2}s_1 - b + e)\right]$$

$$q_{\Gamma 1} = -3.45x10^{-5}\left[100\times 25\times(\frac{1}{2}\times 25 - 50 + 18.75)\right]$$

$$q_{\Gamma 1} = -3.45\times 10^{-5}\left[100\times 25\times(-18.75)\right] = -3.45\times 10^{-5}\left[-46875\right]$$

$\therefore q_{\Gamma 1} = 1.62N/mm$

At point (2); $s_1 = b = 50\ mm$ and $q_\Gamma = -3.45\times 10^{-5}\left[100\, s_1(\frac{1}{2}s_1 - b + e)\right]$

$$q_{\Gamma 2} = -3.45\times 10^{-5}\left[100\times 50\times(\frac{1}{2}\times 50 - 50 + 18.75)\right]$$

$$q_{\Gamma 2} = -3.45\times 10^{-5}\left[100\times 50\times(-6.25)\right] = -3.45\times 10^{-5}\left[-31250\right]$$

$\therefore q_{\Gamma 2} = 1.1N/mm$

<u>In element 2-4</u>: $b \le s \le b + h$

At point (3); $s_2 = b + \frac{1}{2}\ h$

$$\int_0^{s_2} 2A_E t\, ds_2 = \frac{1}{4}bht(2e-b) - et(-\frac{1}{8}h^2) = \frac{1}{4}bht(2e-b) + \frac{1}{8}eh^2t$$

$$q_{\Gamma 3} = E\frac{d^3\theta}{dz^3}\left[\frac{1}{4}bht(2e-b) + \frac{1}{8}eh^2t\right]$$

$$q_{\Gamma 3} = -3.45\times 10^{-5}\left[\frac{1}{4}\times 50\times 100\times 2\times(2\times 18.75 - 50) + \frac{1}{8}\times 18.75\times 100^2\times 2\right]$$

$$q_{\Gamma 3} = -3.45\times 10^{-5}\left[-31250 + 46875\right]$$

$\therefore q_{\Gamma 3} = -0.54N/mm$

The warping shear flow round the other half of the section will be established by inspection of the section symmetry as shown in Fig (5.14), and unit for shear flow, q_Γ is $^N/_{mm}$.

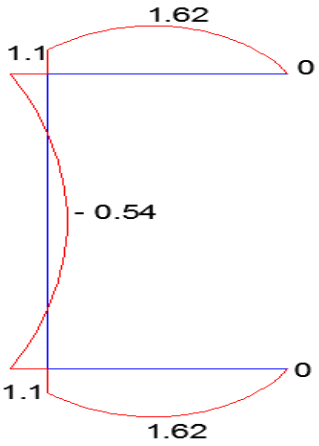

Figure 5.14 Warping shear flow round cross-section at mid-span.

Table 5.9 Warping shear flow results round cross-section at mid-span.

Distance, s (mm)	Warping shear flow, q_Γ $(^N/_{mm})$
0	0
25	1.62
50	1.1
100	-0.54
150	1.1
175	1.62
200	0

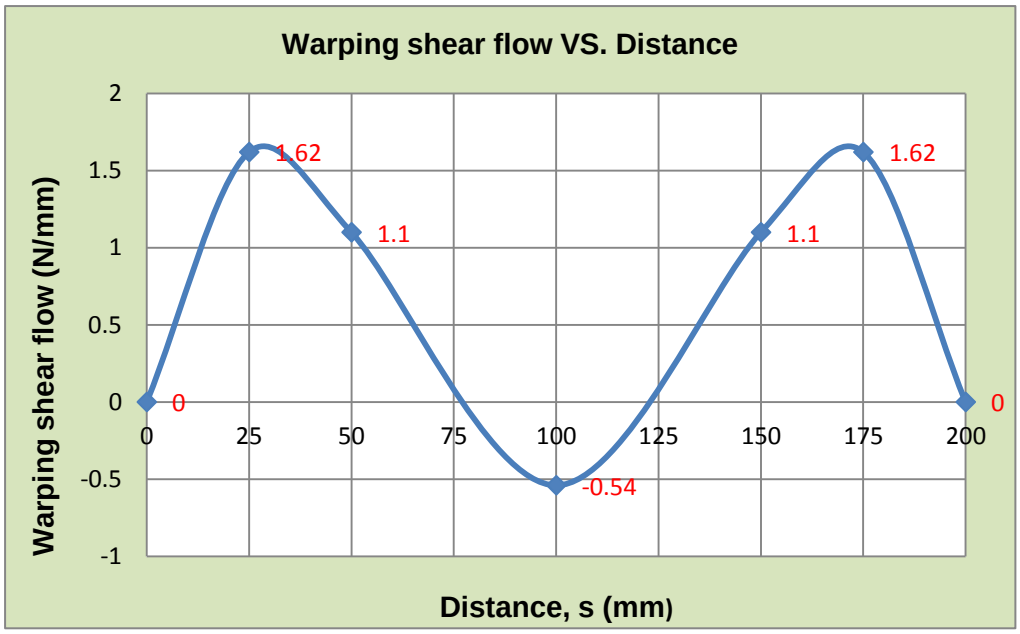

Figure 5.15 Distribution of axial constraint shear flows round cross-section at mid-span.

5.12.2 At built-in end (where Z = 0mm)

From Fig (5.13):

$$\tau_{w1} = -\frac{\int_0^{s_1} 2A_E t\, ds_1 \times \mathrm{T}}{t_f \times I_w}, \quad q_\Gamma = \tau \times t$$

$$\therefore q_{\Gamma 1} = \tau_{w1} \times t_f$$

$$\therefore\ q_{\Gamma 1} = -\frac{\int_0^{s_1} 2A_E t\, ds_1\ \times \mathrm{T}}{I_w}$$

At point (0); s_1 = 0 $mm \rightarrow \therefore q_{\Gamma 0} = 0$

At point (1); $s_1 = \frac{1}{2}\ b$

From section 5.12.1; $\int_0^{s_1} 2A_E t\, ds_1 = \frac{1}{2} hts_1(\frac{1}{2} s_1 - b + e) = \left[-46875\right]$

Also, from section 5.3; $I_w = 1.8 \times 10^8\, mm^6$

$$\therefore\ q_{\Gamma 1} = -\frac{-46875\ \times 9000}{1.8\ \times\ 10^8} =\ 2.34\ {}^{N}/_{mm}$$

At point (2); s_1 = b = 50 mm

From section 5.12.1; $\int_0^{s_1} 2A_E t\, ds_1 = \frac{1}{2} hts_1(\frac{1}{2} s_1 - b + e) = \left[-31250\right]$

$$\therefore\ q_{\Gamma 2} = -\frac{-\ 31250\ \times 9000}{1.8\ \times\ 10^8} =\ 1.6\ {}^{N}/_{mm}$$

At point (3); $s_2 = b + \frac{1}{2}\ h$

From section 5.12.1;

$$\int_0^{s_2} 2A_E t\, ds_2 = \frac{1}{4} bht(2e - b) - et(-\frac{1}{8} h^2) = \frac{1}{4} bht(2e - b) + \frac{1}{8} eh^2 t = 15625$$

$$\therefore\ q_{\Gamma 3} = -\frac{15625 \times 9000}{1.8\ \times\ 10^8} =\ -\ 0.78\ {}^{N}/_{mm}$$

The warping shear flow round the other half of the section will be established by inspection of the section symmetry as shown in Fig (5.16), and unit for warping shear flow, q_Γ is $^N/_{mm}$.

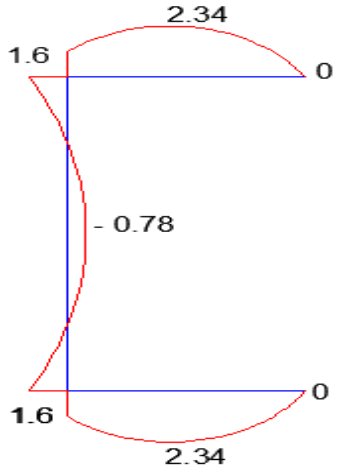

Figure 5.16 Warping shear flow round cross-section at built-in end.

Table 5.10 Warping shear flow results round cross-section at built-in end.

Distance, s (mm)	Warping shear flow, q_Γ $(^N/_{mm})$
0	0
25	2.34
50	1.6
100	-0.78
150	1.6
175	2.34
200	0

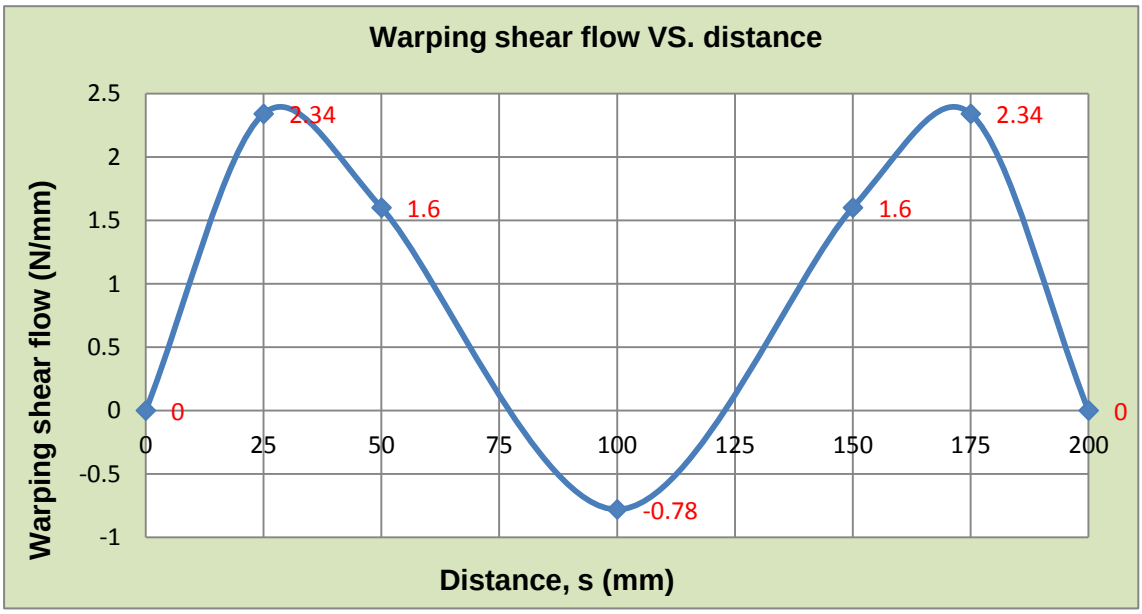

Figure 5.17 Distribution of axial constraint shear flows round cross-section at fix-end.

5.13 Combined (torsion shear & warping shear) flow results; Calculations

5.13.1 At mid-span (where Z = 500mm)

$$\frac{d\theta}{dz} = \frac{T}{GJ}\left[1 - \frac{\cosh \mu(L-z)}{\cosh \mu L}\right]$$

$$\frac{d\theta}{dz} = \frac{T}{GJ}\left[1 - \frac{\cosh \mu(1000-500)}{\cosh \mu L}\right]$$

$$\tau_{T_{(\max)}} = \pm Gt\frac{d\theta}{dz}$$ (St. Venant linear shear stress distribution)

$$\tau_{T_{(\max)}} = \pm Gt\frac{T}{GJ}\left[1 - \frac{\cosh \mu(1000-500)}{\cosh \mu L}\right]$$

$$\tau_{T_{(\max)}} = \pm\frac{tT}{J}\left(1 - \frac{\cosh \mu(500)}{\cosh \mu L}\right)$$

$$\tau_{T_{(\max)}} = \pm\frac{2\times 9000}{533}\left(1 - \frac{\cosh[1.1\times 10^{-3}(500)]}{\cosh(1.1)}\right)$$

$$\therefore \tau_{T_{(\max)}} = \pm 33.77\times(0.31)$$

$$\tau_{T_{(\max)}} = \pm 10.4 N/mm^2$$

$$q_T = \tau_{T_{(\max)}}\times t \Rightarrow q_T = \pm 10.4\times 2$$

$$q_T = \pm 20.8 N/mm$$

The total shear flow distribution due to pure torsion through the all thickness of the cross-section, and maximum occurring at the wall surfaces; as shown in Fig (5.18), and unit for torsion shear flow, q_T is $^{N}/_{mm}$.

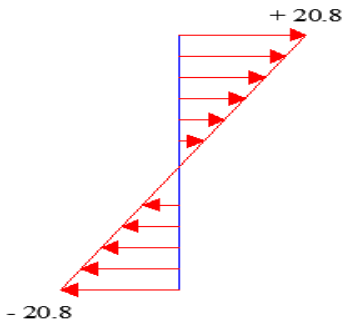

Figure 5.18 Linear shear flow distribution due to pure torsion.

The combined maximum shear flow distribution around profile at mid-span will be found by calculation of torsion shear flow and warping shear flow as shown in Fig (5.19).

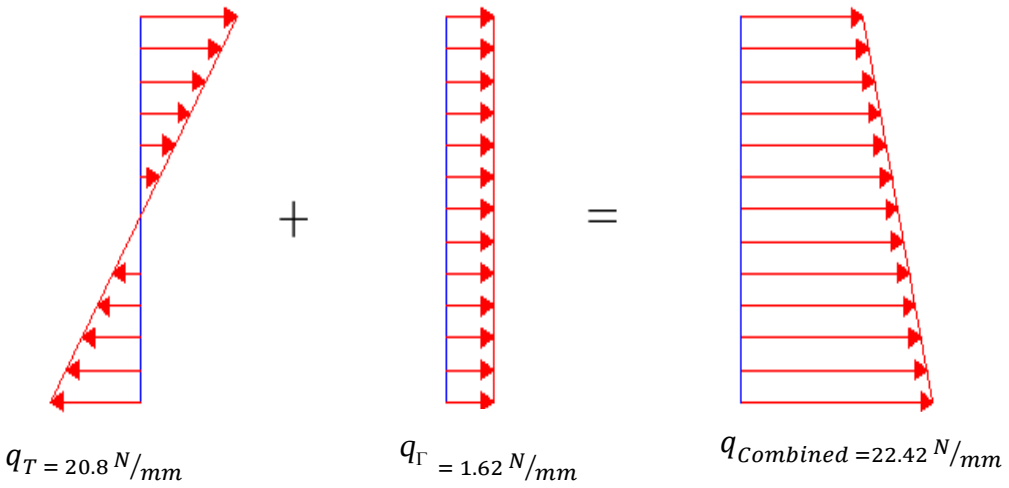

Figure 5.19 Combined maximum shear flow distribution around profile at mid-span for channel beam under restrained torsion.

$q_{Combined} = q_T + q_\Gamma$

$q_{Combined} = 20.8 + 1.62 = 22.42\ ^{N}/_{mm}$

5.13.2 At built-in end (where Z = 0mm)

$$\frac{d\theta}{dz} = \frac{T}{GJ}\left[1 - \frac{\cosh \mu(L-z)}{\cosh \mu L}\right]$$

$\frac{d\theta}{dz} = 0$ (At fix-end)

$\tau_{T_{(max)}} = \pm Gt\frac{d\theta}{dz} = 0$

∴ There is no shear flow due to pure torsion at built-in end. Therefore, there is a warping shear flow due to axial constraint at built-in end, which is calculated in section (5.12.2).

5.13.3 At free end (where Z = 1000mm)

$$\frac{d\theta}{dz} = \frac{T}{GJ}\left[1 - \frac{\cosh \mu(L-z)}{\cosh \mu L}\right]$$

$$\frac{d\theta}{dz} = \frac{T}{GJ}\left[1 - \frac{\cosh \mu(1000-1000)}{\cosh \mu L}\right]$$

$$\therefore \frac{d\theta}{dz} = \frac{T}{GJ}\left[1 - \frac{1}{\cosh \mu L}\right]$$

$$\tau_{T_{(\max)}} = \pm Gt\frac{d\theta}{dz}$$ (St. Venant linear shear stress distribution)

$$\tau_{T_{(\max)}} = \pm Gt\frac{T}{GJ}\left[1 - \frac{1}{\cosh \mu L}\right]$$

$$\tau_{T_{(\max)}} = \pm \frac{tT}{J}\left(1 - \frac{1}{\cosh \mu L}\right)$$

$$\tau_{T_{(\max)}} = \pm \frac{2\times 9000}{533}\left(1 - \frac{1}{\cosh 1.1}\right)$$

$$\therefore \tau_{T_{(\max)}} = \pm 33.77(0.4)$$

$$\tau_{T_{(\max)}} = \pm 13.51 N/mm^2$$

$$q_T = \tau_{T_{(\max)}} \times t \Rightarrow q_T = \pm 13.51 \times 2$$

$$q_T = \pm 27 N/mm$$

The total shear flow distribution due to pure torsion through the all thickness of the cross-section, and maximum occurring at the wall surfaces; as shown in Fig (5.20), which torsion shear flow, q_T unit is $^{N}/_{mm}$.

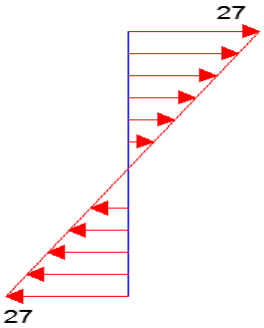

Figure 5.20 Linear shear flow distribution due to pure torsion at free end.

There is no warping shear flow due to axial constraint at free end.

Table 5.11 Summary of stress results due to restrained torsion.

Type of stress	Maximum stress at cross section, $(^{N}/_{mm^2})$		
	Fix-end	Mid-span	Free end
Normal stress due to torsional bending, f_w	62.5	39.1	0

Table 5.12 Summary of combined shear flow results due to restrained torsion.

Type of shear flow	Maximum shear flow at cross section, $(^{N}/_{mm})$		
	Fix-end	Mid-span	Free end
Shear flow due to St. Venant torsion, q_T	0	20.8	27
Shear flows due to warping torsion, q_Γ	2.34	1.62	0
Sum of combined shear flow	2.34	22.42	27

Table 5.13 Summary of combined shear stress results due to restrained torsion.

Type of stress	Maximum shear stress at cross section, $(^{N}/_{mm^2})$		
	Fix-end	Mid-span	Free end
Shear stress due to St. Venant torsion, τ_s	0	10.4	13.51
Shear stress due to warping torsion, τ_w	1.17	0.81	0
Sum of combined shear stresses	1.17	11.21	13.51

In summary, three kinds of stresses arise in any channel section due to torsional loading:

1) Shear stresses τ_s in web and flanges due to rotation of the elements of the cross section (St. Venant torsion,T_J).
2) Shear stresses τ_w in the flanges due to lateral bending (Warping torsion,T_W).
3) Normal stresses due to lateral bending of the flanges (Lateral bending moment on flange).

CHAPTER (6)

FINITE ELEMENT ANALYSIS

6.1 FEA (Strand 7) Results for chapter (3)

Finite element (Strand 7) performed to analysis rectangular cantilever beam. The beam dimensions are illustrated in Fig (3.1), the coordinates for key points are shown in table (6.2) and beam properties are shown in table (6.1).

The Strand 7 software has been used for analysis models to determine the deflection & bending stress along span of the beam, and bending stress & shear stress of the cross-section area at mid-span of the beam, for all mesh diagrams in section (3.3).

The beam restraint in one end and free in other end. The point load is applied at the free end of rectangular cantilever beam which is 1000 N, as indicated in Fig (6.1, 6.2, 6.3, 6.4, 6.5, 6.6 & 6.7).

Using 4-node quadrilateral element to create model one and using 8-node quadrilateral elements to create model two then subdivided model two to create other models by using 8-node quadrilateral element to obtained suitable results. So the finite element model was constructed as following:

- Model (3) four 8-node quadrilateral elements
- Model (4) eight 8-node quadrilateral elements
- Model (5) sixteen 8-node quadrilateral elements
- Own model thirty two 8-node quadrilateral elements

Table 6.1 Beam property for rectangular section cantilever beam.

Beam Element Property				
Materials	Structural		Beam cross section	
Type	Young's Modulus, E (MPa)	Poisson's Ratio, (v)	B (mm)	D (mm)
Steel-Beam	200000	0.3	50	150

Table 6.2 Coordinate key points for rectangular section cantilever beam.

Key points	Coordinate points		
	$X\ (mm)$	$Y\ (mm)$	$Z\ (mm)$
1	0	0	0
2	600	0	0
3	1200	0	0
4	0	75	0
5	1200	75	0
6	0	150	0
7	600	150	0
8	1200	150	0

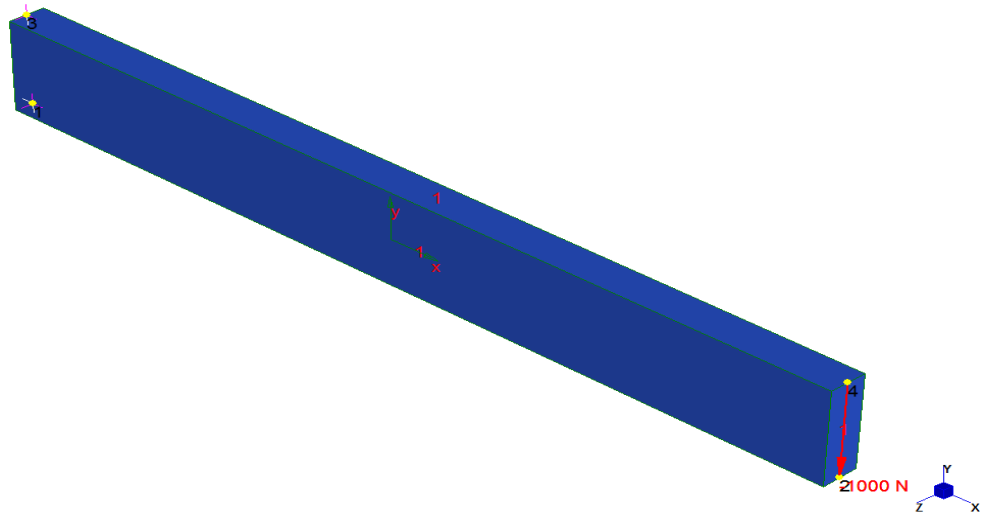

Figure 6.1 4-node quadrilateral element.

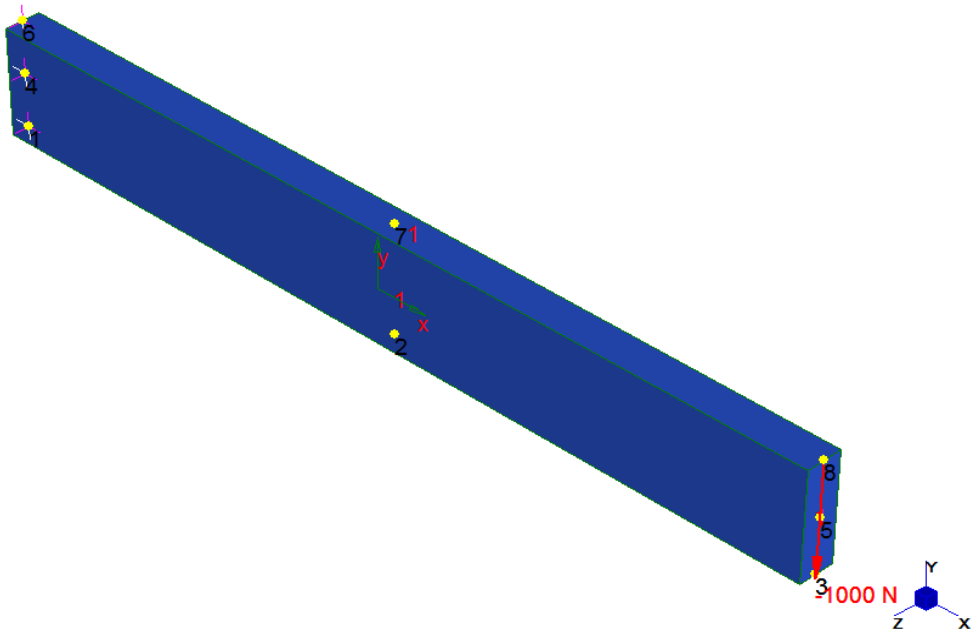

Figure 6.2 8-node quadrilateral element.

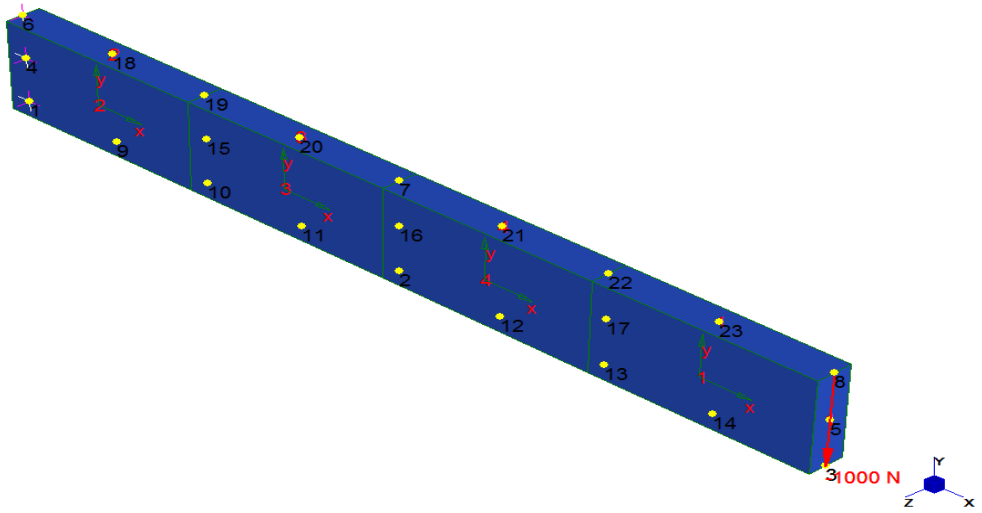

Figure 6.3 Four 8-node quadrilateral elements.

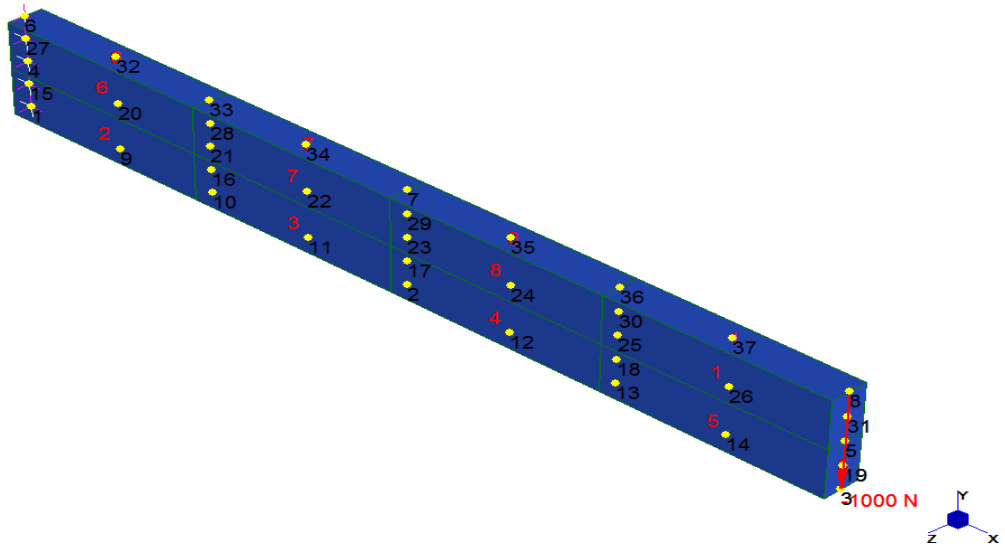

Figure 6.4 Eight 8-node quadrilateral elements.

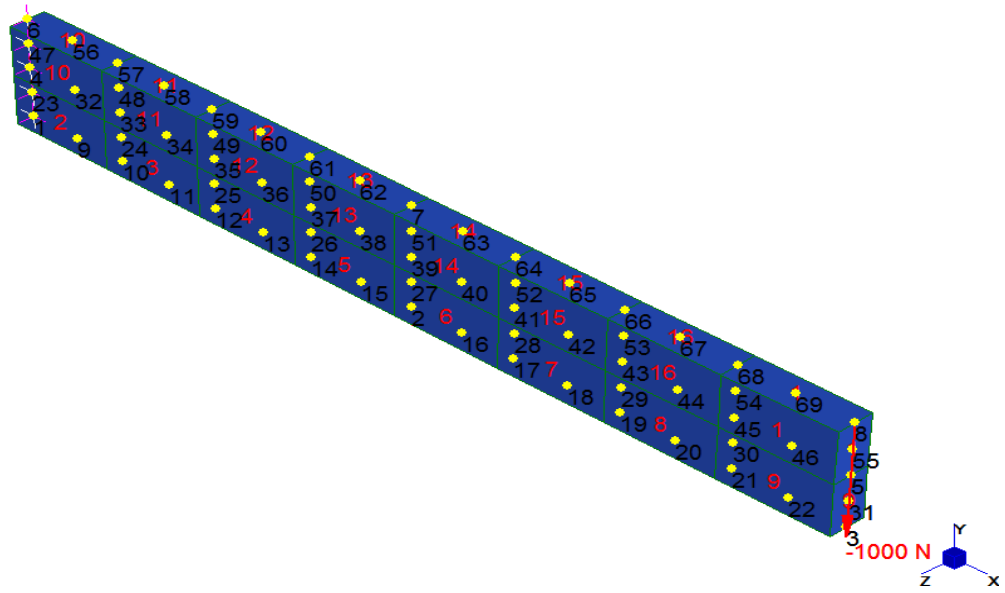

Figure 6.5 Sixteen 8-node quadrilateral elements.

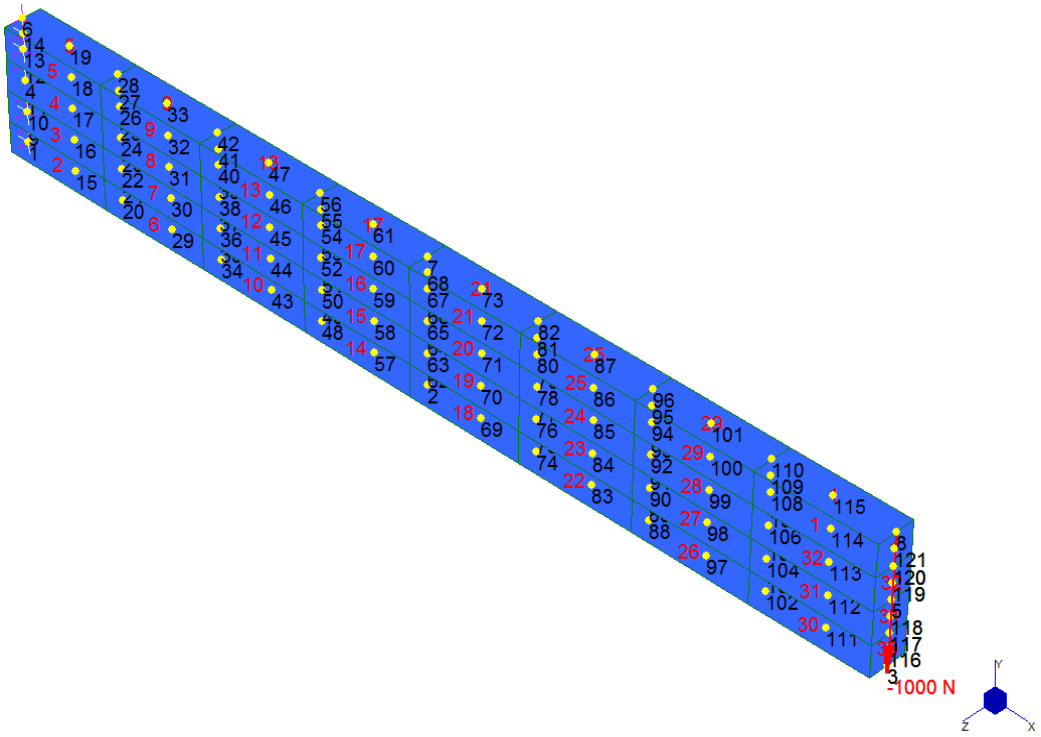

Figure 6.6 Thirty two 8-node quadrilateral elements.

The following table 6.3, 6.4, 6.5 & 6.6 show the results obtained from Strand 7 for all models.

Table 6.3 Vertical deflection results along the top surface of the cantilever beam.

Length (mm)	Node number for own model	Deflection (mm)					
		Strand 7					
		Model 1	Model 2	Model 3	Model 4	Model 5	Own Model
0	6	0.000	0.000	0.000	0.000	0.000	0.000
75	19					-0.001	-0.002
150	28			-0.005	-0.005	-0.005	-0.005
225	33					-0.011	-0.011
300	42			-0.017	-0.018	-0.018	-0.018
375	47					-0.027	-0.027
450	56			-0.037	-0.038	-0.038	-0.038
525	61					-0.051	-0.051
600	7		-0.042	-0.063	-0.064	-0.065	-0.065
675	73					-0.080	-0.080
750	82			-0.093	-0.095	-0.096	-0.096
825	87					-0.113	-0.113
900	96			-0.128	-0.129	-0.130	-0.131
975	101					-0.149	-0.149
1050	110			-0.164	-0.166	-0.168	-0.168
1125	115					-0.187	-0.187
1200	8	-0.142	-0.160	-0.202	-0.204	-0.206	-0.206

Table 6.4 Bending stress results along the top surface of the cantilever beam.

Length (mm)	Node number for own model	Plate number for own model	Bending Stress on top surface of the beam (MPa)					
			Strand 7					
			Model 1	Model 2	Model 3	Model 4	Model 5	Own Model
0	6	5	3.204	3.966	6.295	6.352	6.470	6.598
75	19	5					6.049	6.040
150	28	5,9			5.600	5.646	5.627	5.585
225	33	9					5.180	5.201
300	42	9,13			4.905	4.939	4.782	4.800
375	47	13					4.404	4.405
450	56	13,17			4.000	3.981	3.968	4.000
525	61	17					3.599	3.599
600	7	17,21		3.200	3.414	3.407	3.230	3.249
675	73	21					2.800	2.800
750	82	21,25			2.400	2.403	2.372	2.448
825	87	25					2.000	1.999
900	96	25,29			1.413	1.782	1.572	1.647
975	101	29					1.195	1.200
1050	110	1,29			0.800	0.816	0.818	0.808
1125	115	1					0.480	0.521
1200	8	1	3.196	2.434	0.187	0.216	0.125	0.199

Table 6.5 Bending stress results at mid-span of the cantilever beam.

Depth of beam (mm)	Node number for own model	Plate number for own model	Actual depth from neutral axis (mm)	Bending Stress at Mid-Span (MPa)				
				Strand 7				
				Model 2	Model 3	Model 4	Model 5	Own Model
0	7	17,21	-75	-3.200	-3.414	-3.410	-3.230	-3.249
37.5	67	17,21	-37.5			-1.687	-1.614	-1.597
75	65	15	0		0.000	0.035	0.001	0.000
112.5	63	14,15	37.5			1.687	1.614	1.597
150	2	14,18	75	3.200	3.414	3.407	3.230	3.249

Table 6.6 Shear stress results at mid-span of the cantilever beam.

Depth of beam (mm)	Node number for own model	Plate number for own model	Actual depth from neutral axis (mm)	Shear Stress at Mid-Span (MPa)				
				Strand 7				
				Model 2	Model 3	Model 4	Model 5	Own Model
0	7	17,21	-75	-0.134	-0.140	-0.044	-0.033	-0.008
37.5	67	17,21	-37.5			-0.132	-0.133	-0.158
75	65	15	0		-0.133	-0.231	-0.234	-0.208
112.5	63	14,15	37.5			-0.132	-0.133	-0.158
150	2	14,18	75	-0.134	-0.140	-0.044	-0.033	-0.008

It is clear that the own model give a good results than other models. Hence, own model has been chosen for analysis deflection, bending stress and shear stress, as shown in Fig (6.7 & 6.8).

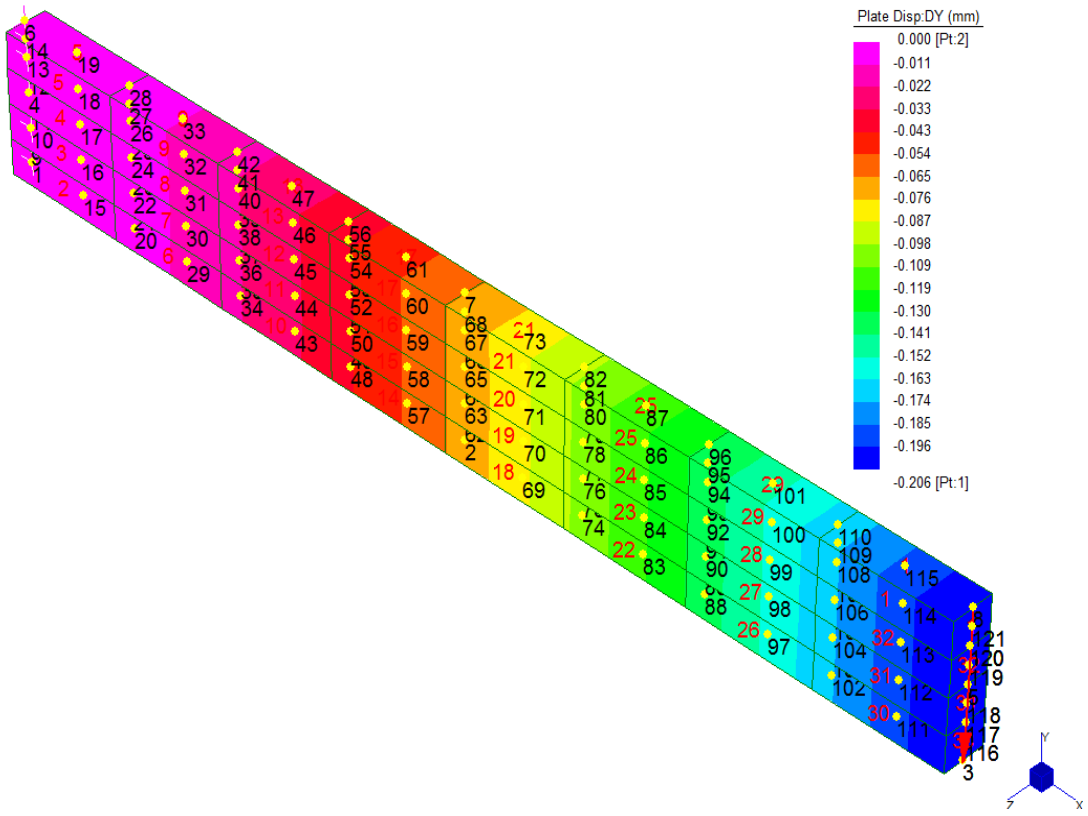

Figure 6.7 Displacement results for thirty-two 8-node elements.

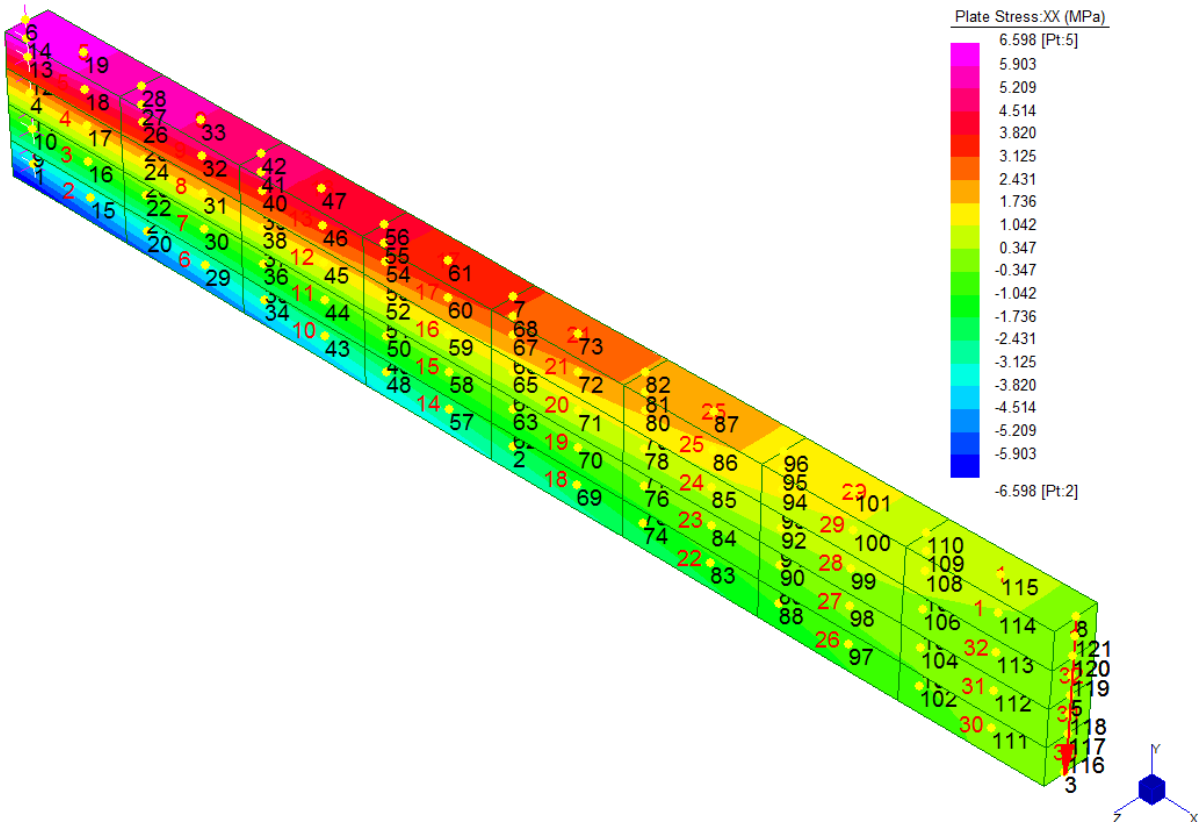

Figure 6.8 Bending stress results for thirty-two 8-node elements.

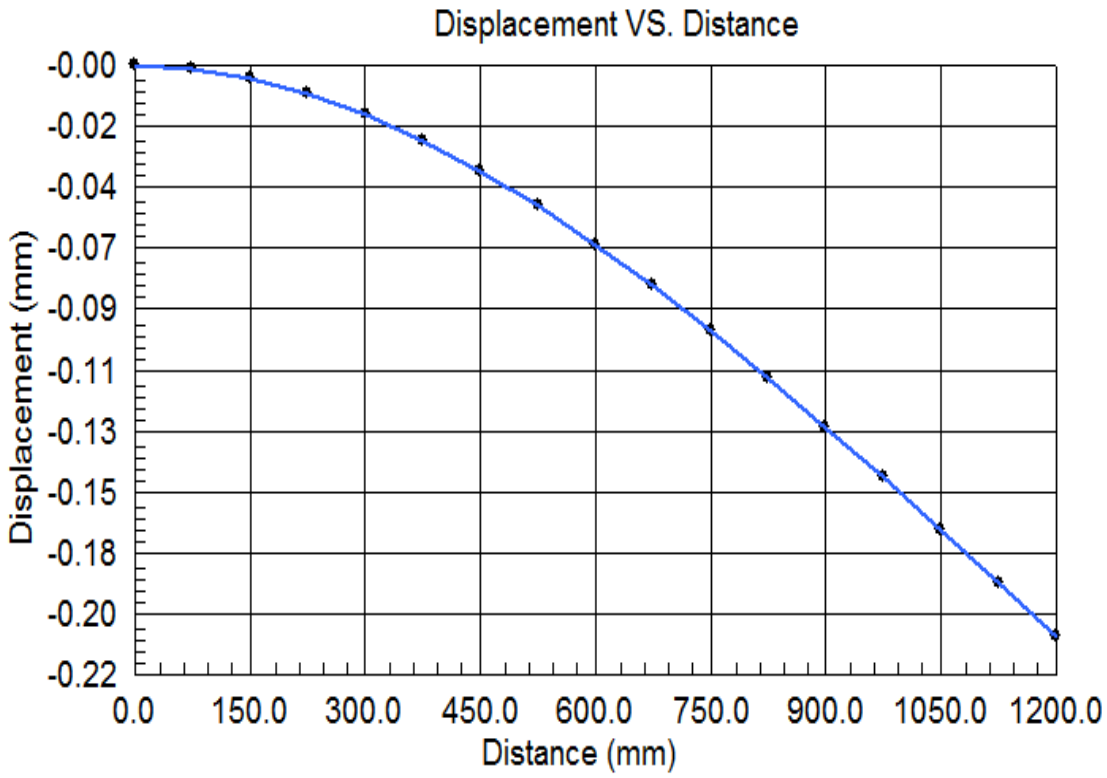

Figure 6.9 Strand 7 graph for deflection along span of the beam (For thirty-two 8-node elements 3D Model).

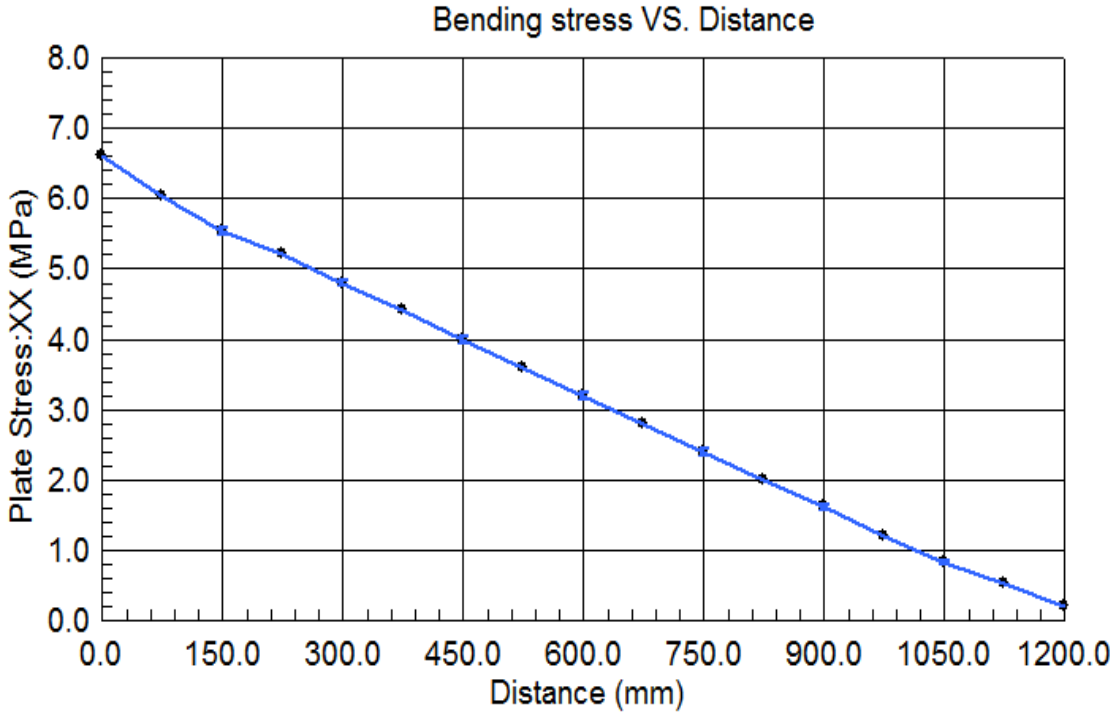

Figure 6.10 Strand 7 graph for bending stress along span of the beam (For thirty-two 8-node elements 3D Model).

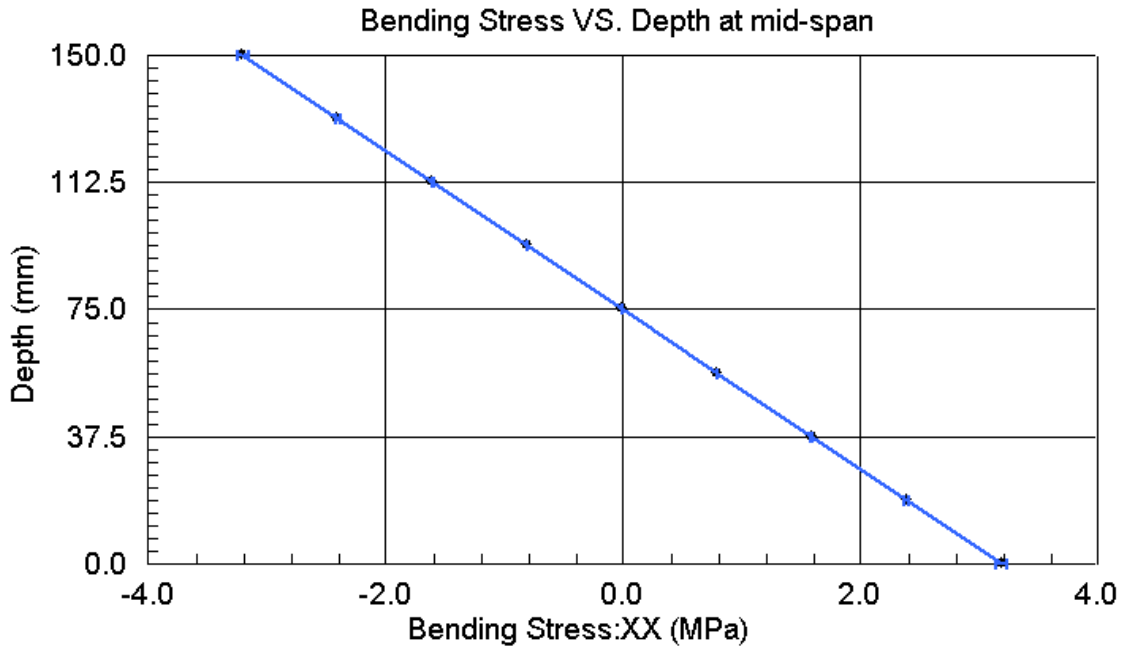

Figure 6.11 Strand 7 graph for bending stress of the cross-section area at mid-span of the beam (For thirty-two 8-node elements 3D Model).

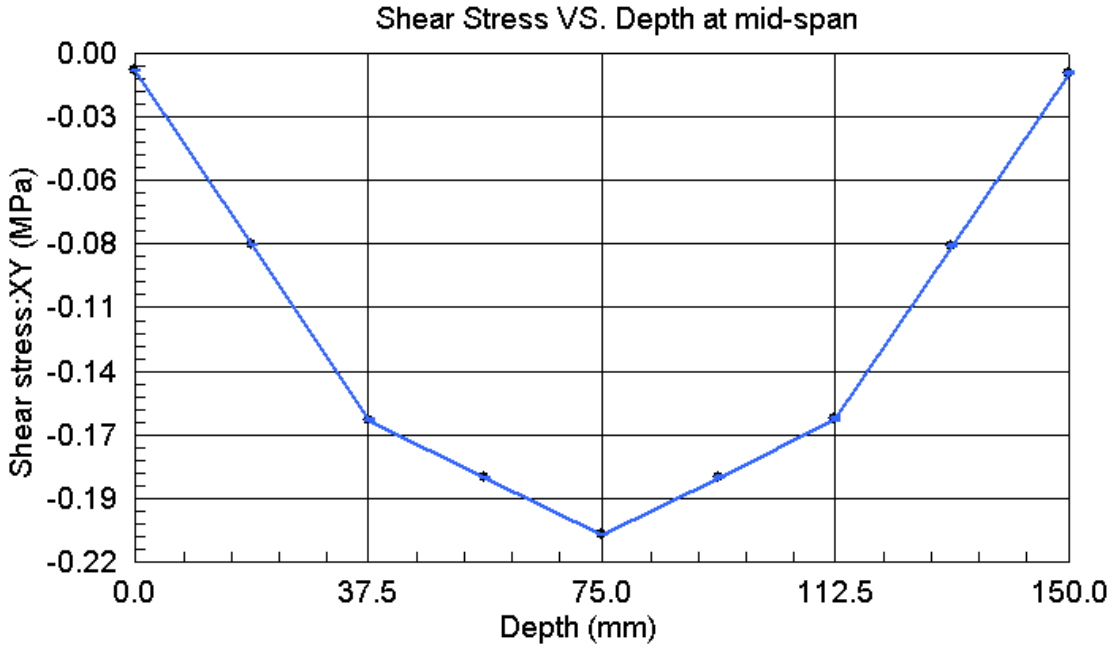

Figure 6.12 Strand 7 graph for shear stress of the cross-section area at mid-span of the beam (For thirty-two 8-node elements 3D Model).

6.2 FEA (Strand 7) Results for chapter (5)

Finite elements analysis has been undertaken for channel section cantilever beam under restrained torsion. The beam dimensions are illustrated in Fig (5.1), plate element properties are shown in table (6.7) and the coordinates for key points are shown in table (6.8). The Strand 7 software has been used for analysis model to determine the behaviour of channel section cantilever beam under torque. The qualities of finite element results depend on the boundary constraint and element material properties. The beam restraint in one end and free in other end. The torque is applied by two imposed point loads at the free end of channel section beam one of them is applied at the flange-web junction and the second point load is applied at the tip of the flange in opposite direction to the first point load and thus, forces of 90 N represent a torque T which is applied to the beam of 9000 N.mm as indicated in Fig (6.13). The finite element analysis has been used to determine the results. Strand 7 procedure is carried out by dividing the both flanges region to (200) elements and the web region to (200) elements by using 8 quadrilateral elements as shown in Fig (6.14). The finite element model was constructed with (400) elements to give the accurate results for warping displacement and warping stresses along the beam in longitudinal direction and around the cross section at mid-span. Also the angle of twist along the beam and warping shear flow around cross-section at mid-span of the beam.

- Warping stress results have been taken from Global axis system in ZZ direction.
- Warping displacement results have been taken from Global axis system in DZ direction.
- Angle of twist results have been taken from Global axis system in RZ direction.
- Shear stress results have been taken from Local axis system in XY direction or can be taken from Global axis system in ZX direction.

Table 6.7 Element property for channel section cantilever beam.

Plate element property				
Materials		Structural		Geometry
Type	Material	Young's Modulus, E (MPa)	Poisson's Ratio, (v)	Membrane Thickness, t (mm)
Plate	Isotropic	69000	0.334	2

Table 6.8 Coordinate key points for channel section cantilever beam.

Key points	Coordinate points		
	X (mm)	Y (mm)	Z (mm)
1	50	0	0
2	25	0	0
3	0	0	0
4	0	50	0
5	0	100	0
6	25	100	0
7	50	100	0
8	50	0	500
9	0	0	500
10	0	100	500
11	50	100	500
12	50	0	1000
13	25	0	1000
14	0	0	1000
15	0	50	1000
16	0	100	1000
17	25	100	1000
18	50	100	1000

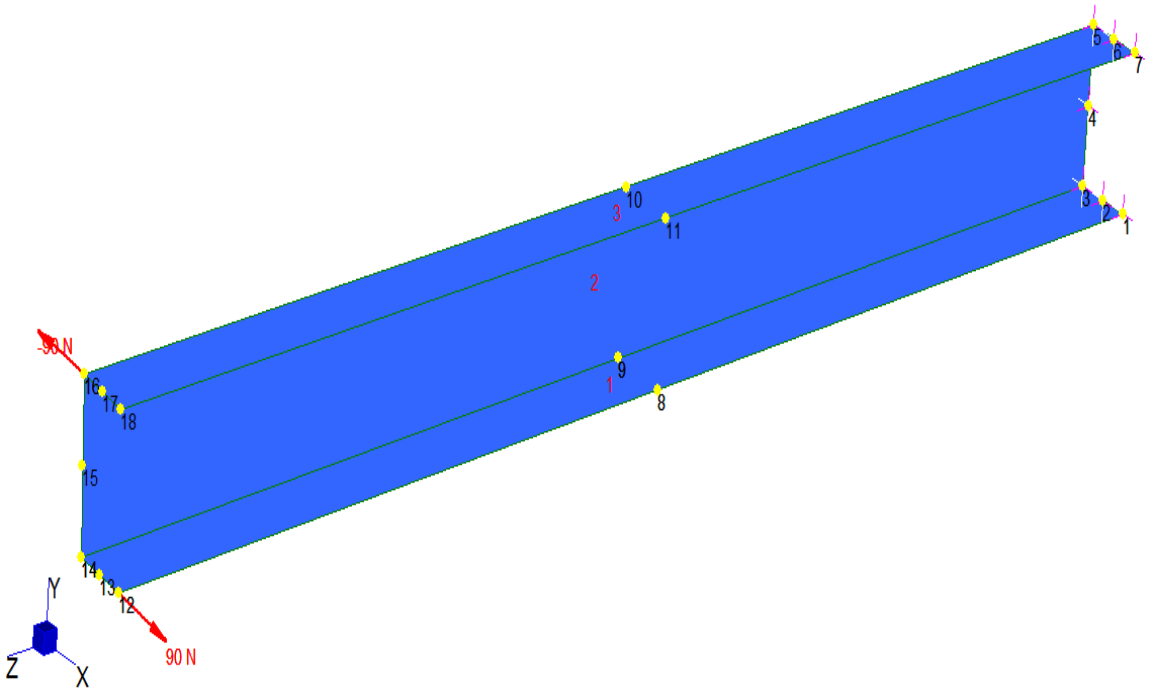

Figure 6.13 A thin-walled channel section cantilever beam subjected to restrained torsion.

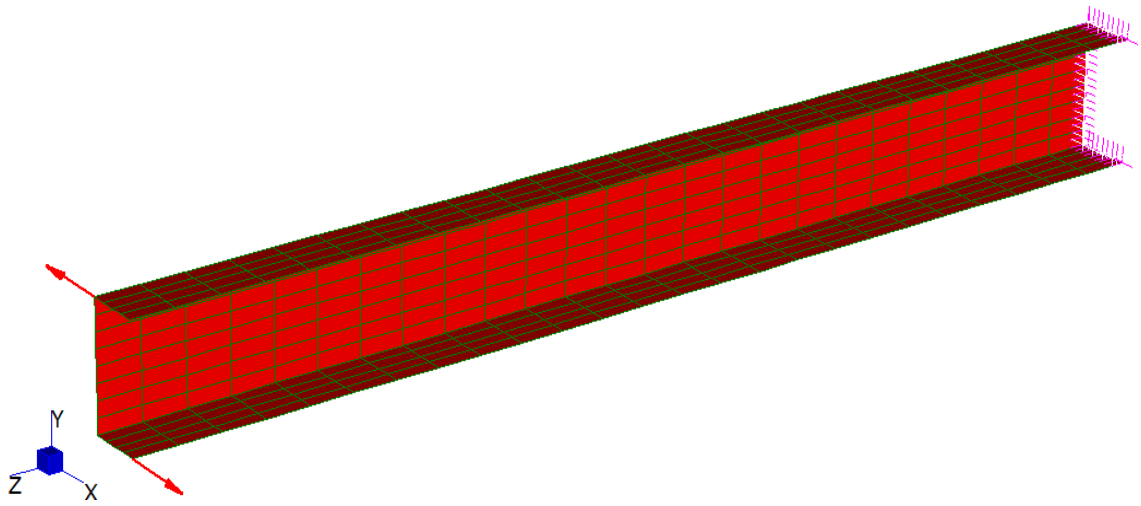

Figure 6.14 A thin-walled channel section cantilever beam with meshing subjected to restrained torsion.

6.3 Warping stress average results obtained by finite elements analysis

(Strand 7)

6.3.1 Warping stress results at top flange tip – along span

The distance (0) mm, start from the fix-end.

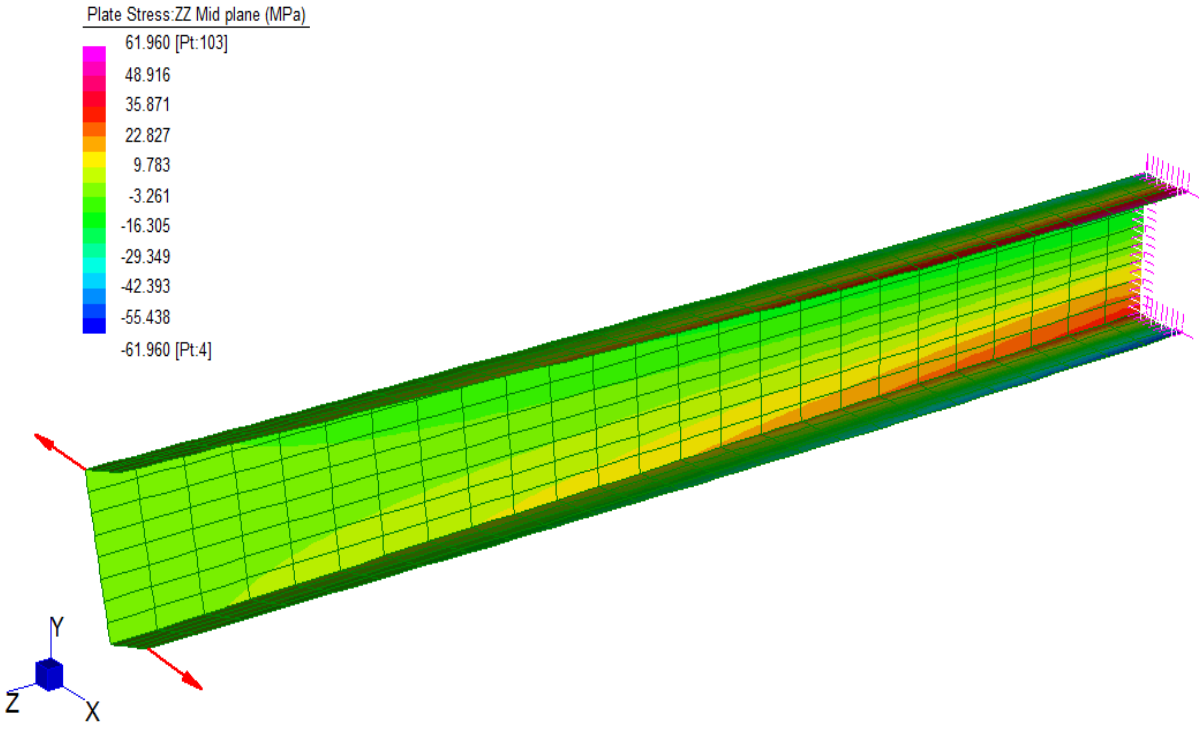

Figure 6.15 Warping stress along the span of the beam (Global Axis System).

Table 6.9 Warping stress results at top flange tip – along span.

Length, Z (mm)	Node number	Plate number	Warping stress, f_{ZZ} (MPa)
0	7	103	61.96
100	404	111	50.586
200	437	119,123	43.787
300	474	131	37.327
400	507	143	31.268
500	11	151	25.720
600	575	163,159	20.434
700	612	171	15.235
800	645	179,183	10.333
900	682	191	5.377
1000	18	199	0

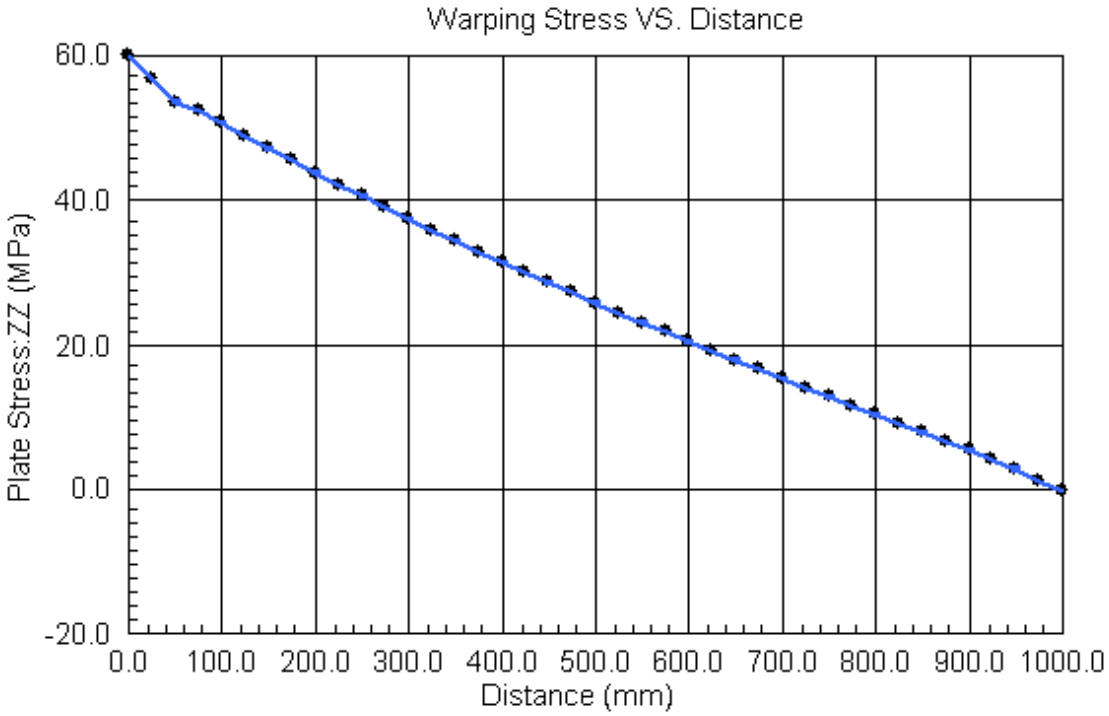

Figure 6.16 Warping stress at top flange tip-along the span of the beam from (Strand7).

6.3.2 Warping stress results at mid-span

Table 6.10 Warping stress results at mid-span.

Distance, s (mm)	Node number	Plate number	Warping stress, f_{ZZ} (MPa)
0	8	52	25.720
50	9	298,55	-15.428
100	1002	301,302	0.000
150	10	305,154	15.428
200	11	151	-25.720

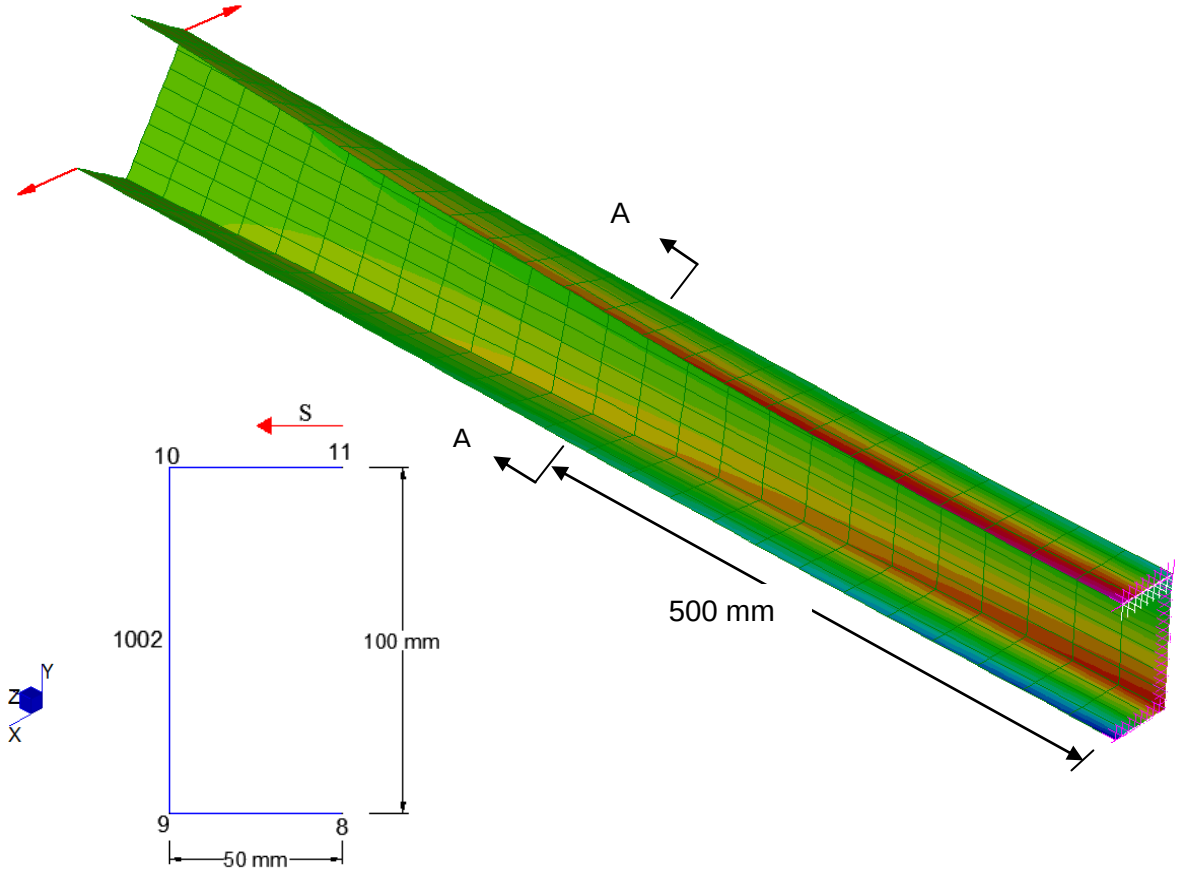

Section A-A at mid-span

Figure 6. 17 Warping stress for a cross-section A-A at mid-span.

6.3.3 Warping stress results at fix-end span

Table 6.11 Warping stress results at fix-end span.

Distance, s (mm)	Node number	Plate number	Warping stress, f_{zz} (MPa)
0	1	4	61.96
50	3	7,202	-36.713
100	4	205,206	0.000
150	5	106,209	36.713
200	7	103	-61.96

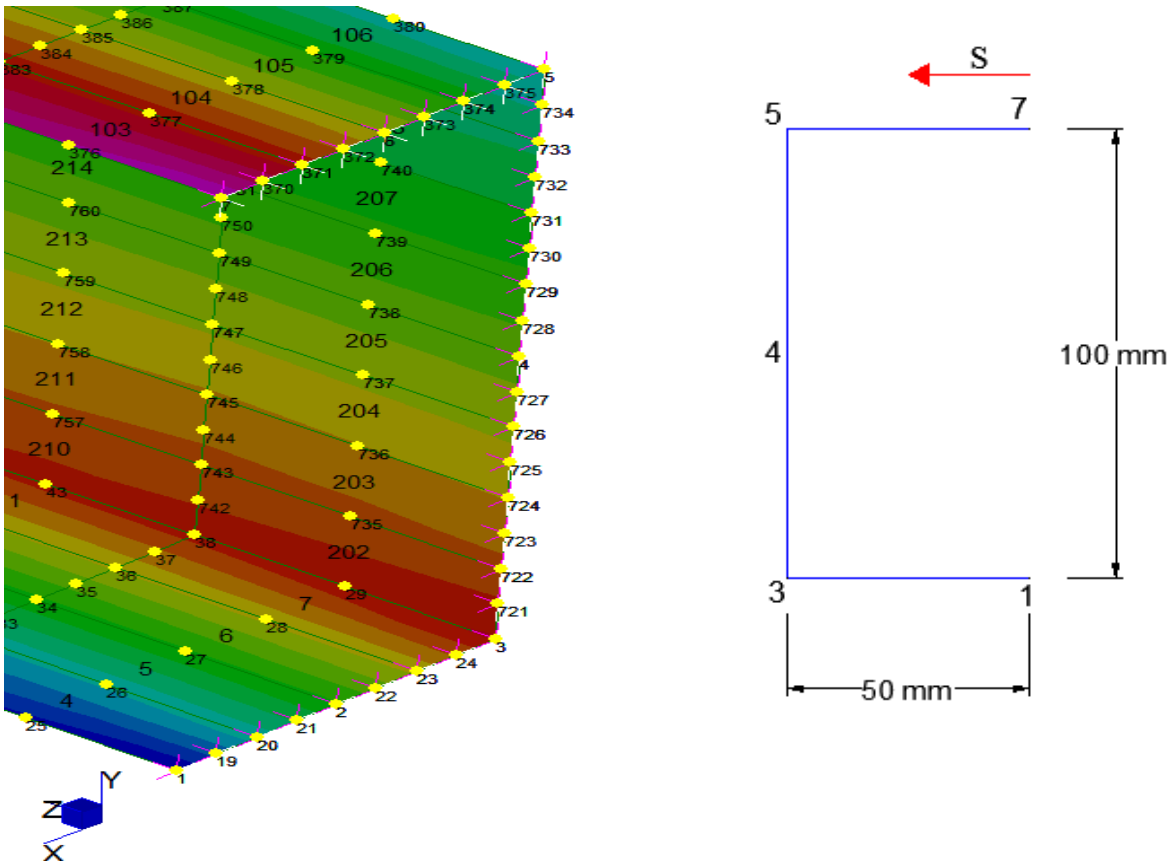

Figure 6.18 Warping stresses round profile at fix-end of the beam.

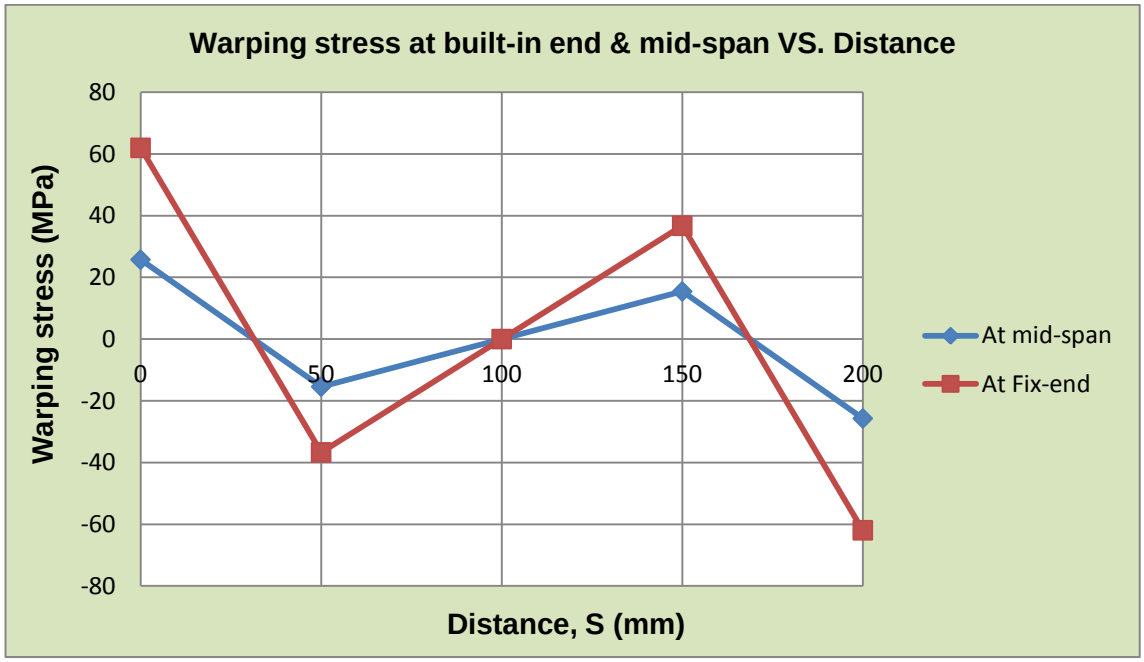

Figure 6.19 Distribution of axial constraint direct stress round section at built-in end and mid-span of the beam from (strand 7) results.

6.4 Warping displacement results obtained by finite elements analysis

(Strand 7)

6.4.1 Warping displacement results at top flange tip – along span

The distance (0) mm, start from the fix-end.

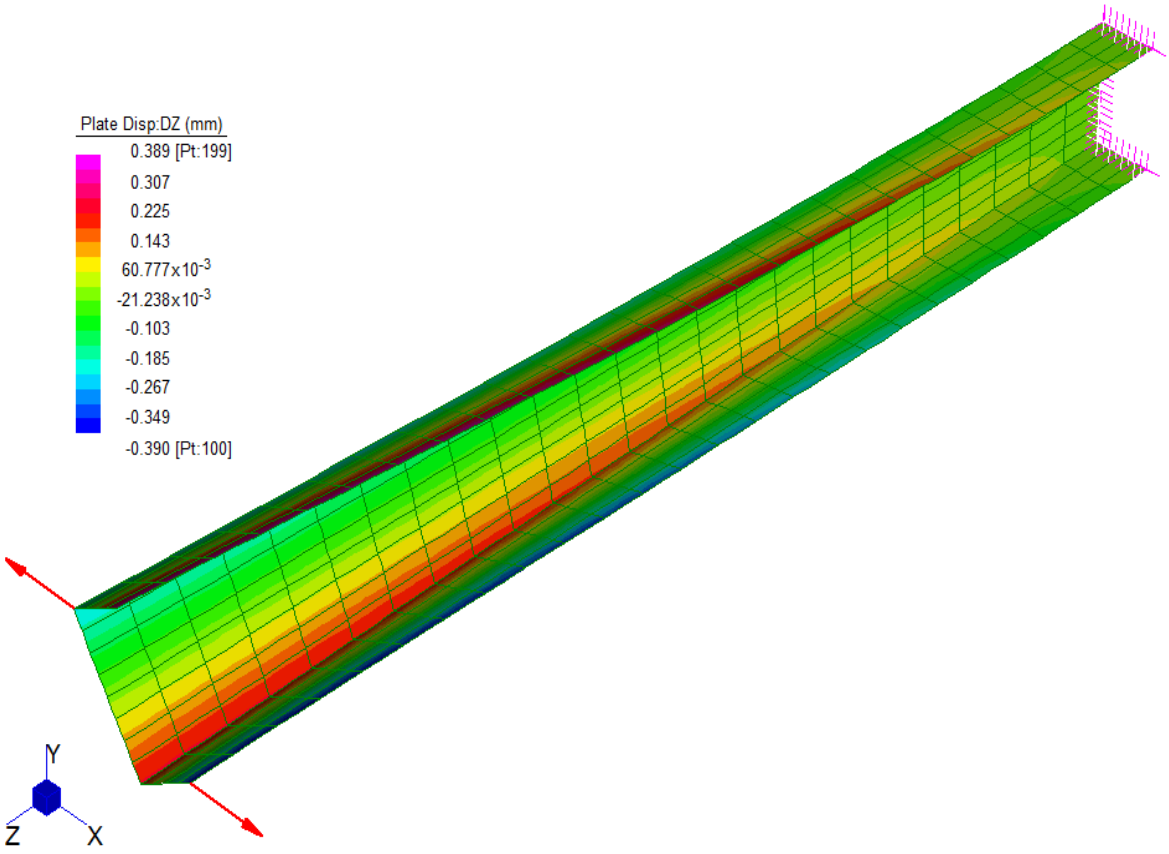

Figure 6. 20 Warping displacement along the span of the beam (Global Axis System).

Table 6.12 Warping displacement results at top flange tip – along span.

Length, Z (mm)	Node number	Warping , DZ (mm)
0	7	0
100	404	0.078
200	437	0.146
300	474	0.205
400	507	0.255
500	11	0.296
600	575	0.329
700	612	0.355
800	645	0.374
900	682	0.385
1000	18	0.389

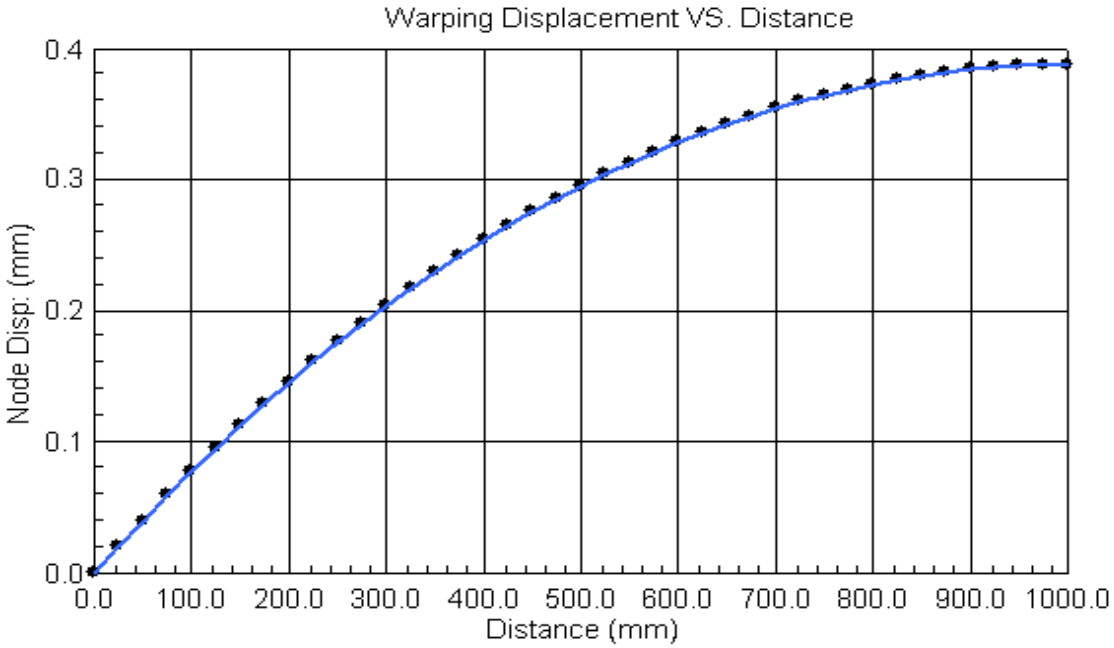

Figure 6.21 Warping displacement at top flange-along the span of the beam from (Strand7).

6.4.2 Warping displacement results at mid-span

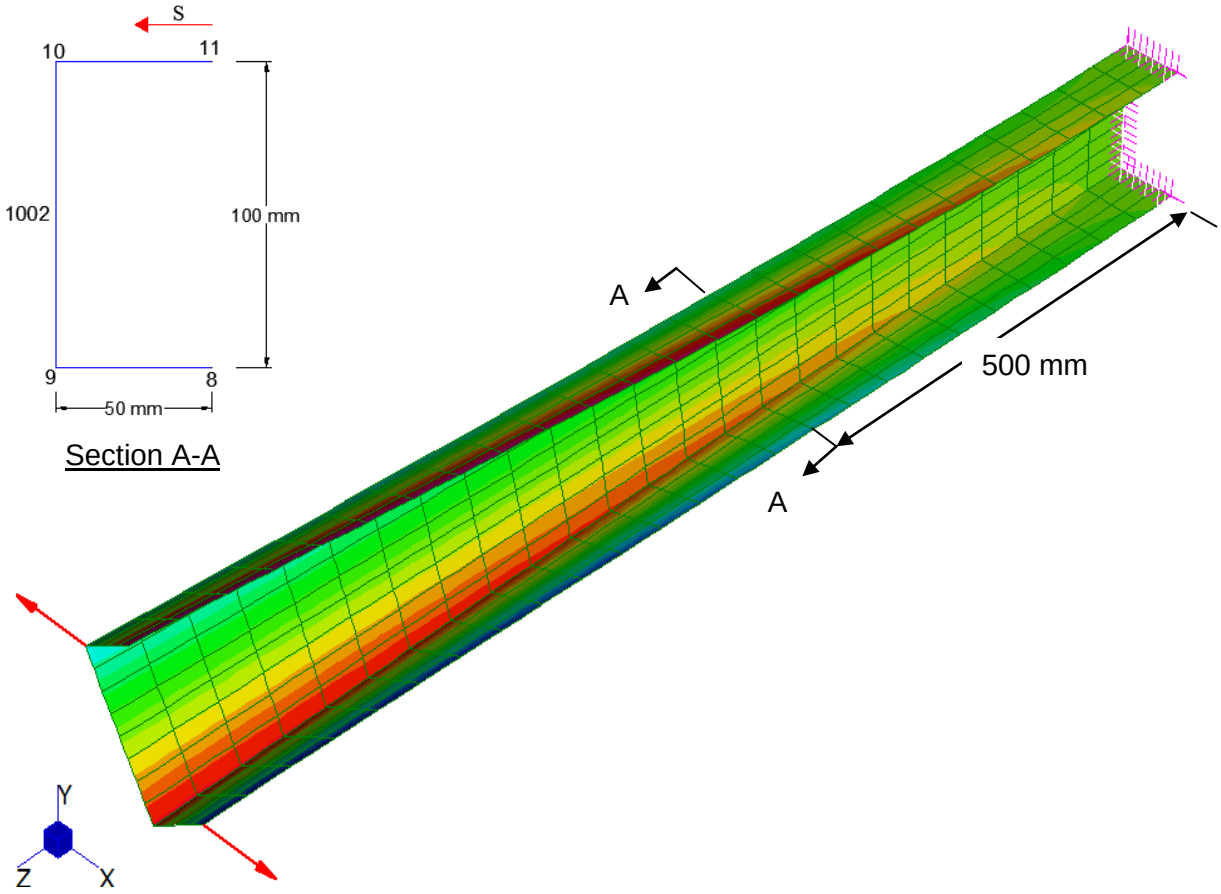

Figure 6.22 Warping displacement for a cross-section A-A at mid-span.

Table 6.13 Warping displacement results at mid-span.

Distance, s (mm)	Node number	Warping stress, DZ (mm)
0	8	0.296
50	9	-0.178
100	1002	0.000
150	10	0.178
200	11	-0.296

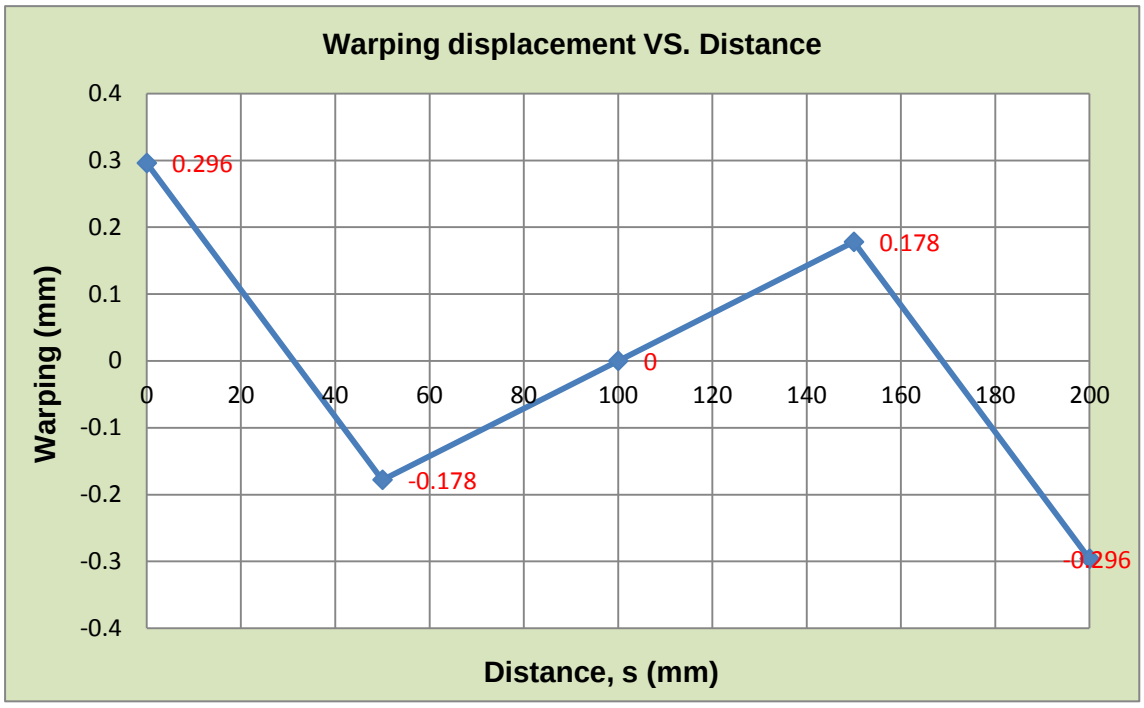

Figure 6.23 Warping displacement round cross-section at mid-span of the beam from (Strand 7) results.

6.5 Angle of twist results obtained by finite elements analysis (Strand 7)

Table 6.14 Angle of twist results at top flange tip – along span.

Length, Z (mm)	Node number	Angle of twist, θ_z $(degree)$
0	7	0.000
100	404	0.185
200	437	0.607
300	474	1.252
400	507	2.095
500	11	3.105
600	575	4.252
700	612	5.506
800	645	6.835
900	682	8.142
1000	18	8.898

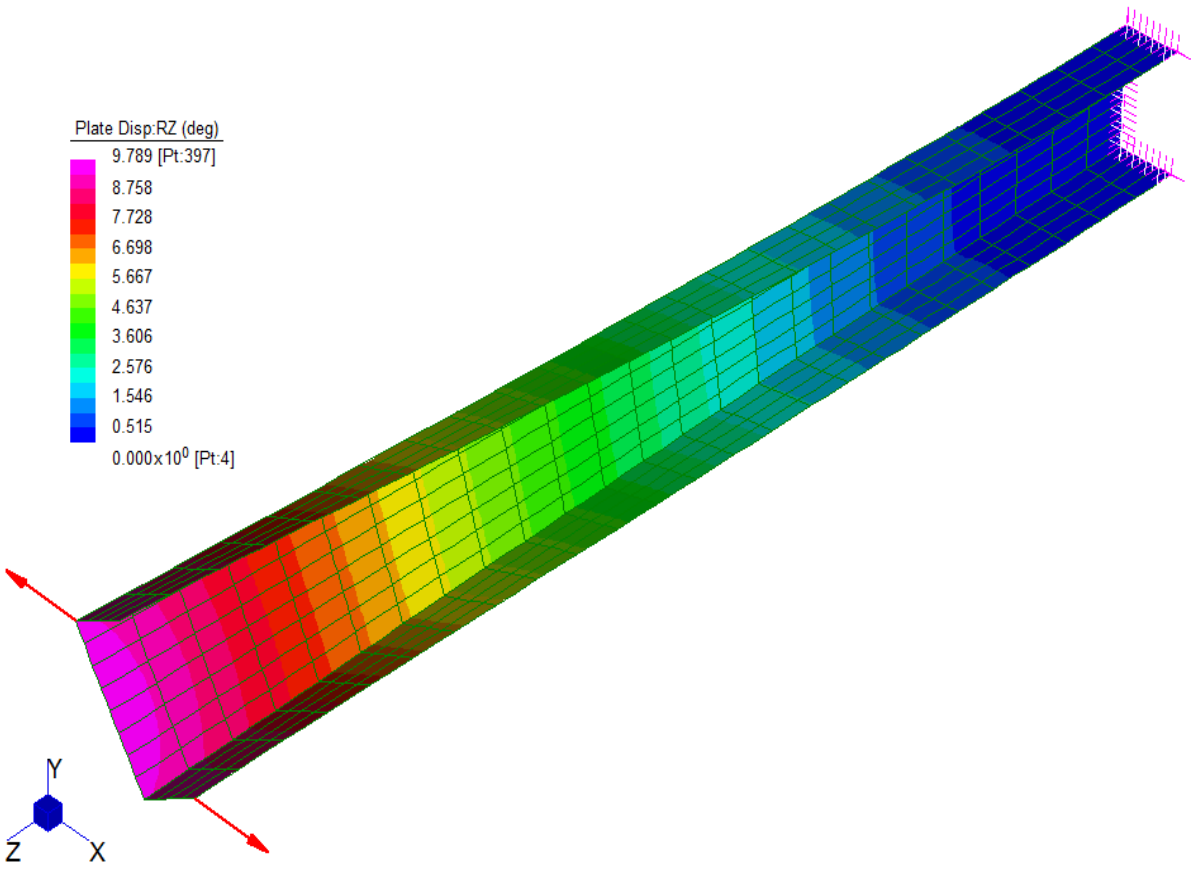

Figure 6.24 Angle of twist along the span of the beam (Global Axis System).

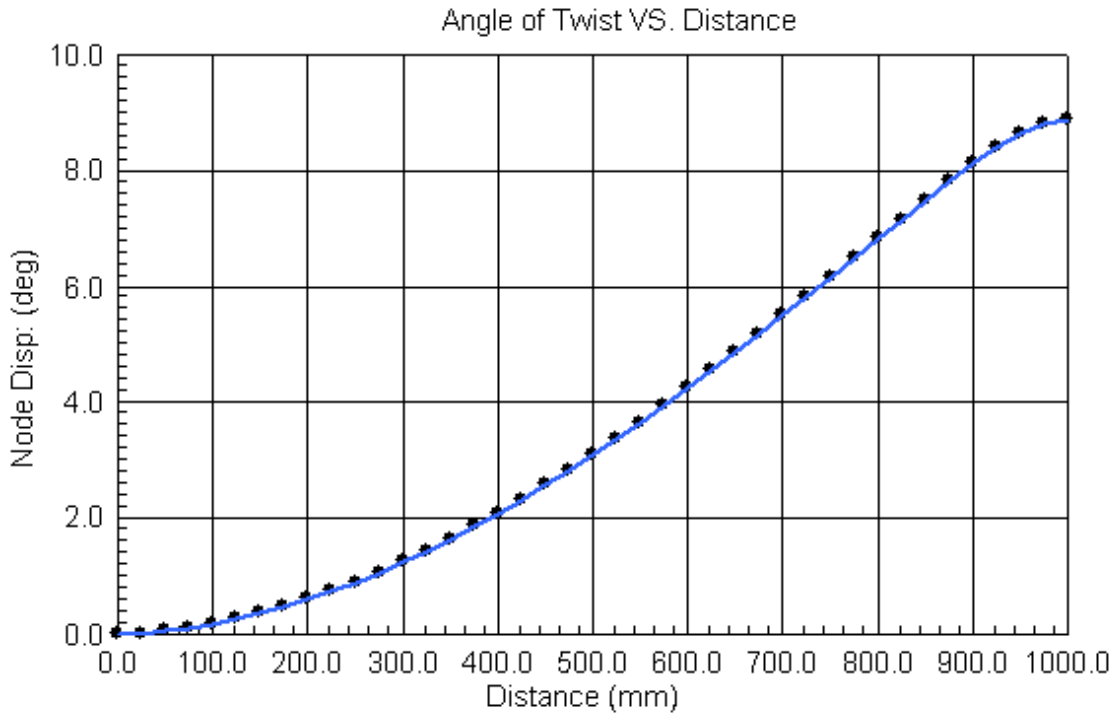

Figure 6.25 Angle of twist at top flange-along the span of the beam from (Strand 7).

6.6 Warping shear flow results round section profile at mid-span obtained by finite element analysis (Strand 7)

Table 6.15 Warping shear flow results at mid-span.

Distance, s (mm)	Node number	Plate number	Thickness, t (mm)	Shear stress, τ_{xy} (MPa)	Shear stress, q_r $(^N/_{mm})$, $q_r = \tau_{xy} \times t$
0	8	52	2	0.000	0.00
25	194	53,54	2	0.846	1.69
50	9	298	2	0.540	1.10
100	1002	301	2	-0.282	-0.56
150	10	305	2	0.540	1.10
175	545	152,153	2	0.846	1.69
200	11	151	2	0.000	0.00

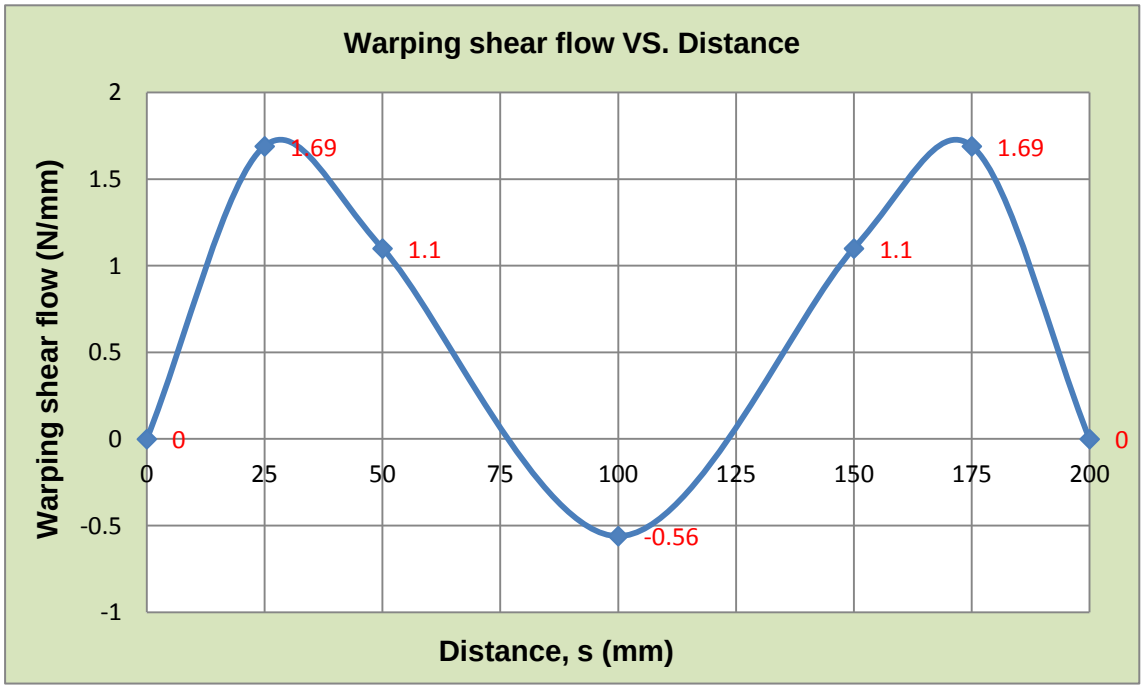

Figure 6.26 Distribution of axial constraint shear flows round cross-section at mid-span of the beam from (Strand 7) results

The combined maximum shear flow distribution around profile at mid-span has been found at node 545 at middle of the flange as shown in table (6.16).

Table 6.16 Combined maximum shear flow result around profile at mid-span.

Distance, s (mm)	Node number	Plate number	Thickness, t (mm)	Shear stress, τ_{xy} (MPa)	Shear stress, q_Γ $(^N/_{mm})$, = $\tau_{xy} \times t$
175	545	152,153	2	10.661	21.3

CHAPTER (7)

COMPARISON OF RESULTS AND DISCUSSION

Comparison between finite element analysis (Strand 7) and theoretical calculation for:

- Rectangular cantilever beam under point load at free end.
- Thin-walled channel cantilever beam under restrained torsional loading.

7.1 Rectangular cantilever beam under point load at free end

In this section the percentage differences are calculated for all the models and compared with the theoretical results. The following tables summarize all the percentage differences for each model.

The deflection results between theoretical and Strand 7 is shown in table (7.1). Also the percentage of error between theoretical and finite element analysis are shown in table (7.2). However, the results have ignored where the theoretical values are smaller than the other Strand 7 modelling results values.

Table 7.1 Vertical deflection results along the top surface of the beam.

Length (mm)	Deflection (mm)						
	Strand 7						Theoretical Result
	Model 1	Model 2	Model 3	Model 4	Model 5	Own Model	
0	0.000	0.000	0.000	0.000	0.000	0.000	0.000
75					-0.001	-0.002	-0.001
150			-0.005	-0.005	-0.005	-0.005	-0.005
225					-0.011	-0.011	-0.010
300			-0.017	-0.018	-0.018	-0.018	-0.017
375					-0.027	-0.027	-0.027
450			-0.037	-0.038	-0.038	-0.038	-0.038
525					-0.051	-0.051	-0.050
600		-0.042	-0.063	-0.064	-0.065	-0.065	-0.064
675					-0.080	-0.080	-0.079
750			-0.093	-0.095	-0.096	-0.096	-0.095
825					-0.113	-0.113	-0.112
900			-0.128	-0.129	-0.130	-0.131	-0.130
975					-0.149	-0.149	-0.148
1050			-0.164	-0.166	-0.168	-0.168	-0.167
1125					-0.187	-0.187	-0.185
1200	-0.142	-0.160	-0.202	-0.204	-0.206	-0.206	-0.204

Table 7.2 Percentage difference for deflection along beam span.

Length (mm)	Theoretical Result	Percentage of error (%)					
		Model 1	Model 2	Model 3	Model 4	Model 5	Own Model
0	0.000	0	0	0	0	-	-
75	-0.001					-	-
150	-0.005			0	0	-	-
225	-0.010					-	-
300	-0.017			0	0	-	-
375	-0.027					-	-
450	-0.038			0	0	-	-
525	-0.050					-	-
600	-0.064		-34.4	-1.6	0	-	-
675	-0.079					-	-
750	-0.095			-2.1	0	-	-
825	-0.112					-	-
900	-0.130			-1.5	-0.8	-	-
975	-0.148					-	-
1050	-0.167			-1.8	-0.6	-	-
1125	-0.185					-	-
1200	-0.204	-30.4	-21.6	-1	0	-	-
Average percentage error difference		30.4	28	1.6	0.7	0	0

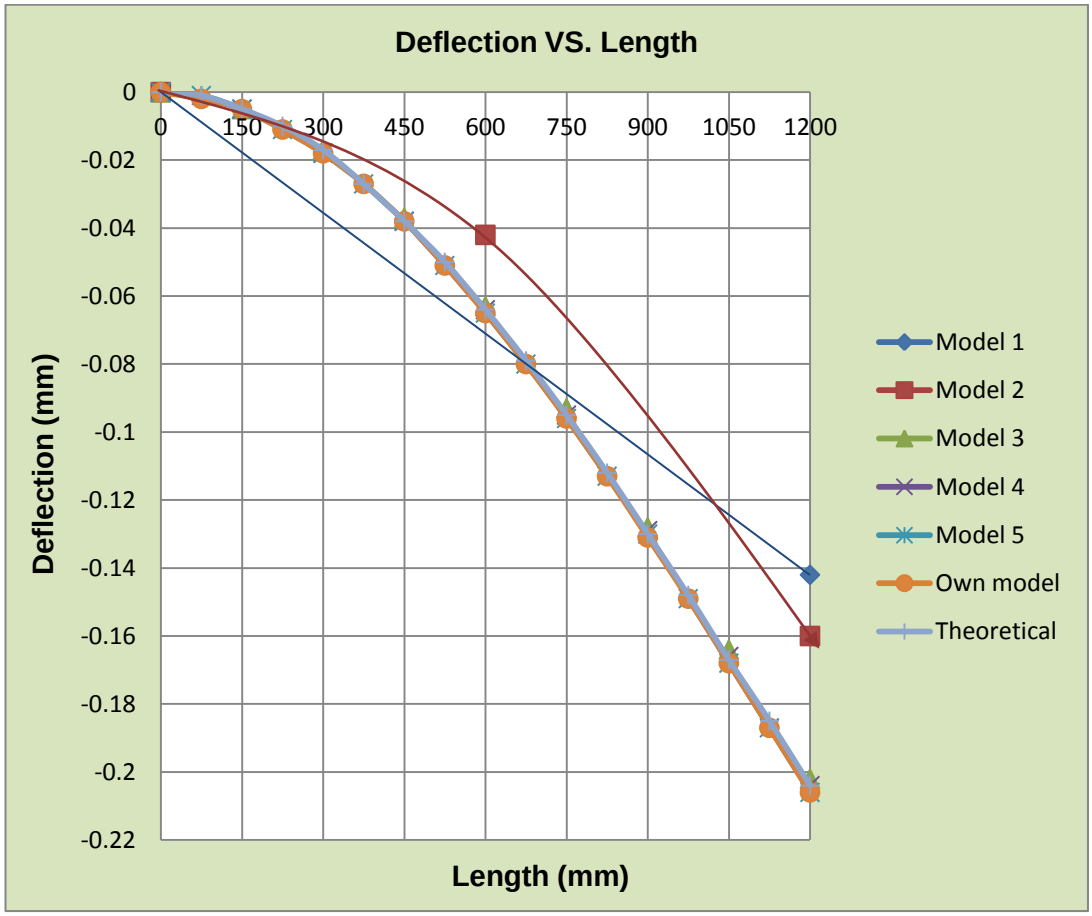

Figure 7.1 Vertical deflection along the top surface of the beam.

In table (7.2); the maximum percentage difference occurs in model 1 (30.4%) and it can be seen that the major difference is in Model 1 and model 2. This difference is clearly shown in Fig (7.1). This difference is because these two models contain just 1 element. The model (3 & 4) contains very small percentage difference and at model (5 & own model) is zero. This shows that the beam should have at least four elements for it to work and to produce accurate results. Therefore, it clear to see that model (3, 4, 5, 6 & own model) are very close to each other. Also the maximum deflections occur at the free end of the beam and it is zero at the fix end of the beam as shown in Fig (7.1).

Table 7.3 Bending stress results along the top surface of the beam.

Length (mm)	Bending Stress on top surface of the beam (MPa)						
	Strand 7						Theoretical Result
	Model 1	Model 2	Model 3	Model 4	Model 5	Own Model	
0	3.204	3.966	6.295	6.352	6.470	6.598	6.400
75					6.049	6.040	6.000
150			5.600	5.646	5.627	5.585	5.600
225					5.180	5.201	5.200
300			4.905	4.939	4.782	4.800	4.800
375					4.404	4.405	4.400
450			4.000	3.981	3.968	4.000	4.000
525					3.599	3.599	3.600
600		3.200	3.414	3.407	3.230	3.249	3.200
675					2.800	2.800	2.800
750			2.400	2.403	2.372	2.448	2.400
825					2.000	1.999	2.000
900			1.413	1.782	1.572	1.647	1.600
975					1.195	1.200	1.200
1050			0.800	0.816	0.818	0.808	0.800
1125					0.480	0.521	0.400
1200	3.196	2.434	0.187	0.216	0.125	0.199	0.000

In table (7.4); the maximum percentage difference for bending stress on the top surface of the beam occurs in model 1 which is (50%) and the value for model 2 is also quite big (38%). This big difference can be seen in Fig (7.2). The two lines for model 1 and model 2 do not match the lines of the rest of the models. The percentage difference for the rest of the models is very small and it is minimum for the own model which shows that the own model is very adequate compared to the others. The same theory applies here also. The more elements, the more adequate is the result. Also the maximum bending stresses occur at the fix end of the beam and it is zero at the free end.

Table 7.4 Percentage difference for bending stress along beam span.

Length (mm)	Theoretical Result	Percentage of error (%)					
		Model 1	Model 2	Model 3	Model 4	Model 5	Own Model
0	6.400	50	38	1.6	0.8		
75	6.000						
150	5.600			0			0.3
225	5.200					0.4	
300	4.800					0.4	0.7
375	4.400					0	0
450	4.000			0	0.5	0.8	0
525	3.600					0	0
600	3.200		0				
675	2.800					0	0
750	2.400			0		1.2	
825	2.000					0	0
900	1.600			11.7		1.7	
975	1.200					0.4	0
1050	0.800			0			
1125	0.400						
1200	0.000						
Average percentage error difference		50	38	6.65	0.65	0.8	0.5

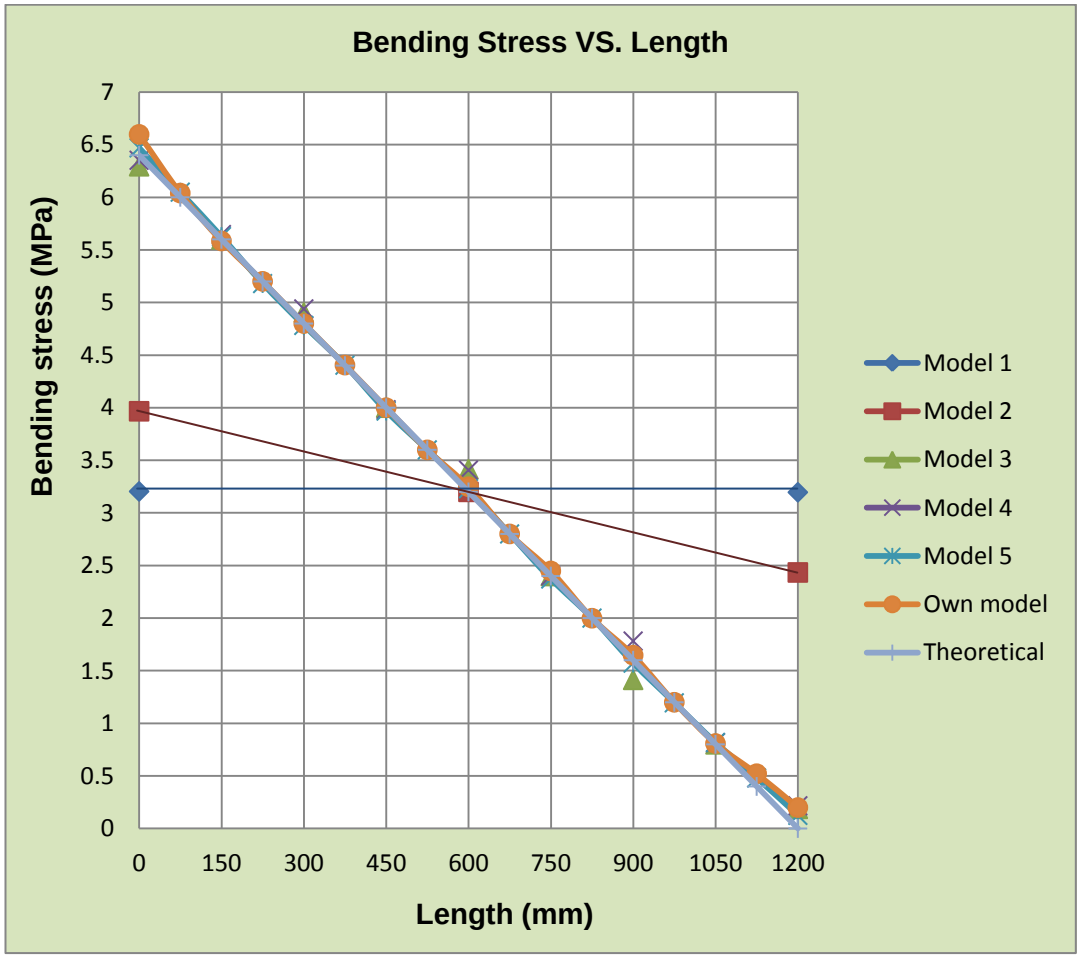

Figure 7.2 Bending stress along the top surface of the beam.

Table 7.5 Bending stress results at mid-span of the beam.

Depth of beam (mm)	Actual depth from neutral axis (mm)	Bending Stress at Mid-Span (MPa)					
		Strand 7					Theoretical Result
		Model 2	Model 3	Model 4	Model 5	Own Model	
0	-75	-3.200	-3.414	-3.410	-3.230	-3.249	-3.200
37.5	-37.5			-1.687	-1.614	-1.597	-1.600
75	0		0.000	0.035	0.001	0.000	0.000
112.5	37.5			1.687	1.614	1.597	1.600
150	75	3.200	3.414	3.410	3.230	3.249	3.200

Table 7.6 Percentage difference for bending stress at mid-span of the beam.

Actual depth from neutral axis (mm)	Theoretical Result	Percentage of error (%)				
		Model 2	Model 3	Model 4	Model 5	Own Model
-75	-3.200	0	6.7	6.6	0.9	1.5
-37.5	-1.600			5.4	0.9	0.2
0	0.000		0	0	0	0
37.5	1.600			5.4	0.9	0.2
75	3.200	0	6.7	6.6	0.9	1.5
Average percentage error difference		0	6.7	6	0.9	0.85

In table (7.6); the percentage difference is zero at model 2. This means that the bending stress at mid-span does not depend on how many elements are present in the model which is not the case for bending stress along the top surface of the beam. Also Fig (7.3) shows how the results for the different models are almost similar. All the graphs nearly fit on the same line. The maximum bending stresses occur at the surface of the cross section of the beam and it is zero at neutral axis. Moreover, it varies linearly as illustrated in Fig (7.3).

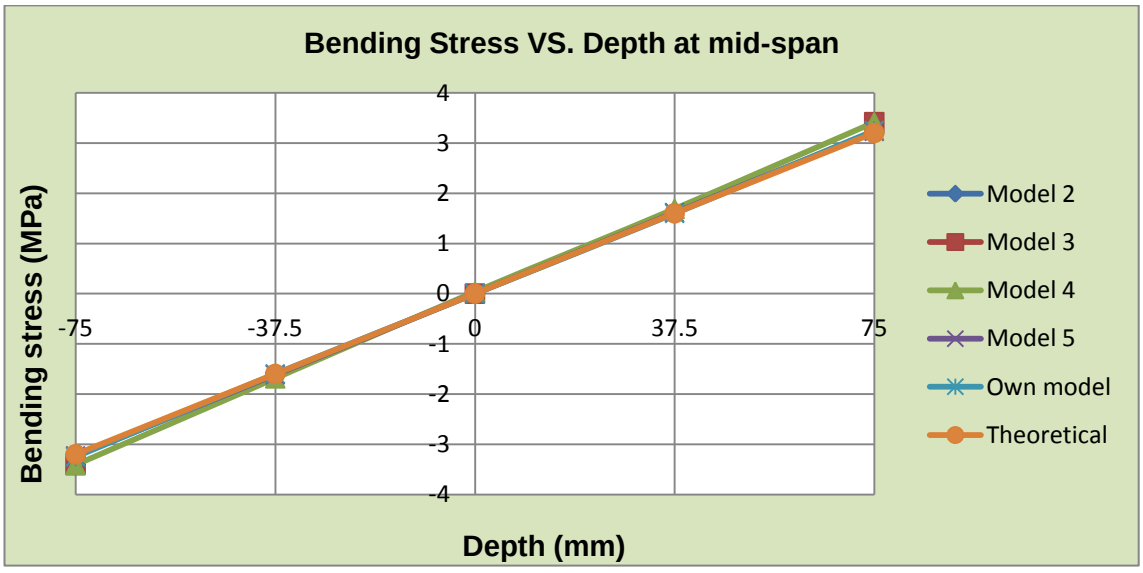

Figure 7.3 Bending stress at mid-span of the beam.

Table 7.7 Shear stress results at mid-span of the beam.

Depth of beam (mm)	Actual depth from neutral axis (mm)	Shear Stress at Mid-Span (MPa)					
		Strand 7					Theoretical Result
		Model 2	Model 3	Model 4	Model 5	Own Model	
0	-75	-0.134	-0.140	-0.044	-0.033	-0.008	0.000
37.5	-37.5			-0.132	-0.133	-0.158	-0.150
75	0	0.000	-0.133	-0.231	-0.234	-0.208	-0.197
112.5	37.5			-0.132	-0.133	-0.158	-0.150
150	75	-0.134	-0.140	-0.044	-0.033	-0.008	0.000

Table 7.8 Percentage difference for shear stress at mid-span of the beam.

Actual depth from neutral axis (mm)	Theoretical Result	Percentage of error (%)				
		Model 2	Model 3	Model 4	Model 5	Own Model
-75	0.000	-	-	-	-	-
-37.5	-0.150			12	11	5
0	-0.197		32	17	18	5.6
37.5	-0.150			12	11	5
75	0.000	-	-	-	-	-
Average percentage error difference		-	32	13.7	13	5.2

In table (7.8); the maximum percentage difference occurs in model 3 (32%) and in Fig (7.4) it can be seen that the major difference is in model 2 and 3. The model (4 & 5) contains very small percentage difference and at own model is (5.2%) which is a better value. This shows that the beam should have at least four elements for it to work and to produce accurate results. The maximum shear stresses occur at the centre of the cross section of the beam as shown in Fig (7.4).

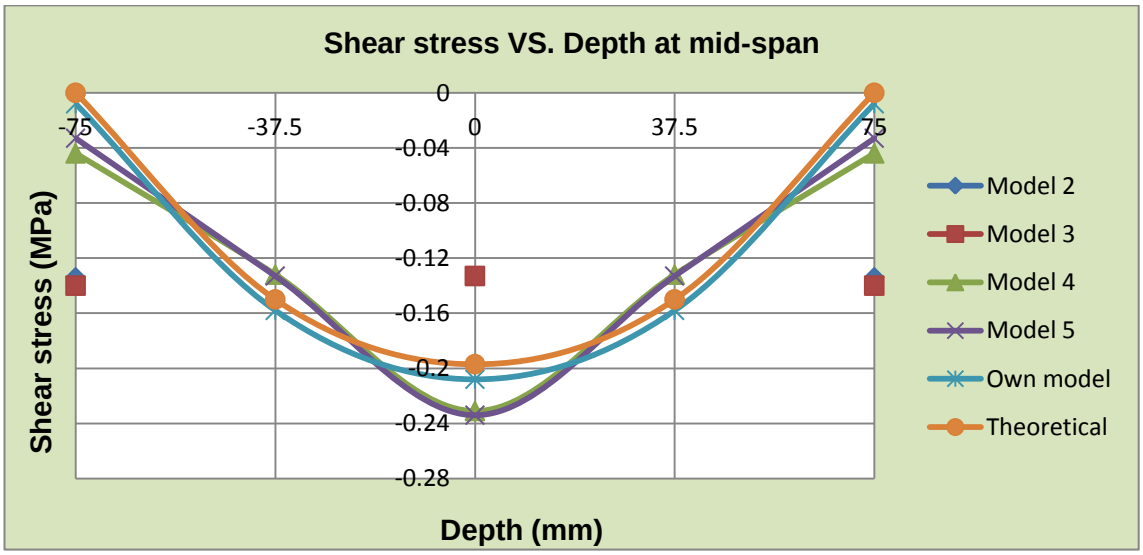

Figure 7.4 Shear stress at mid-span of the beam.

7.2 Thin-walled C-channel cantilever beam under restrained torque loading

In this section the percentage differences are calculated between theoretical and finite element analysis (Strand 7). It is very important to check and compare theoretical results with finite element analysis to obtained accurate results.

7.2.1 Comparison of warping at top flange tip–along the span

Table 7.9 Percentage of error for warping displacement results at flange tip–along span.

Length, Z (mm)	Warping displacement (mm)		Percentage of error (%)
	Theoretical, (W)	Strand 7, (DZ)	
0	0.00	0.000	0
100	0.08	0.078	2.5
200	0.16	0.146	8.75
300	0.22	0.205	6.8
400	0.27	0.255	5.6
500	0.31	0.296	4.5
600	0.35	0.329	6
700	0.38	0.355	6.6
800	0.40	0.374	6.5
900	0.41	0.385	6.1
1000	0.41	0.389	5
Average percentage error (%)			5.8

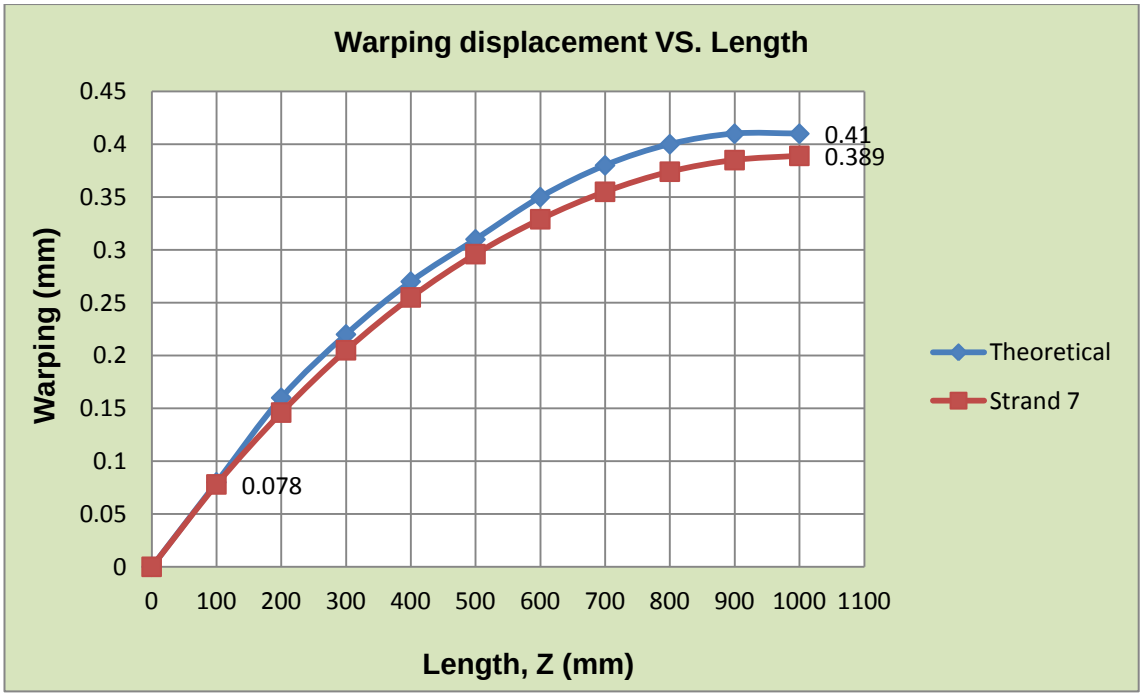

Figure 7.5 Comparison of warping at top flange tip–along the span between theoretical and Strand 7.

In the table (7.9); it shows that the average percentage along the span between theoretical and Strand 7 is (5%) which is small value and good adjustment for channel section behaviour under constraint torsion. In the Fig (7.5); the warping displacement is linearly started from zero (mm) to 0.078 (mm), which point (0.078) is intersection point between theoretical and Strand 7 at distance of 100 mm, then warping from that point is started non linearly till distance of 1000 mm. It is clear that theoretical value is not match exactly with Strand 7 by 5% differences. However, at both state the maximum warping displacement occurs at the free end of the thin-walled channel section cantilever beam under constraint torsion and it is zero at the fix end of the beam.

7.2.2 Comparison of warping round cross-section at mid-span

Table 7.10 Percentage of error for warping displacement at mid-span.

Distance, s (mm)	Warping displacement (mm)		Percentage of error (%)
	Theoretical, (W)	Strand 7, (DZ)	
0	0.31	0.296	4.5
50	-0.19	-0.178	6.3
100	0.00	0.000	0
150	0.19	0.178	6.3
200	-0.31	-0.296	4.5
Average percentage error (%)			5.4

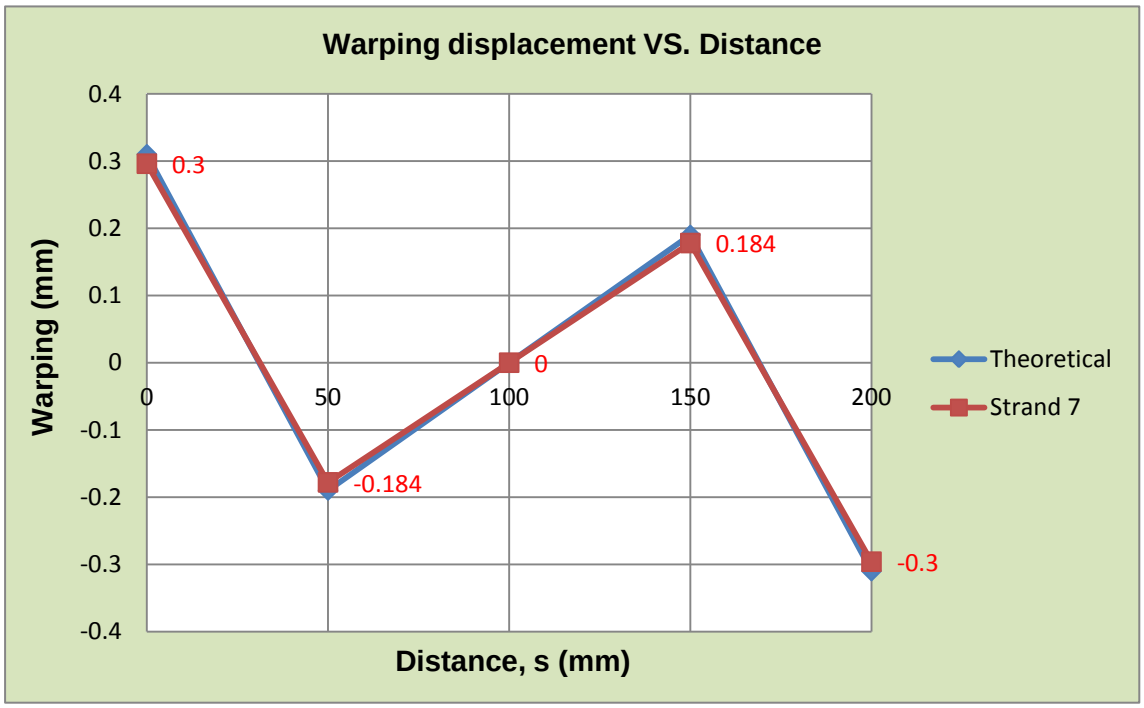

Figure 7.6 Comparison of warping at mid-span between theoretical and Strand 7.

The average percentage error is (5.4%) between theoretical and Strand 7 as shown in table (7.10). However, Fig (7.6) shows how the results between theoretical and Strand 7 are almost similar. Moreover, both graphs nearly fit on the same line and warping displacement are varies linearly at the flange and the web, and it is zero at the middle of the web as indicated. Also, the values which are shown on Fig (7.6) are representing the average value between theoretical and Strand 7.

7.2.3 Comparison of warping stress at top flange tip–along the span

Table 7.11 Percentage of error for warping stress results at flange tip–along span.

Length, Z (mm)	Warping stress (MPa)		Percentage of error (%)
	Theoretical, (f_w)	Strand 7, (f_{ZZ})	
0	62	61.96	0
100	53.8	50.586	6
200	46.3	43.787	5.4
300	39.4	37.327	5.3
400	32.9	31.268	5
500	26.8	25.720	4
600	21.1	20.434	3.2
700	15.6	15.235	2.3
800	10.3	10.333	0
900	5.1	5.377	5.4
1000	0	0	0
Average percentage error (%)			4.6

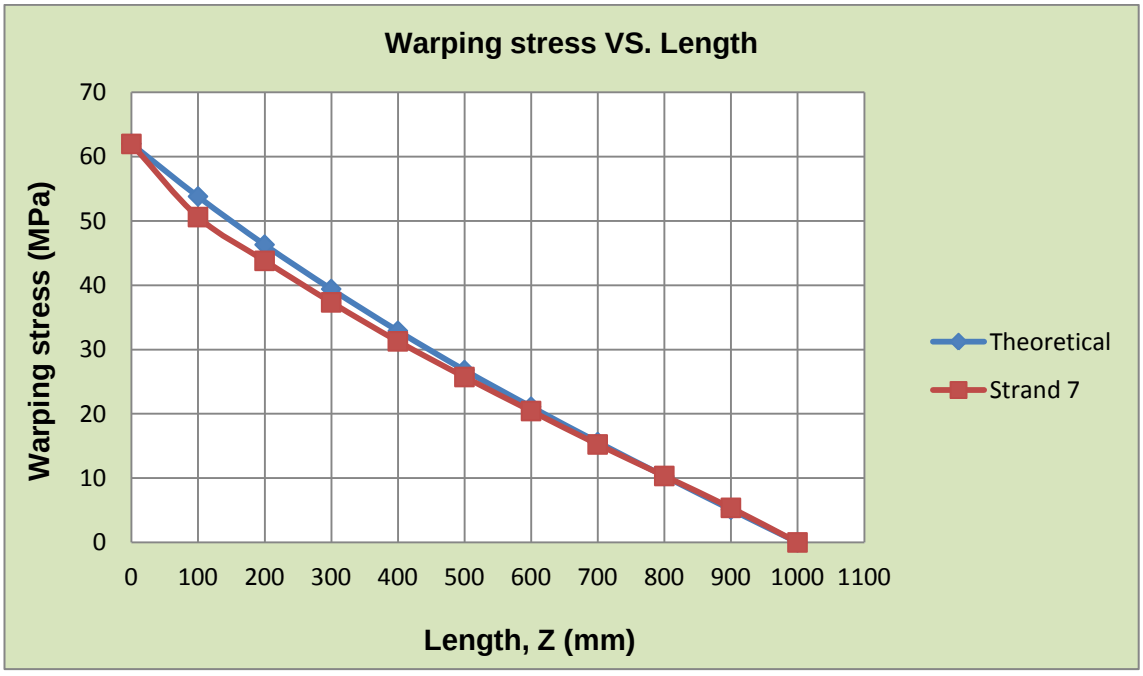

Figure 7.7 Comparison of warping stress at top flange tip-along span between theoretical and Strand 7.

In the table (7.11); the average percentage error is (4.6%) between theoretical and strand 7. Also Fig (7.7) shows how the results between theoretical and Strand 7 are almost similar. Moreover, the maximum warping stresses occur at the restrained end of the beam and it is zero at the free end because there is no axial constraint. Fig (7.8) is clearly shows the differences between warping displacements and warping stresses versus length of the beam. A good agreement is obtained between theoretical and Strand 7 results for channel section behaviour under constraint torsion because the finite element model was constructed with (400) elements which is indicated in Fig (6.14). In addition the maximum warping displacement occurs at the free end of the beam and it is zero at the fix end due to St. Venant theory.

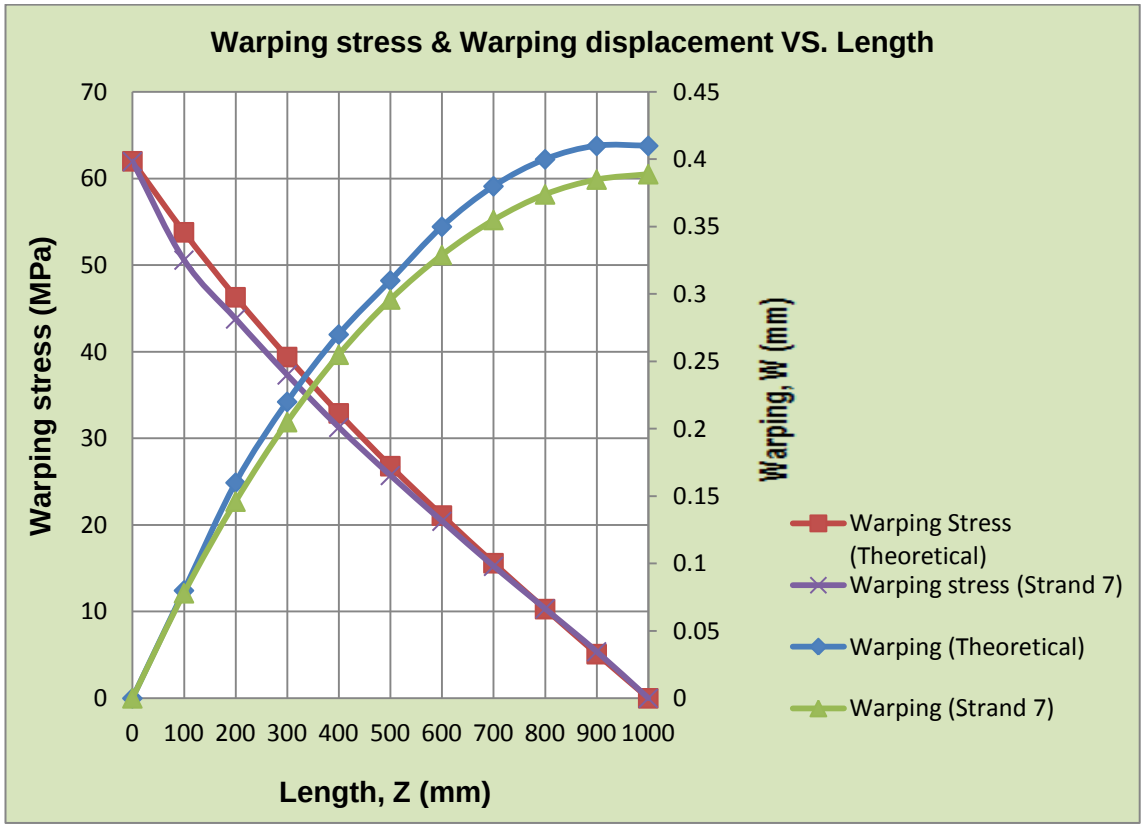

Figure 7.8 Comparison of warping displacement & warping stress at top flange tip- along the span between theoretical and strand 7.

7.2.4 Comparison of warping stress round cross-section at mid-span & built-in end

Table 7.12 Percentage of error for warping stress at mid-span.

Distance, s (mm)	Warping stress (MPa)		Percentage of error (%)
	Theoretical, (f_w)	Strand 7, (f_{zz})	
0	39.1	25.720	34
50	-23.4	-15.428	34.1
100	0.00	0.000	0
150	23.4	15.428	34
200	-39.1	-25.720	34.1
Average percentage error (%)			34

Table 7.13 Percentage of error for warping stress at built-in end.

Distance, $s(mm)$	Warping stress (MPa)		Percentage of error (%)
	Theoretical, (f_w)	Strand 7, (f_{zz})	
0	62.5	61.96	0
50	-37.5	-36.713	2.1
100	0.00	0.000	0
150	37.5	36.713	2.1
200	-62.5	-61.96	0
Average percentage error (%)			2.1

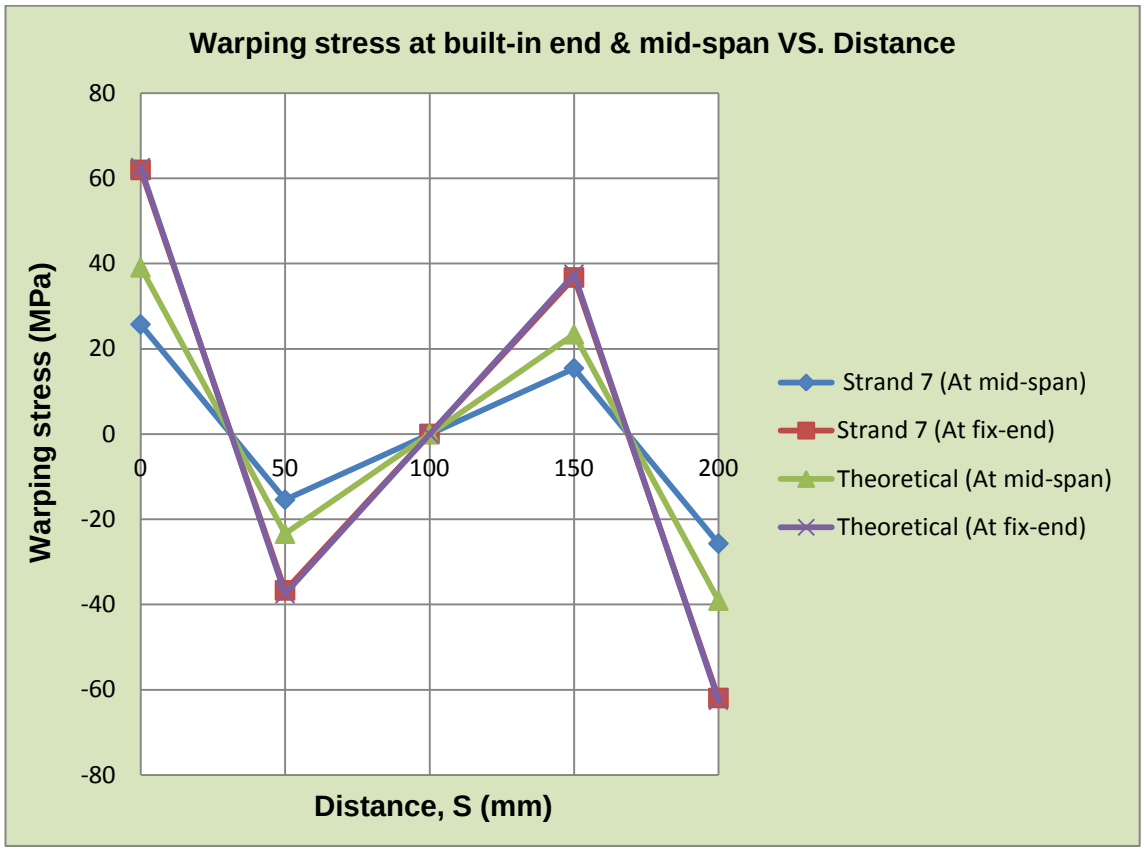

Figure 7.9 Comparison of distribution of axial constraint direct stress around cross section between theoretical and strand7.

In tables (7.12 & 7.13); the average percentage error at mid-span is (34%) which is quite bigger than the average percentage error at fix-end of the beam, which is (2.1%) this differences between mid-span and fix-end is refer to constraint torsion at fix-end of the beam. However, the angle of rotation is zero at fix-end.

Fig (7.9) shows how the results between theoretical and Strand 7 are almost similar for warping stress at built-end and both graphs nearly fit on the same line. Also it is noted that warping stress at mid-span is slightly different between theoretical and Strand 7 due to occurs rotation at mid-span. The warping stresses are varies linearly at the flanges and the web, and it is zero at the middle of the web for both cases as indicated in Fig (7.9). Furthermore, the maximum warping stresses occur at the flange tip where the distance (s = 0). The improved accuracy and precision between theoretical and Strand 7 results is provided by increasing the number of elements in finite element analysis.

7.2.5 Comparison of angle of twist at top flange tip–along the span

Table 7.14 Percentage of error for angle of twist results at flange tip–along span.

Length, Z (mm)	Angle of twist, θ_z $(degree)$		Percentage of error (%)
	Theoretical	Strand 7	
0	0.000	0.000	0
100	0.099	0.185	46.5
200	0.551	0.607	9
300	1.248	1.252	0
400	2.155	2.095	2.8
500	3.237	3.105	4.1
600	4.460	4.252	4.7
700	5.796	5.506	5
800	7.215	6.835	5.3
900	8.688	8.142	6.3
1000	10.188	8.898	12.7
Average percentage error (%)			10.7

In the table (7.14); the average percentage error is (10.7%) between theoretical and strand 7 which identify a good agreement. Also Fig (7.10) shows how the results between theoretical and Strand 7 are almost similar. Moreover, the maximum angle of rotation occurs at the free end of the beam and it is zero at the built-in of the beam because there is axial constraint at fix end.

Fig (7.10) is clearly shows that the angle of rotation is non-linearly changes along thin-walled channel section cantilever beam under restrained torsion.

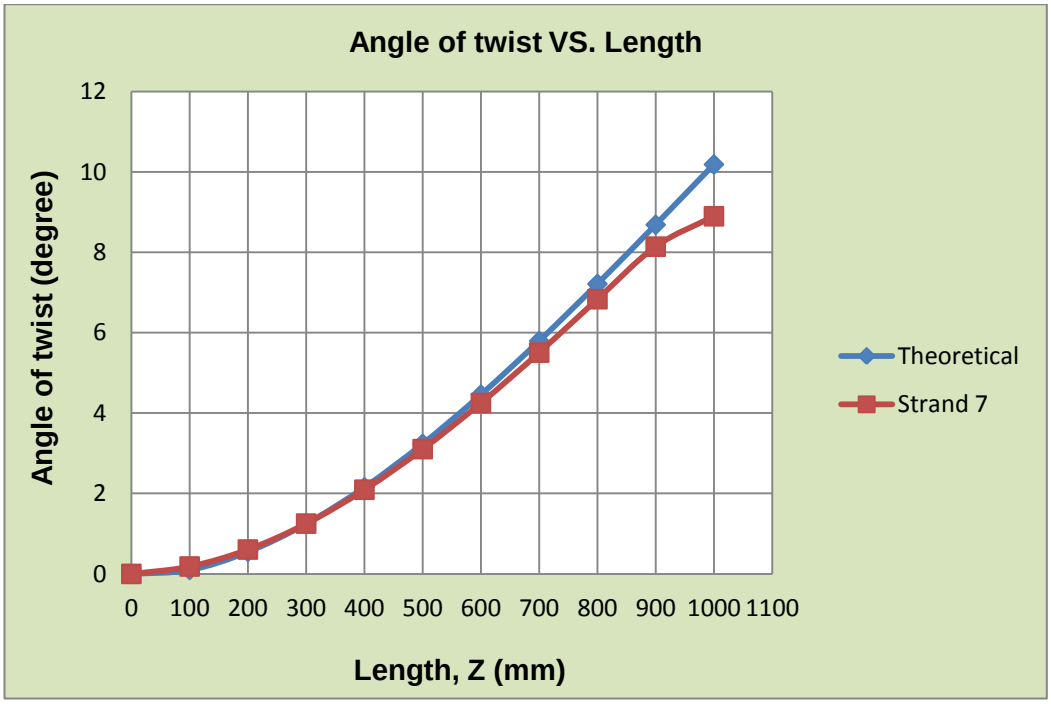

Figure 7.10 Comparison of angle of twist at top flange tip-along the span due to axial constraint.

7.2.6 Comparison of angle of twist at free end due to axial constraint

To check the angle of twist at the free end due to the effect of constraint and compared with St. Venant rotation for channel thin-walled cantilever beam under restrained torsional loading shown in Fig (7.11) illustrates the stiffening effect of axial constraint;

$$\theta = \frac{T\,z}{G\,J} = \frac{9000\ \times 1000}{25862\ \times 533} = 0.653\,rad$$

$$\theta = 0.653 \times \frac{180}{\pi} = 37.4^{\,o} \qquad (\,due\ to\ St.Venant)$$

From table (7.14) the angle of twist at free end is:

$$\theta = \ 10.188^{\,o} \qquad (\,due\ to\ axial\ constraint)$$

Table 7.15 Angle of twist at free end.

Length (mm)	Angle of twist, $\theta_z\ (degree)$		Percentage of error (%)
	St. Venant	Wagner	
0	0	0	0
1000	$37.4^{\,o}$	$10.188^{\,o}$	72.6
Average percentage error (%)			72.8

In the table (7.15); the average percentage error is (72.8%), which is very high due to axial constraint. The decrease in the effect of axial constraint towards the free end of the beam is demonstrated by the variation of the St. Venant (T_J) and Wagner (T_W) torques along the length of the beam as shown in Fig (7.11).

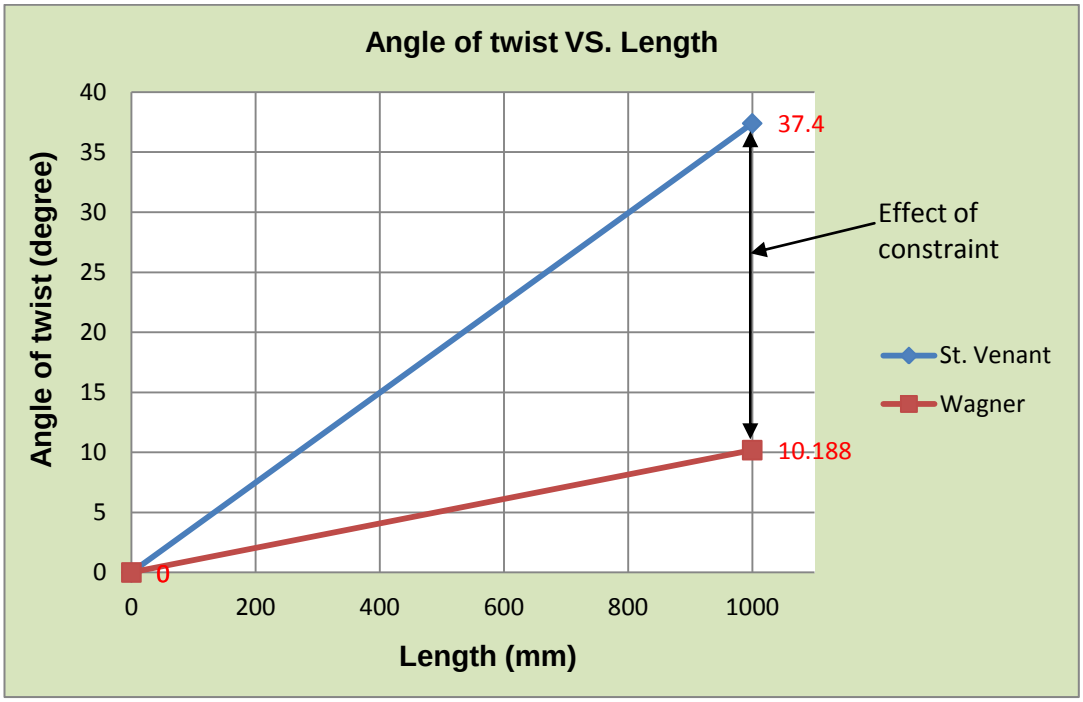

Figure 7.11 Stiffening effect of axial constraint.

7.2.7 Comparison of St. Venant torsion and Wagner torsion-bending along span

Table 7.16 St. Venant torsion and Wagner torsion-bending results along span.

Length, Z (mm)	$\frac{T_J}{T}$	$\frac{T_W}{T}$
0	0.000	1.000
100	0.082	0.918
200	0.153	0.847
300	0.214	0.786
400	0.265	0.735
500	0.308	0.692
600	0.342	0.658
700	0.368	0.632
800	0.386	0.613
900	0.397	0.603
1000	0.401	0.599

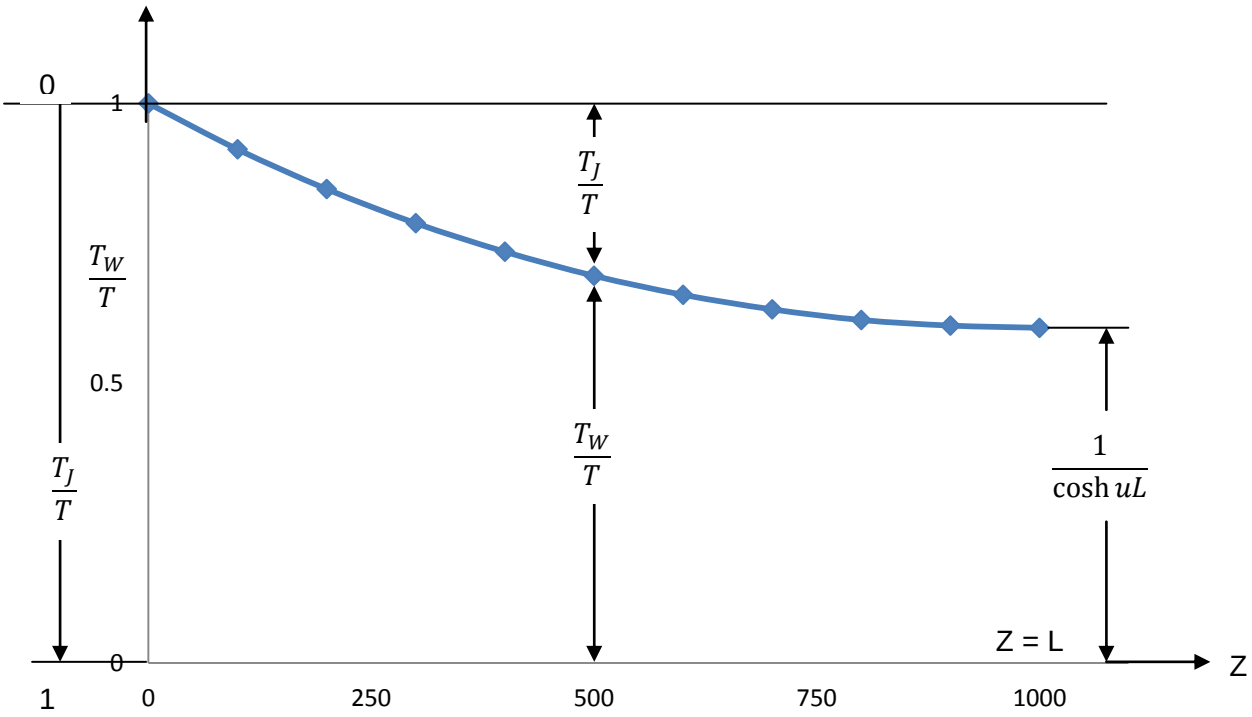

Figure 7.12 Distribution of St. Venant and torsion bending techniques along open section beam.

(T_J) and (T_W) are now plotted against (z) as fractions of the total torque (T) Fig (7.12). At the built-in end the entire torque is resisted by axial constraint stresses, but although the constraint effect diminishes towards the free end it does not disappear entirely. This is due to the fact that the axial constraint shear flow, does not vanish at $(z = L)$, at this section, $\frac{d^3\theta}{dz^3}$ is not zero.

7.2.8 Comparison of warping shear flow round cross-section at mid-span

Table 7.17 Percentage of error for warping shear flow results round cross-section at mid-span.

Distance, s (mm)	Warping shear flow, q_Γ (N/mm)		Percentage of error (%)
	Theoretical	Strand 7	
0	0	0.00	0
25	1.62	1.69	4
50	1.1	1.10	0
100	-0.54	-0.56	3.6
150	1.1	1.10	0
175	1.62	1.69	4
200	0	0.00	0
Average percentage error (%)			3.9

The average percentage error of warping shear flow is (3.9%) between theoretical and Strand 7 for channel round cross section at mid-span of the cantilever beam under torsional loading as shown in table (7.17). However, Fig (7.13) shows how the results between theoretical and Strand 7 are almost similar and the values which are shown on this graph representing the average value between theoretical and Strand 7. Moreover, both graphs nearly fit on the same line and warping shear flow are varies non-linearly (parabolic distribution) at the flanges and the web. The maximum warping shear flows occur at middle of the flanges and it is zero at the distance where (s = 0 & s = 200) mm as indicated in Fig (7.13) and this is shows that the section is distorted in their own plane during torsion-bending.

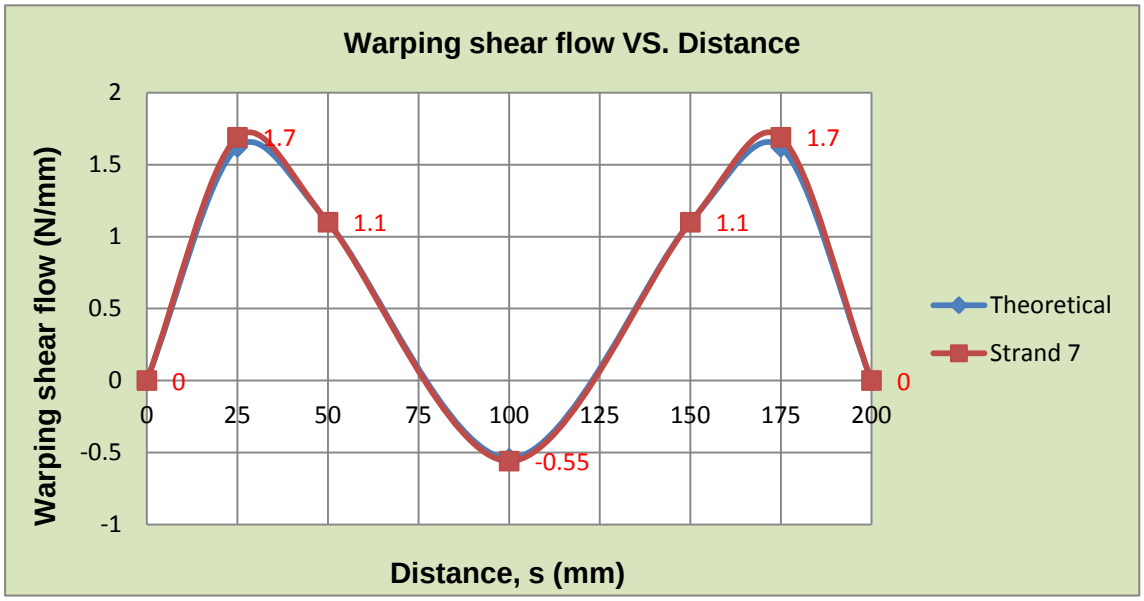

Figure 7.13 Comparison of distribution of axial constraint of shear flows round cross-section at mid-span.

7.2.9 Comparison of combined shear flow round cross-section at mid-span

The average percentage error of combined shear flow is (5.3%) between theoretical and Strand 7 which identify a good agreement for channel round cross section at mid-span of the cantilever beam under restrained torsion as shown in table (7.18).

Table 7.18 Percentage of error for combined shear flow results round cross-section at mid-span.

Combined shear flow, q_{Γ} (N/mm)		Percentage of error (%)
Theoretical	Strand 7	
22.42	21.3	5.3

CHAPTER (8)

CONCLUSIONS AND RECOMMENDATIONS

Chapter 8: Conclusions and recommendations

8.1 Conclusions

This project proposed to describe the behaviour of St. Venant principle, Wagner torsion-bending and Vlasov assumption on thin-walled open section cantilever beam under restrained torsion. A thin-walled open section cantilever beam has been developed for determining the behaviour of warping stress, warping displacement distribution, angle of twist and axial shear flow under restrained torsion.

When the end of a torsion member is restrained so that the cross-section is prevented from warping, tension and compression forces develop at the restraint and axial stresses are introduced. The angle of twist depends on the dimensions of the cross-section, thickness and the length of the member. By increasing the number of elements this will achieve more accurate results for bending stress and displacement as shown in chapter 3.

The secondary warping has been ignored due to significant values for the primary warping in thin-walled channel section cantilever beam subjected to restrained torsion.

Warping shear flow is zero at the free end due to being restrained at the built-in end and the maximum warping displacement with maximum angle of twist are occur at free end. Also, the maximum warping stress occurs at fix-end and varies linearly around profile and it is zero at the middle of the web. In addition, the maximum warping stress occurs at the flange tip at built-in end. The maximum axial constrained shear flow distribution occurs first at the middle of the flanges and second at the flange-web junction at the built-in end of the beam.

Theoretical analysis is showed that warping shear flow is proportional to young's modulus, third derivative of angle of twist, cross section dimensions and the integration of the first sectorial moment.

Previous studies in literature review are discussed and similar results are exposed with Loughlan, J. and Ata, M. Research, which the flange shows identical parabolic

behaviour for shear flow results and the maximum value occurs at the middle of the flange under restrained torsion.

It has been revealed that the location of the shear centre is very important and it depends on the shape of the cross section.

Comparisons are made between theoretical calculation and finite element analysis to define the percentage of error and have shown the excellent agreements of obtained results. Hence, the accuracy of the result depends on the number of elements.

It has been noticed that warping stress results around cross section due to restrained torsion is more accurate at built-in end than mid-span. This could be due to that there is no rotation at built-in end. Also, warping shear flow distribution results were getting more accurate in the web than the flanges; this may be due to both loads being applied through the flange area to create a torque.

8.2 Recommendations

- Additional work can be done to assess restrained torsion bending behaviour in different cross section as Z-section, I-section and angle section.
- Experiment should be carried out to investigate and compare results with theoretical and finite element analysis.
- Further study can be carried out to expose the effects of secondary warping behaviour on T-section under restrained torsion.
- Additional load can be applied to find out lateral torsional buckling behaviour.
- Closed section can be used instead channel section under restrained torsion to investigate behaviour of warping displacement, warping stress and warping shear flow, and compared with channel section.
- The same process can be done for different material to get comparison behaviour of different material under restrained torsion.

References

1) Allen, D. H. and Haisler, W. E. (1985), Introduction to Aerospace Structural Analysis, John Wiley & Sons Inc, Canada.
2) Bazant, Z. P. and Cedolin, L. (2010), Stability of Structures, Scientific Publishing Co. Pte. Ltd, USA.
3) Bruhn, E. F. (1973), Analysis and Design of Flight Vehicle Structures, Jacobs Publishing Inc, USA.
4) Beer, F. P., Johnston, E. R., and Dewolf, J. T. (2006), Mechanics of Materials, McGraw-Hill, USA.
5) Datoo, M. H. (2012), Thin Walled Beam-Stress Analysis, MSc-Structural Engineering Note, London South Bank University, London.
6) Englekirk, R. (1994), Steel Structures, John Wiley & Sons Inc, University of California at Los Angeles, USA.
7) Gjelsvik, Atle. (1981), The Theory of Thin Walled Bars, John Wiley & Sons Inc, New York.
8) Gotluru, B. P., Schafer, B. W. and Pekoz, T. (2000), Torsion in Thin-Walled Cold-Formed Steel Beams, Cornell University, USA.
9) Heins, C. P. (1975), Bending and Torsional Design in Structural Members, D. C. Heath and Company, University of Maryland, USA.
10) Heyman, J. (1982), Elements of Stress Analysis, University of Cambridge, UK.
11) Kollbrunner, C. F. and Basler, K. (1969), Torsion in Structures, Springer-Verlag, Berlin/Heidelberg, Germany.
12) Macleod, I. A. (1990), analytical Modelling of Structural Systems, University of Strathclyde, UK.
13) Megson, T. H. G. (1999), Aircraft Structures for Engineering Students, Third Edition, UK.
14) Megson, T. H. G. (2007), Aircraft Structures for Engineering Students, Fourth Edition, UK.

15) Megson, T. H. G. (1974), Linear Analysis of Thin-Walled Elastic Structures, Surry University Press, UK.

16) Megson, T. H. G. (2005), Structural and Stress Analysis, Second Edition, UK.

17) Murray, N.W. (1986), Introduction to the Theory of Thin Walled Structures, Second Edition, Clarendon Press, Oxford, UK.

18) Pilkey, W. D. (1994), Formulas for Stress, Strain, and Structural Matrices, John Wiley & Sons Inc, USA.

19) Rhodes, J. and Spence, J. (1984), Behaviour of Thin-Walled Structures, USA.

20) Rhodes, J. and Walker, A. C. (1980), Thin-Walled Structures, Granada PL, UK.

21) Salmon, C. G. and Johnson, J. E. (1990), Steel Structures; Design and Behavior, Harper & Row, Third edition, USA.

22) Sun, C. T. (2006), Mechanics of Aircraft Structures, John Wiley & Sons, Second Edition, USA.

23) Sechler, Ernest. E., and Dunn, L. G. (1942), Airplane Structural Analysis and Design, John Wiley & Sons Inc, New York.

24) Steinbacher, F. R., and George Gerard, Sc. D. (1952), Aircraft Structural Mechanics, Canada.

25) Shanmugam, N. E., Richard Liew, J. Y. and Thevendran, V. (1998), Thin-Walled Structures, National University of Singapore, Singapore.

26) Seaburg, P. A. and Carter, C. J. (1997), Torsional Analysis of Structural Steel Members, American Institute of Steel Construction Inc, USA.

27) Timoshenko, S. P. and Goodier, J. N. (1970), Theory of Elasticity, Third Edition, McGraw-Hill Book Company, New York.

28) Timoshenko, S. P. and Gere, J. M. (1961), Theory of Elastic Stability, Second Edition, McGraw-Hill, New York.

29) Timoshenko, S. P. (1940), Strength of Materials Part I & II, Second Edition, D. Van Nostrand Company, New York.

30) Trahair, N. S., Bradford, M. A., Nethercot, D. A., and Gardner, L. (2008), The Behaviour and Design of Steel Structures to EC3, Fourth Edition, Taylor & Francis, London, UK.

31) V. Dias da Silva. (2006), Mechanics and Strength of Materials, Netherlands.

32) Williams, A. (2011), Steel Structures Design, McGraw-Hill Book Company Inc, USA.

33) Williams, D. (1960), an Introduction to the Theory of Aircraft Structures, UK.

34) Young, W. C. (19869), Roark's Formulas for Stress and Strain, Sixth Edition, McGraw-Hill Book Company, Singapore.

35) Zbirohowski-Koscia, K. (1967), Thin Walled Beams, Crosby Lockwood & Son Ltd, First edition, London.
Available from, http://0-www.sciencedirect.com.lispac.lsbu.ac.uk/science
(Acceded 04-10-2012)

36) Loughlan, J. and Ata, M. (1995), The Restrained Torsional Response of Open section Carbon Fibre Composite Beams, Cranfield University, UK.
Available from, http://0-www.sciencedirect.com.lispac.lsbu.ac.uk/science
(Acceded 02-10-2012)

37) Resatoglu, R. (2005). Three Dimensional Analysis of Non-Planar Coupled shear Walls Subjected to Lateral Forces. University of Cukurova, Available from http://library.cu.edu.tr/tezler/5531.pdf (Acceded 9/7/2009)

38) Shakourzadeh. H., Guo, Y. Q. and Batoz. J. L. (1993). A Torsion Bending Element for Thin-Walled Beams with Open and Closed cross sections.
Available from, http://0-www.sciencedirect.com.lispac.lsbu.ac.uk/science
(Acceded 03-10-2012)

39) Thin-Walled Beams, Chapter 6 ,Available from
http://mae.ucdavis.edu/vlasaponara/BauchauCraig_ch6.pdf
(Acceded 12-09-2012)

40) Torsion in Structural Design, Available from
http://people.virginia.edu/~ttb/torsion.pdf (Acceded 03-09-2012)

41) Vlassov's torsion theory, Chapter 7 (2006), Available from

http://homepage.tudelft.nl/p3r3s/CT5141_chap7.pdf (Acceded 30-09-2012)

Appendix: A

Torsion properties of thin-walled cross sections

TABLE A-3. PROPERTIES OF SECTIONS

O = shear center J = torsion constant C_w = warping constant

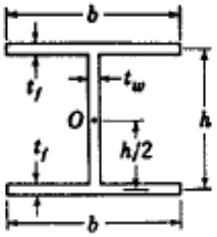	$J = \frac{2bt_f^3 + ht_w^3}{3}$ $C_w = \frac{t_f h^2 b^3}{24}$	If $t_f = t_w = t$: $J = \frac{t^3}{3}(2b + h)$
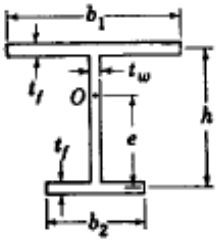	$e = h\frac{b_1^3}{b_1^3 + b_2^3}$ $J = \frac{(b_1 + b_2)t_f^3 + ht_w^3}{3}$ $C_w = \frac{t_f h^2}{12}\frac{b_1^3 b_2^3}{b_1^3 + b_2^3}$	If $t_f = t_w = t$: $J = \frac{t^3}{3}(b_1 + b_2 + h)$
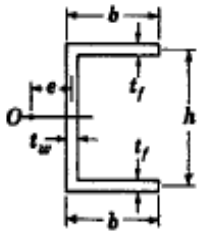	$e = \frac{3b^2 t_f}{6bt_f + ht_w}$ $J = \frac{2bt_f^3 + ht_w^3}{3}$ $C_w = \frac{t_f b^3 h^2}{12}\frac{3bt_f + 2ht_w}{6bt_f + ht_w}$	If $t_f = t_w = t$: $e = \frac{3b^2}{6b + h}$ $J = \frac{t^3}{3}(2b + h)$ $C_w = \frac{tb^3h^2}{12}\frac{3b + 2h}{6b + h}$
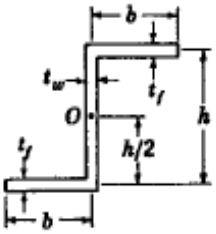	$J = \frac{2bt_f^3 + ht_w^3}{3}$ $C_w = \frac{b^3h^2}{12(2b + h)^2}$ $\times [2t_f(b^2 + bh + h^2) + 3t_w bh]$	If $t_f = t_w = t$: $J = \frac{t^3}{3}(2b + h)$ $C_w = \frac{tb^3h^2}{12}\frac{b + 2h}{2b + h}$
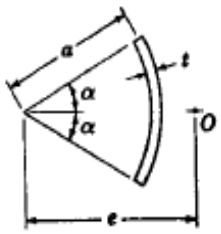	$e = 2a\frac{\sin\alpha - \alpha\cos\alpha}{\alpha - \sin\alpha\cos\alpha}$ $J = \frac{2a\alpha t^3}{3}$ $C_w = \frac{2ta^5}{3}$ $\times \left[\alpha^3 - \frac{6(\sin\alpha - \alpha\cos\alpha)^2}{\alpha - \sin\alpha\cos\alpha}\right]$	If $2\alpha = \pi$: $e = \frac{4a}{\pi}$ $J = \frac{\pi a t^3}{3}$ $C_w = \frac{2ta^5}{3}\left(\frac{\pi^2}{8} - \frac{12}{\pi}\right)$ $= 0.0374ta^5$

Source: S. P. Timoshenko and J. M. Gere, Theory of Elastic Stability. 2nd ed., McGraw-Hill, New York, 1961.

Appendix: B

Shear stress (τ_{xy}) results at Mid-plane & +Z plane; from Strand 7 for channel section.

SYSTEM: Strand7 Release 2.1.1
FILE C:\Users\hallogull\Documents\My dissertation 2012\Strand 7 files\Chapter 6\Chapter 6 Strand 7\Mesh Original.st7
TIME: 21 October 2012 1:46 pm

TITLE: Finite Element Analysis for Channel Section Cantilevered Beam Subject to Restrained Torsional Loading
DESCRIPTION: Channel Section Cantilevered Beam Subject to Restrained Torsional Loading
USER NAME: Osman Karim Abdullah
REF NUMBER: London South Bank University (ID: 2528740)

Model: Mesh Original
Result type: Plate stress
Coordinate system: Local coordinate system
Plane: PLANE: Mid-plane
Freedom case: 1: Freedom Case 1
Result case: 1: Load Case 1
Group: Model
Property: 1: Plate property 1

	Stress(xx) (MPa)	Stress(yy) (MPa)	Stress(xy) (MPa)	Stress(xz) (MPa)	Stress(yz) (MPa)	Stress(User) (MPa)
Plate 52: Node 8	378.320e-6	-25.720	22.836e-3	-3.654e-3	1.097	0.000e+0
Plate 53: Node 194	-6.271e-3	-5.152	0.846	-4.146e-3	-0.122	0.000e+0
Plate 54: Node 194	-6.422e-3	-5.152	0.846	-4.147e-3	0.123	0.000e+0
Plate 151: Node 11	-378.337e-6	25.720	22.835e-3	-3.654e-3	1.097	0.000e+0
Plate 152: Node 545	6.270e-3	5.152	0.846	-4.145e-3	-0.122	0.000e+0
Plate 153: Node 545	6.421e-3	5.152	0.846	-4.147e-3	0.123	0.000e+0
Plate 298: Node 9	-284.985e-6	15.428	0.540	12.701e-3	1.099	0.000e+0
Plate 301: Node 1002	-31.130e-6	53.471e-6	-0.282	12.210e-3	-2.838e-3	0.000e+0
Plate 305: Node 10	282.476e-6	-15.428	0.540	12.697e-3	-1.099	0.000e+0

SYSTEM: Strand7 Release 2.1.1
FILE C:\Users\hallogull\Documents\My dissertation 2012\Strand 7 files\Chapter 6\Chapter 6 Strand 7\Mesh Original.st7
TIME: 21 October 2012 2:10 pm

TITLE: Finite Element Analysis for Channel Section Cantilevered Beam Subject to Restrained Torsional Loading
DESCRIPTION: Channel Section Cantilevered Beam Subject to Restrained Torsional Loading
USER NAME: Osman Karim Abdullah
REF NUMBER: London South Bank University (ID: 2528740)

Model: Mesh Original
Result type: Plate stress
Coordinate system: Local coordinate system
Plane: PLANE: +Z Plane
Freedom case: 1: Freedom Case 1
Result case: 1: Load Case 1
Group: Model
Property: 1: Plate property 1

	Stress(xx) (MPa)	Stress(yy) (MPa)	Stress(xy) (MPa)	Stress(xz) (MPa)	Stress(yz) (MPa)	Stress(User) (MPa)
Plate 152: Node 545	-0.604	4.228	10.661	-4.145e-3	-0.122	0.000e+0
Plate 153: Node 545	-0.605	4.228	10.661	-4.147e-3	0.123	0.000e+0

Appendix: C

Warping displacement (DZ) and angle of twist (RZ) results at Mid-plane; from Strand 7 for channel section.

SYSTEM: Strand7 Release 2.1.1
FILE C:\Users\hallogull\Documents\My dissertation 2012\Strand 7 files\Chapter 6\Chapter 6 Strand 7\Mesh Original.st7
TIME: 21 October 2012 2:34 pm

TITLE: Finite Element Analysis for Channel Section Cantilevered Beam Subject to Restrained Torsional Loading
DESCRIPTION: Channel Section Cantilevered Beam Subject to Restrained Torsional Loading
USER NAME: Osman Karim Abdullah
REF NUMBER: London South Bank University (ID: 2528740)

Model: Mesh Original
Result type: Node displacement
Coordinate system: Global XYZ
Freedom case: 1: Freedom Case 1
Result case: 1: Load Case 1
Group: Model
Property: 1: Plate property 1

	DX (mm)	DY (mm)	DZ (mm)	RX (deg)	RY (deg)	RZ (deg)
Node 7	0.000e+0	0.000e+0	0.000e+0	0.000e+0	0.000e+0	0.000e+0
Node 8	2.690	3.712	-0.296	-0.740	0.000e+0	3.105
Node 9	2.689	1.004	0.178	-0.209	0.539	3.093
Node 10	-2.689	1.004	-0.178	-0.209	-0.539	3.093
Node 11	-2.690	3.712	0.296	-0.740	0.000e+0	3.105
Node 18	-8.423	11.043	0.389	-0.536	0.000e+0	8.898
Node 404	-0.133	0.210	78.076e-3	-0.205	0.000e+0	0.185
Node 437	-0.498	0.713	0.146	-0.366	0.000e+0	0.607
Node 474	-1.065	1.488	0.205	-0.512	0.000e+0	1.252
Node 507	-1.805	2.500	0.255	-0.636	0.000e+0	2.095
Node 575	-3.695	5.089	0.329	-0.823	0.000e+0	4.252
Node 612	-4.794	6.595	0.355	-0.887	0.000e+0	5.506
Node 645	-5.964	8.193	0.374	-0.925	0.000e+0	6.835
Node 682	-7.181	9.799	0.385	-0.871	0.000e+0	8.142
Node 1002	-163.469e-9	1.002	0.000e+0	0.000e+0	-181.627e-9	3.076

Warping stresses (f_{zz}) results at Mid-plane; from Strand 7 for channel section.

SYSTEM: Strand7 Release 2.1.1
FILE C:\Users\hallogull\Documents\My dissertation 2012\Strand 7 files\Chapter 6\Chapter 6 Strand 7\Mesh Original.st7
TIME: 21 October 2012 3:39 pm

TITLE: Finite Element Analysis for Channel Section Cantilevered Beam Subject to Restrained Torsional Loading
DESCRIPTION: Channel Section Cantilevered Beam Subject to Restrained Torsional Loading
USER NAME: Osman Karim Abdullah
REF NUMBER: London South Bank University (ID: 2528740)

Model: Mesh Original
Result type: Plate stress
Coordinate system: Global XYZ
Plane: PLANE: Mid-plane
Freedom case: 1: Freedom Case 1
Result case: 1: Load Case 1
Group: Model
Property: 1: Plate property 1

	Stress(XX) (MPa)	Stress(YY) (MPa)	Stress(ZZ) (MPa)	Stress(XY) (MPa)	Stress(YZ) (MPa)	Stress(ZX) (MPa)	Stress(User) (MPa)
Plate 4: Node 1	-14.573	0.000e+0	-61.960	10.141e-3	-876.978e-6	6.213	0.000e+0
Plate 7: Node 3	8.917	0.000e+0	36.713	-79.458e-3	0.689	2.031	0.000e+0
Plate 103: Node 7	14.573	0.000e+0	61.960	10.141e-3	-876.975e-6	-6.213	0.000e+0
Plate 106: Node 5	-8.917	0.000e+0	-36.713	-79.458e-3	0.689	-2.031	0.000e+0
Plate 111: Node 404	0.129	0.000e+0	50.586	5.894e-3	0.312	-59.386e-3	0.000e+0
Plate 119: Node 437	23.677e-3	0.000e+0	43.787	7.307e-3	0.551	-26.597e-3	0.000e+0
Plate 123: Node 437	-36.001e-3	0.000e+0	43.607	6.239e-3	0.538	-27.594e-3	0.000e+0
Plate 131: Node 474	-703.644e-6	0.000e+0	37.327	5.299e-3	0.759	-25.667e-3	0.000e+0
Plate 143: Node 507	-26.518e-3	0.000e+0	31.268	4.389e-3	0.940	-24.483e-3	0.000e+0
Plate 151: Node 11	-378.337e-6	0.000e+0	25.720	3.654e-3	1.097	-22.835e-3	0.000e+0
Plate 159: Node 575	23.727e-3	0.000e+0	20.434	2.748e-3	1.224	-21.534e-3	0.000e+0
Plate 163: Node 575	-23.923e-3	0.000e+0	20.292	2.620e-3	1.219	-22.008e-3	0.000e+0
Plate 171: Node 612	-198.596e-6	0.000e+0	15.235	2.066e-3	1.314	-20.961e-3	0.000e+0
Plate 179: Node 645	22.862e-3	0.000e+0	10.333	1.629e-3	1.368	-20.073e-3	0.000e+0
Plate 183: Node 645	-21.843e-3	0.000e+0	10.199	2.917e-3	1.368	-20.339e-3	0.000e+0
Plate 191: Node 682	-10.255e-3	0.000e+0	5.377	-12.258e-3	1.215	-27.136e-3	0.000e+0
Plate 199: Node 18	-12.696e-3	0.000e+0	-0.219	-71.735e-3	-46.221e-3	56.439e-3	0.000e+0
Plate 202: Node 3	0.000e+0	8.609	36.597	-55.529e-3	4.217	0.329	0.000e+0
Plate 205: Node 4	0.000e+0	-0.228	-83.767e-3	7.671e-3	-1.971	-5.677e-3	0.000e+0
Plate 206: Node 4	0.000e+0	0.228	83.767e-3	7.671e-3	-1.971	5.677e-3	0.000e+0
Plate 209: Node 5	0.000e+0	-8.609	-36.597	-55.529e-3	4.217	-0.329	0.000e+0

Appendix: D

Deflection results (DY); from Strand 7 for Own model rectangular section cantilever beam.

SYSTEM: Strand7 Release 2.1.1
FILE F:\Dissertation 2012\My MSc Dissertation 2012\Dissertation\My Dissertation by Strand7\3D from 2D\Own 3D\Mesh6.st7
TIME: 13 August 2012 12:59 pm

Model: Mesh6
Result type: Node displacement
Coordinate system: Global XYZ
Freedom case: 1: Freedom Case 1
Result case: 1: Load Case 1
Group: Model
Property: 1: Plate Property 1

	DX (mm)	DY (mm)	DZ (mm)	RX (deg)	RY (deg)	RZ (deg)
Node 1	0.000	0.000	0.000	0.000	0.000	0.000
Node 2	-0.014	-0.065	0.000	0.000	0.000	0.000
Node 3	-0.019	-0.206	0.000	0.000	0.000	0.000
Node 9	0.000	0.000	0.000	0.000	0.000	0.000
Node 11	0.000	0.000	0.000	0.000	0.000	0.000
Node 12	0.000	0.000	0.000	0.000	0.000	0.000
Node 13	0.000	0.000	0.000	0.000	0.000	0.000
Node 14	0.000	0.000	0.000	0.000	0.000	0.000
Node 15	-0.002	-0.002	0.000	0.000	0.000	0.000
Node 29	-0.006	-0.011	0.000	0.000	0.000	0.000
Node 43	-0.010	-0.027	0.000	0.000	0.000	0.000
Node 57	-0.013	-0.051	0.000	0.000	0.000	0.000
Node 69	-0.015	-0.080	0.000	0.000	0.000	0.000
Node 83	-0.017	-0.113	0.000	0.000	0.000	0.000
Node 97	-0.018	-0.149	0.000	0.000	0.000	0.000
Node 100	0.009	-0.149	0.000	0.000	0.000	0.000
Node 111	-0.019	-0.187	0.000	0.000	0.000	0.000

Bending stress (f_{xx}) and shear stress (τ_{xy}) results; from Strand 7 for Own model rectangular section cantilever beam.

SYSTEM: Strand7 Release 2.1.1
FILE F:\Dissertation 2012\My MSc Dissertation 2012\Dissertation\My Dissertation by Strand7\3D from 2D\Own 3D\Mesh6.st7
TIME: 13 August 2012 2:58 pm

Model: Mesh6
Result type: Plate stress
Coordinate system: Global XYZ
Plane: PLANE: Mid-plane
Freedom case: 1: Freedom Case 1
Result case: 1: Load Case 1
Group: Model
Property: 1: Plate Property 1

	Stress(XX) (MPa)	Stress(YY) (MPa)	Stress(ZZ) (MPa)	Stress(XY) (MPa)	Stress(YZ) (MPa)	Stress(ZX) (MPa)	Stress(User) (MPa)
Plate 14: Node 2	-3.249	-0.016	0.000	-0.008	0.000	0.000	0.000
Plate 18: Node 2	-3.249	0.012	0.000	-0.008	0.000	0.000	0.000
Plate 5: Node 6	6.598	1.369	0.000	-0.466	0.000	0.000	0.000
Plate 17: Node 7	3.249	0.017	0.000	-0.008	0.000	0.000	0.000
Plate 21: Node 7	3.249	-0.012	0.000	-0.008	0.000	0.000	0.000
Plate 1: Node 8	0.199	-0.579	0.000	-0.076	0.000	0.000	0.000
Plate 5: Node 19	6.040	0.374	0.000	-0.118	0.000	0.000	0.000
Plate 5: Node 28	5.585	-0.621	0.000	0.230	0.000	0.000	0.000
Plate 9: Node 28	5.585	-0.048	0.000	-0.037	0.000	0.000	0.000
Plate 9: Node 33	5.201	-0.028	0.000	-0.011	0.000	0.000	0.000
Plate 9: Node 42	4.8	-0.008	0.000	0.016	0.000	0.000	0.000
Plate 13: Node 42	4.8	0.031	0.000	-0.018	0.000	0.000	0.000
Plate 13: Node 47	4.405	0.016	0.000	-0.012	0.000	0.000	0.000
Plate 13: Node 56	4.0	0.000	0.000	-0.005	0.000	0.000	0.000
Plate 17: Node 56	4.0	-0.023	0.000	-0.008	0.000	0.000	0.000
Plate 17: Node 61	3.599	-0.003	0.000	-0.008	0.000	0.000	0.000
Plate 15: Node 63	-1.597	-0.001	0.000	-0.158	0.000	0.000	0.000
Plate 14: Node 63	-1.597	0.004	0.000	-0.158	0.000	0.000	0.000
Plate 15: Node 65	0.000	0.001	0.000	-0.208	0.000	0.000	0.000
Plate 17: Node 67	1.597	-0.005	0.000	-0.158	0.000	0.000	0.000
Plate 21: Node 67	1.597	-0.001	0.000	-0.158	0.000	0.000	0.000
Plate 21: Node 73	2.800	0.001	0.000	-0.010	0.000	0.000	0.000
Plate 21: Node 82	2.448	0.013	0.000	-0.012	0.000	0.000	0.000
Plate 25: Node 82	2.448	-0.011	0.000	-0.010	0.000	0.000	0.000
Plate 25: Node 87	1.999	-0.001	0.000	-0.005	0.000	0.000	0.000
Plate 25: Node 96	1.647	0.009	0.000	0.000	0.000	0.000	0.000
Plate 29: Node 96	1.570	0.020	0.000	0.021	0.000	0.000	0.000
Plate 29: Node 101	1.2	-0.016	0.000	-0.032	0.000	0.000	0.000
Plate 29: Node 110	0.808	-0.052	0.000	-0.085	0.000	0.000	0.000
Plate 1: Node 110	0.808	0.336	0.000	0.102	0.000	0.000	0.000
Plate 1: Node 115	0.521	-0.122	0.000	0.013	0.000	0.000	0.000

Appendix: E

Stiffness Matrix for the Vlasov Torsion Theory

$$x=0 \rightarrow \varphi_1=\varphi,\quad \theta_1=\frac{d\varphi}{dx},\quad T_1=-M_t,\quad B_1=B$$

$$x=l \rightarrow \varphi_2=\varphi,\quad \theta_2=\frac{d\varphi}{dx},\quad T_2=M_t,\quad B_2=-B$$

$$\begin{bmatrix} T_1 \\ T_2 \\ B_1 \\ B_2 \end{bmatrix} + \begin{bmatrix} \frac{1}{2}l \\ \frac{1}{2}l \\ \frac{1}{2}\frac{l^2}{\beta^2\lambda} \\ -\frac{1}{2}\frac{l^2}{\beta^2\lambda} \end{bmatrix} m_x = \begin{bmatrix} \frac{GI_t}{l}\eta & -\frac{GI_t}{l}\eta & GI_t\lambda & GI_t\lambda \\ -\frac{GI_t}{l}\eta & \frac{GI_t}{l}\eta & -GI_t\lambda & -GI_t\lambda \\ GI_t\lambda & -GI_t\lambda & \frac{EC_w}{l}\xi & \frac{EC_w}{l}\mu \\ GI_t\lambda & -GI_t\lambda & \frac{EC_w}{l}\mu & \frac{EC_w}{l}\xi \end{bmatrix} \begin{bmatrix} \varphi_1 \\ \varphi_2 \\ \theta_1 \\ \theta_2 \end{bmatrix}$$

$$\eta=\frac{\beta(e^{\beta}+1)}{\beta+2+(\beta-2)e^{\beta}}$$

$$\lambda=\frac{e^{\beta}-1}{\beta+2+(\beta-2)e^{\beta}}$$

$$\mu=\frac{\beta}{e^{\beta}-1}\,\frac{e^{2\beta}-2\beta e^{\beta}-1}{\beta+2+(\beta-2)e^{\beta}}$$

$$\xi=\frac{\beta}{e^{\beta}-1}\,\frac{\beta+1+(\beta-1)e^{2\beta}}{\beta+2+(\beta-2)e^{\beta}}$$

$$\beta=l\sqrt{\frac{GI_t}{EC_w}}$$

Source: http://homepage.tudelft.nl/p3r3s/CT5141_chap7.pdf